# NANOTUBE MEMBRANES FOR CHEMICAL AND BIOCHEMICAL SENSING AND SEPARATION

By

LACRAMIOARA TROFIN

A DISSERTATION PRESENTED TO THE GRADUATE SCHOOL
OF THE UNIVERSITY OF FLORIDA IN PARTIAL FULFILLMENT
OF THE REQUIREMENTS FOR THE DEGREE OF
DOCTOR OF PHILOSOPHY

UNIVERSITY OF FLORIDA

2005

This dissertation is dedicated to my parents, Lucia and Nicolae Darie.

## ACKNOWLEDGMENTS

I think if any of us honestly reflects on who we are, and how we got here, we discover a debt to others that spans nearly our whole lives.

The work and support of some people made my life easier everyday. Some people have directly shaped my life and my work.

I would like to acknowledge the inspiration and guidance that I received from my Ph.D. advisor, Dr. Charles R. Martin. He encouraged and supported my work. He also taught me how to effectively communicate science and successfully write scientific papers. I am grateful for the many suggestions and comments that I received from the members of the Martin group. I have been fortunate to be a member of such a diverse, team-oriented research group. Many colleagues contributed directly to my research projects with their ideas and energies. David T. Mitchell introduced me to the field of nanomaterials. He taught me how to make alumina membranes, silica nanotubes and he gave me excellent training in electron microscopy. SangBok Lee gave me insightful advice on the microbattery project. Marc Wirtz taught me the fundamentals of impedance spectroscopy. I am grateful to Punit Kohli for his help in the protein separation project and for his contagious enthusiasm for science. The many hours I spent chatting with Zuzanna Siwy have led to fruitful developments. She contributed directly with her knowledge and energy to my scientific development. I would like to thank David T. Mitchell and Elizabeth Heins for the endless hours they spent, teaching me English. For that, I am especially grateful to them. Damian Odom, Scott Miller,

Elizabeth Heins, David Mitchell, Shufang Yu, Punit Kohli, Marc Wirtz gave me ideas and helped me in preparing the talks that I presented during graduate school. I am very grateful to Myungchan Kang, who helped me with the microarrays project. He taught me about plasma etching technique and fluorescence spectroscopy. I am indebted to Miguel O. Mota, who did his best to improve on my best. Miguel spent many hours making alumina membranes and solutions necessary for my projects. I also want to thank Heather Hillebrenner who has shared her needs and experiences with me. I have had the wonderful experience to truly believe that in some small way I helped her; that means so very much to me. I am also grateful to Zuzanna Siwy and Lane Baker who proofread this dissertation and, by their feedback, they helped me structure better the dissertation.

My life during the graduate school would have been much less interesting without my friends Isabela and Calin Briciu, Zuzanna Siwy , Cristina Cosma, Nathalie Kohli, and Violeta Bacanu. I would like to specially thank my boyfriend, Hermann Schulte auf'm Erley, for his love and continuous support during my last years of graduate school.

I would like to thank to my chemistry high school teacher, Ion Dumbrava, and my mentor, Dr. Gheorghe Ivan from CERELAST-Bucharest, for their untiring support and seemingly unlimited belief in me.

Special gratitude is reserved to my parents, Lucia and Nicolae Darie, who have encouraged me in so many ways to pursue my life dreams.

TABLE OF CONTENTS

Page

LIST OF TABLES

LIST OF FIGURES

Abstract of Dissertation Presented to the Graduate School
of the University of Florida in Partial Fulfillment of the
Requirements for the Degree of Doctor of Philosophy

# NANOTUBE MEMBRANES FOR CHEMICAL AND BIOCHEMICAL SENSING AND SEPARATION

By

Lacramioara Trofin

May 2005

Chair: Charles R. Martin
Major Department: Chemistry

The discovery of novel materials, processes, and phenomena at the nanoscale, as well as the development of new experimental and theoretical techniques for research, provide fresh opportunities for the development of innovative nanodevices and nanostructured materials. Nanostructured materials can be made with unique nanostructures and properties, and finding various and unique applications of these is a continuous challenge for researchers in this field. As part of this emerging research, the work presented here is focused on development of new nanostructures based on nanoporous membranes, and investigation of their applications as sensors and separation devices. A template synthesis method is used to produce nanotubes inside the pores of both aluminum oxide and polymeric membranes. After an introduction in the template synthesis method and the processes of fabrication of the porous membranes, the dissertation is centered on investigating new applications of these nanotube membranes.

There are three applications of the nanotube alumina membranes, and one application of the single nanotube polymeric membranes that are explored.

Porous alumina is used to mimic the function of the ligand-gated ion channel by applying a porous battery cathode film to one face of the hydrophobic membrane and a porous battery anode film to the other face. Hence, in analogy to the naturally occurring channel case, we have a membrane with a built in electrochemical potential difference across the membrane.

The application of silica nanotube membranes in selective separation of proteins is presented. The membranes were modified with antibodies that selectively bind one analyte. These nanotube systems lead to the transport at much higher rates of the analyte which binds to the membrane.

Another application studied is the fabrication of the protein microarrays which features a three dimensional substrate based on porous aluminum oxide membranes. These membranes represent distinct microfeatures on a robust platform, and they have cylindrical pores with monodisperse nanoscopic diameters. The advantages of using this substrate and its application in antibody specificity screening are presented.

Finally, a new family of protein biosensors based on a single conical nanotube membrane is described. Three different protein systems were investigated: (i) biotin/streptavidin, (ii) protein-G/immunoglobulins, and (iii) anti-ricin/ricin.

# CHAPTER 1
# INTRODUCTION AND BACKGROUND

## Introduction

Nanotechnology refers to technologies in which matter is manipulated on the atomic and molecular level to create new materials and observe new processes. It is not just the study of the very small; it is also the practical application of that knowledge. Nanotechnology is a truly interdisciplinary field. Materials scientists, electronic and mechanical engineers, as well as medical researchers are working together with biologists, physicists and chemists. Research at the nanoscale is unified by the need to share the knowledge and expertise required to work at the atomic and molecular level. Powerful new concepts and capabilities, such as atomic-scale imaging and manipulation, self-assembly and biological structure-function relationship, together with increasingly powerful computing tools are rapidly converging from different research areas. Nanotechnology is not a new area, though. Mother Nature serves as a model for having many materials and processes that functions at the nanoscale (1); small molecular building blocks are joined together to produce nanostructures with defined geometries and functions. The top-down approach becomes increasingly difficult, as the final products approach the nanometer levels. It has become evident that Nature's bottom-up approach can be emulated to produce new materials with nanosized dimensions and engineered properties.

Nanoparticles (2,3) and nanotubes (4,5) are the two principal branches of nanostructured materials. Historically, nanoparticles were mainly restricted to gold and

silver particles. More recently, a wider variety of nanoparticles have been synthesized; for example, commercially available magnetic beads are used for cell preparation (6,7), quantum dots are used for long-term fluorescence assay in cells (8), and colloidal gold has been used for gene therapy (9). Since the discovery of carbon nanotubes in 1991 (10), the synthesis and functionalization of the nanotubular materials has become one of the most highly energized research areas (11). Nanotubes have numerous potential commercial and technological applications, including their use in nanoelectronics (12,13,14,15), catalysis (16,17,18), hydrogen storage (19), scanning probe microscopy (20), biosensors (21,22) and drug delivery systems (23).

Research in the field of nanotube membranes will have a great impact on membrane technology. Membranes are utilized to perform separations for a wide range of applications such as water and wastewater treatment, electrodialysis, gas separation, and fuel cell development (24). The use of membranes and biological tools are important in the development of biomedical and biotechnological applications (25). Recently, membranes have been gaining attention as options for biological sensors (26). However, modern biotechnology and separation science have presented new challenges to membrane technology, including the requirement of pores with diameters similar to those of molecules under study, therefore as small as several nanometers. Nanometer scale pores are necessary in achieving optimal control of the flow of biomolecules as well as in developing sensors for their detection (27-30). Another challenge is the development and characterization of membranes possessing well-controlled, stable, and uniform nanometer dimension pores capable of the separation and sensing of molecules in a restricted manner.

In light of these challenges, Martin's group has pioneered a bottom-up method for the production of nanotube membranes, called template synthesis (31). This method involves synthesizing nanotubes inside of a porous membrane (template). This chapter provides background information on the following: membrane-based template synthesis, fabrication and applications of porous alumina (one type of membrane template), sol-gel and silane chemistry, carrier facilitated transport, and single pore polymeric membranes. An overview of the dissertation is also presented. This information will be used in the next chapters.

## Background

### Membrane-Based Template Synthesis

In recent years, the Martin group has been investigating a versatile method to produce nanomaterials, called template synthesis (31). In this approach, a membrane with uniform dispersed, micro or nanometer diameter pores acts as a template. When material is deposited into the cylindrical pores of the membranes, it adopts their shape. If the template is dissolved, the material can retain the high aspect ratio of the pores, yielding wires or tubes with nanometer diameters. The method is versatile with regard to the type of materials that can be prepared. For instance, track-etched polymeric membranes have been used to prepared nanostructures composed of metals (32,33), insulating polymers (34) or conductive polymers (35,36).

### Membrane templates

Two types of template are most often used for this approach: polycarbonate and alumina membranes. Polycarbonate membranes are prepared by the "track-etch" method (37) and have been commercialized by companies like Nucleopore and Osmonics Poretics. These membranes have pores with diameters between 10 nm and 10 μm, and

pore densities approaching $10^9$ pores/cm$^2$. Alumina membranes are prepared electrochemically from aluminum foils (38). They are commercially available (Whatman International), or can be prepared in the laboratory. The process of making alumina membranes and their applications will be discussed in detail in the following section.

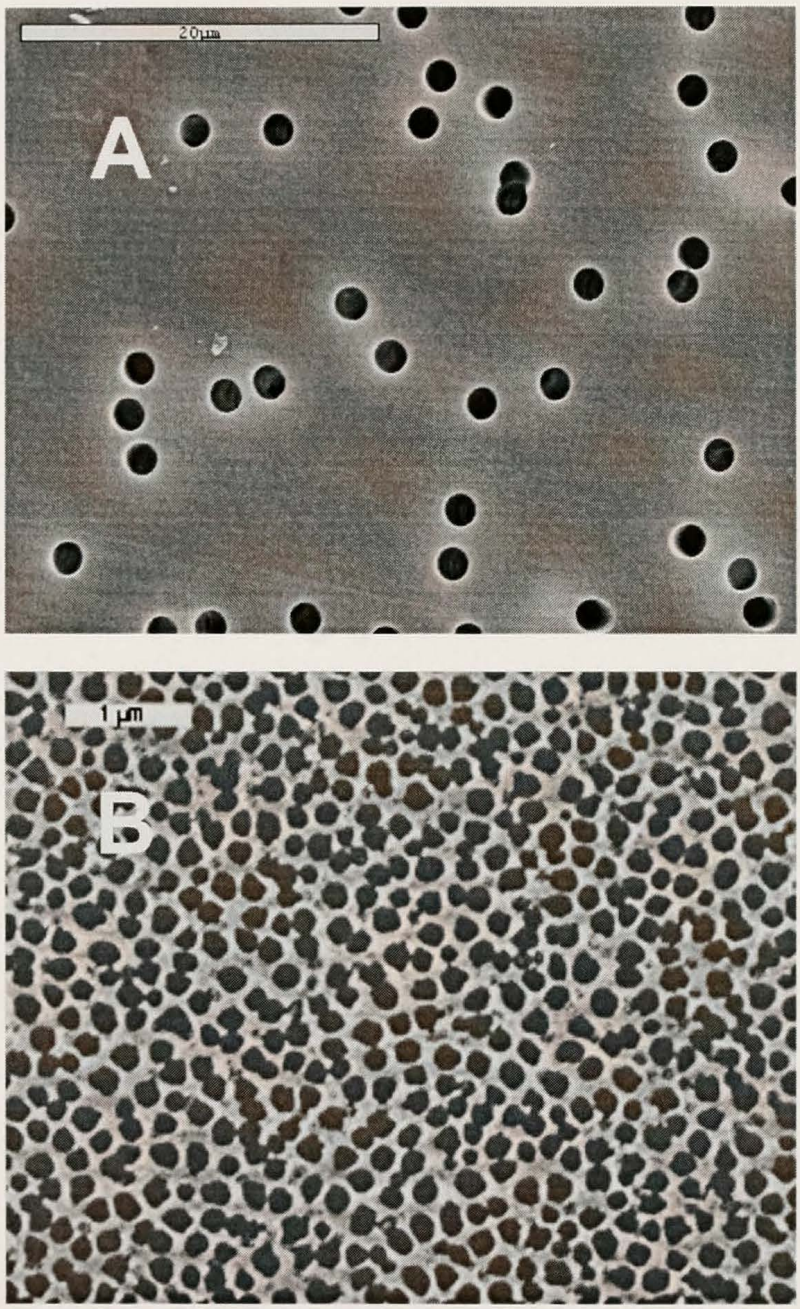


Figure 1-1. Scanning electro micrographs of the 3 µm pore diameter polycarbonate (A) and 200 nm pore diameter alumina (B) membrane surfaces.

Figure 1-1 shows scanning electron micrographs of the surfaces of the polycarbonate and alumina membranes, respectively. Templates with diamond shapes pore in mica have also been reported (39).

The sensing and transport properties of the gold nanotube membranes prepared by the electroless deposition method (40) were investigated extensively in the Martin group (40-47).

**Electroless deposition**

Electroless deposition involves a chemical reducing agent which is used to plate a metal from a solution onto a surface. The method for electroless deposition of gold can be summarized as follows. The membrane is first "sensitized" by exposing it to a solution of $SnCl_2$. This results in deposition of $Sn^{II}$ onto the membrane surfaces and the pore walls. After the sensitization, the membrane is immersed into an ammonia silver nitrate solution. A surface redox reaction occurs (Equation 1-1) and $Ag^{I}$ is reduced by $Sn^{II}$, which results in absorbtion of Ag nanoscopic particles on the membrane surfaces.

$$Sn^{II}_{surf} + 2Ag^{I}_{sol} \rightarrow Sn^{IV}_{surf} + 2Ag^{0}_{surf} \qquad (1\text{-}1)$$

The subscripts "surf" and "sol" denote species absorbed to the membrane surfaces and species in solution, respectively. Then, the membrane is immersed into a gold plating solution at $4^0$C. A second redox reaction occurs, and $Au^0$ displaces the Ag particle, yielding the membrane surfaces to be coated with Au particles (Equation 1-2).

$$Au^{I}_{sol} + Ag^{0}_{surf} \rightarrow Au^{0}_{surf} + Ag^{I}_{sol} \qquad (1\text{-}2)$$

These $Au^0$ particles are excellent autocatalysts for the reduction of $Au^I$ to $Au^0$, using formaldehyde as reducing agent. As a result, the Au deposition begins at the pore walls, forming Au nanotubes or nanowires, depending on the plating time (33).

**Applications of gold nanotube membranes**

Gold nanotube membranes are a new class of molecular filters, capable of sensing and transporting both small and large molecules. Jiraje et al. took advantage of the excess charge density present on the inner walls of the gold nanotubes and showed the regulation of ion transport through the membranes (40). They showed the fluxes of anionic and cationic permeates changed with the potential applied to the gold nanotube membranes. The tubes transport ions which have the opposite charge as the gold nanotubes (40). Because the inner diameter of the gold tubes can be of molecular dimensions ( <1 nm), nanotube membranes have also been used to separate small molecules on the basis of molecular size (41). In these experiments, a large molecule, (a tris-bipyridal complex of $Ru_{(II)}$ $Ru(bpy)_3^{2+}$), and a small molecule (methyl viologen $MV^{2+}$), were used. A selectivity coefficient was defined as the ratio between the fluxes of $MV^{2+}$ and $Ru(bpy)_3^{2+}$ through the membranes. They report a selectivity coefficient of 50 when the inner diameter of the gold tubes was 5.5 nm. They have also showed that as the inner diameter decreases, the selectivity coefficient increases, reaching a value of 172 for a 2 nm inner diameter (41). The gold nanotube membranes were also used to study the DNA transport, both by diffusion and electrophoretically. The flux of the single-stranded homooligonucleotides made of thymidine bases (poly($T_n$) – where n represents the number of bases – decreased as the size (base number) of the poly($T_n$) increased (42).

Another way of introducing chemical and biochemical transport selectivity is by adsorbing thiols on the gold nanotubes (43,44,45). Hydrophobic thiols yield membranes that preferentially transport hydrophobic species and hydrophilic thiols form tubes that preferentially transport hydrophilic species (43,44). The absorbtion of L-cysteine on the

gold tubes was used to make pH-switchable ion transport membranes. Depending on the solution pH, the membrane can have excess positive charge (low pH), no net charge (isoelectric point ), or excess negative charge (high pH ). As a result, these membranes can be switched between cation-, non-ion-permselective, and anion-transporting states (45). By controlling the inner diameter of the gold tubes, these membranes can also show good selectivity for transport of proteins on the basis of molecular size (46). In this work, chemisorbtion of a PEG-thiol prevented the non-specific adsorbtion of the protein on the gold tubes. A transmembrane pressure was applied to the feed solution to force the solution through the membrane. The effect of nanotube diameter on the flux and selectivity for lysozyme, bovine serum albumin and β-lactoglobulin A was investigated (46). Recently, through the immobilization of molecular recognition elements, gold nanotube membranes were used to obtain DNA single base mismatch transport selectivity (47). Single-stranded DNA molecules with a thiol at one end were chemisorbed on the inner walls of the tubes. These DNA functionalized tubes selectively recognize and transport the DNA sequences which are complementary to the DNA on the tubes, relative to the uncomplementary DNA sequences.

**Porous Alumina Membranes**

Electrochemical oxidation (anodization) of aluminum surfaces under controlled conditions can produce aluminum oxide or alumina with a structure of essentially cylindrical, parallel pores (48). Anodic porous alumina membranes can be made with pore diameters varying between few nanometers to 200 nm, with lengths up to 300 μm (49). Pore densities can range from $10^9$-$10^{12}$ pores/cm$^2$. Solutions of dilute acidic

solutions (*e.g.* phosphoric acid (49), oxalic acid (50) and sulfuric acid) are used as electrolyte (51).

In recent years, there has been a growing interest in preparing alumina membranes with a perfect pore array architecture, having a high aspect ratio at the nanometer scale. This interest was drawn by the possibility of applying these membranes as hosts or templates for the fabrication of the nanodevices.

There are two reported methods for the fabrication of highly ordered anodic porous alumina membranes. One is the two-step anodization method which will be discussed in detail in the next section; this is the method that is used in our laboratory to make the alumina membranes (52,53). In the other method, the layout of the initiation sites for hole development in anodic alumina is achieved by a process based on nanoindentation of the aluminum substrate. In this process, an array of shallow depressions is formed on aluminum by indentation, and these depressions serve as initiation sites for hole generation at the initial stage of generation. Masuda et al. (54) used a SiC mold to form an array of concave features with the desired arrangement (square, triangular) on aluminum. In addition, Mikulskas et al. (55) showed that the nanoindentation twice with commercially available optical grating rotated by an angle of $60^0$ to each other, can create pre-structures with rombohedral ridges on aluminum. The advantage of this patterning is that it eliminates the high cost of the mold, which requires electron beam lithography to produce it. Masuda et al. (56) reported another patterning method, by using a nanoindentation apparatus attached to a scanning probe microscope.

**Two-step anodization method**

This method involves two successive steps of anodization of an aluminum foil in order to obtain very highly ordered porous alumina membranes.

**Polishing of aluminum foils.** In order to obtain a high quality alumina film, the starting material, aluminum, must be very smooth. High purity aluminum foils (99.99 %) are first mechanically polished with a slurry of alumina particles. Larger particles (>10μm) are used to remove material fast, and polishing is continued with slurries of progressively smaller particles of submicron size. If the aluminum foils have severe scratches, mechanically polishing with fine sand paper is applied until the scratches disappear. This mechanical polishing is followed by an electrochemical one. In this process, a potential difference of 15 V is applied between the aluminum foil (which serves as the anode) and a lead plate which serves as the cathode. The polishing solution (95% concentrated phosphoric acid, 5% concentrated sulfuric acid and 20 g/L chromic oxide) is heated to $70^0$C. This process is analogous with that of alumina film formation, but the electrolyte, being a very concentrated acidic solution at high temperature, favors immediate dissolution of alumina. The electropolishing step (usually 5 minutes) is repeated as many times as it is necessary, until the aluminum foil has a mirror-like surface.

**Anodization steps.** Electropolished aluminum is electrochemically oxidized into a first step at a constant voltage, using an electrochemical cell setup like the one presented in figure 1-2.

In the process of forming the alumina film referred in the literature as the growth process, the aluminum is the anode and a stainless steal plate is used as the cathode. Both anode and cathode are immersed into an electrolyte solution and a voltage is applied using a power supply. The temperature (usually between $0^0$ and $15^0$C) is controlled using a cooling bath. The expansion of aluminum during the oxidation process depends

strongly on experimental conditions, such as temperature, voltage applied, type of electrolyte and concentration of the electrolyte (57-59). Smaller pore sizes require lower applied voltages and therefore more conductive electrolytes (such as sulfuric acid) (48). Larger pores need larger voltages, which causes a high rate of dissolution in highly conductive electrolytes (62).

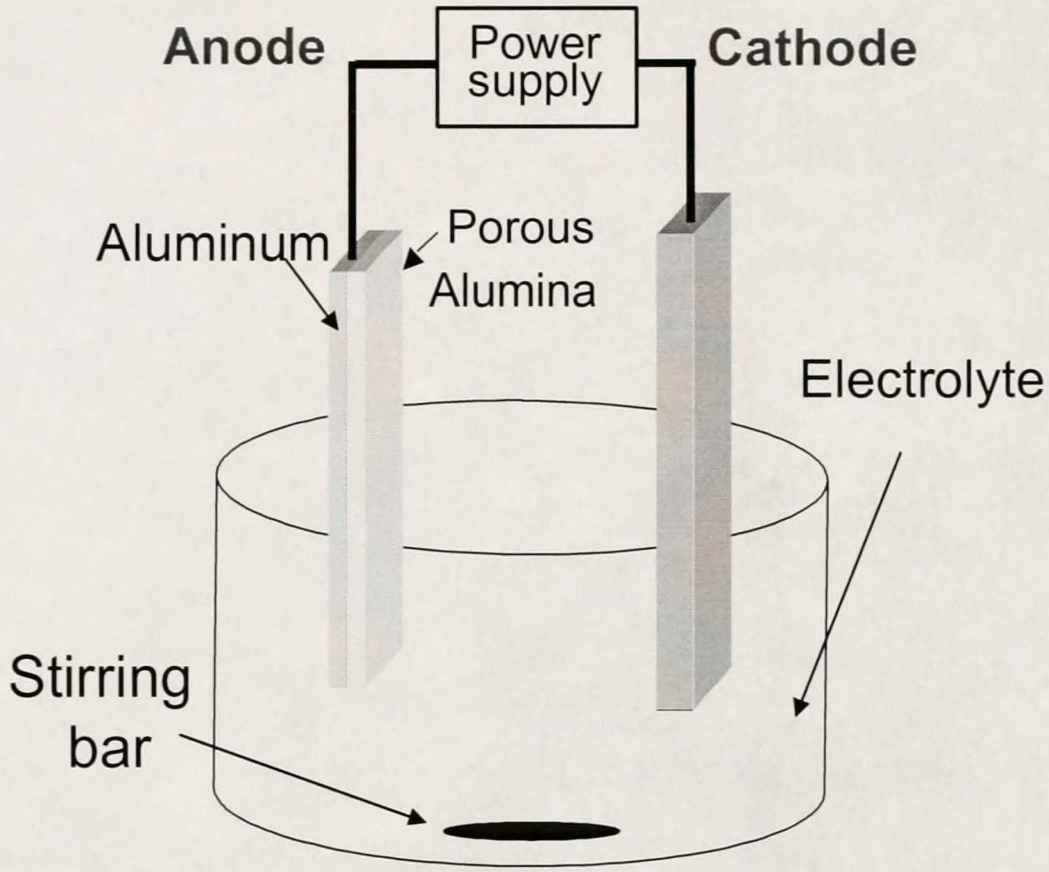


Figure 1-2. Electrochemical cell setup for alumina growth.

Thus, the formation of large pores will require lower conductivity electrolytes, such as oxalic acid. The pore diameter in the grown alumina films varies in direct proportion to the voltage applied and the concentration of the electrolyte. Figure 1-3 shows the dependence of the pore diameter on the voltage applied, when using 5% oxalic acid as electrolyte. Figure 1-4 shows the variation of the pore diameter with the concentration of

electrolyte solution, when 50 V was applied. The thickness of the formed alumina film depends on the anodization time; longer anodization times yield thicker membranes.

After the first anodization, alumina film is removed in a solution which is 0.4 M in phosphoric acid and 0.2 M in chromic oxide at $60^0$C. The removal of alumina film leaves behind aluminum with a hexagonal scalloped pattern, due to the self-organizing into a hexagonal arrays of the pores during the anodization (50). That is, the removal of the alumina leaves indentations, or pits, in the aluminum that correspond to each pore.

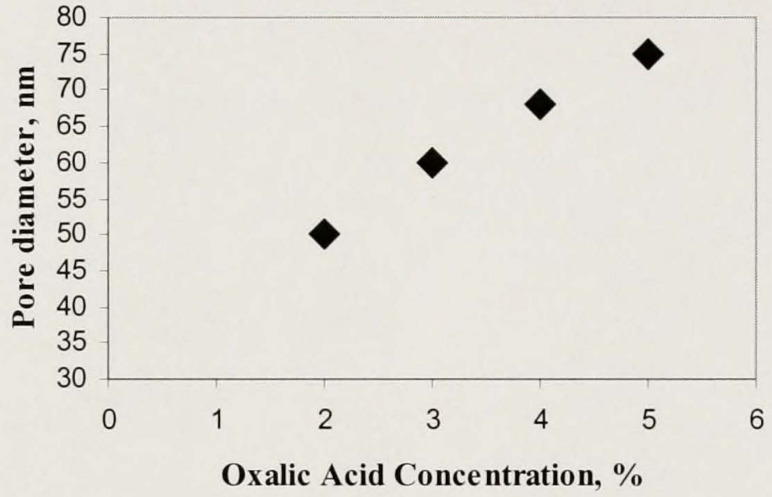


Figure 1-3. Variation of pore diameter with applied voltage.

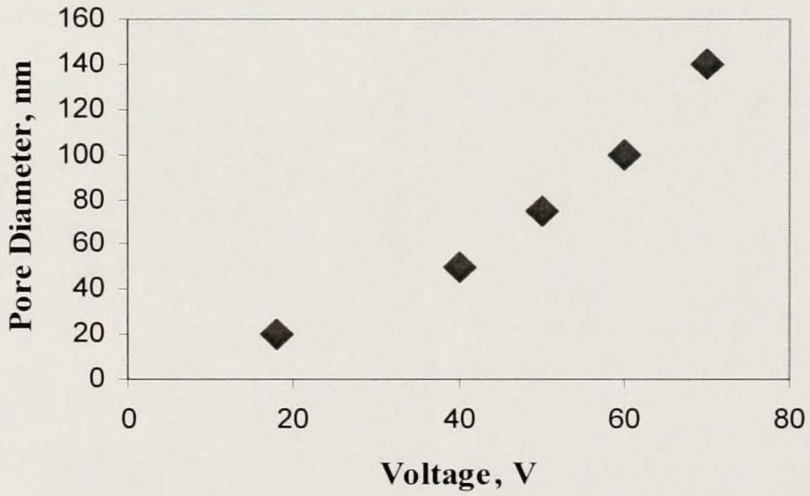


Figure 1-4. Variation of pore diameter with electrolyte concentration.

To obtain this pattern on aluminum, the duration of the anodization process must at least 12 hours.

The pre-patterned aluminum is then re-anodized in exactly the same conditions, which were used in the first anodization step. The pores nucleate in the pits which are already highly ordered and monodisperse (52). The second anodization step is carried out for a length of time, depending on the thickness of alumina membranes desired. In our laboratory, we obtained alumina membranes of thicknesses between 0.3 and 150 μm.

**Detaching.** After the second anodization step, alumina can be detached from the unoxidized aluminum by two methods. One method utilizes dissolving the aluminum in a saturated solution of $HgCl_2$. One side of the formed alumina membrane, which faced during the growth the electrolyte solution has open pores while pores on the other side are closed (60). The two sides are called "solution" and "barrier" side, respectively. Figure 1-5 shows the scanning electron micrographs of the solution side and barrier side of an alumina membrane obtained in our laboratory.

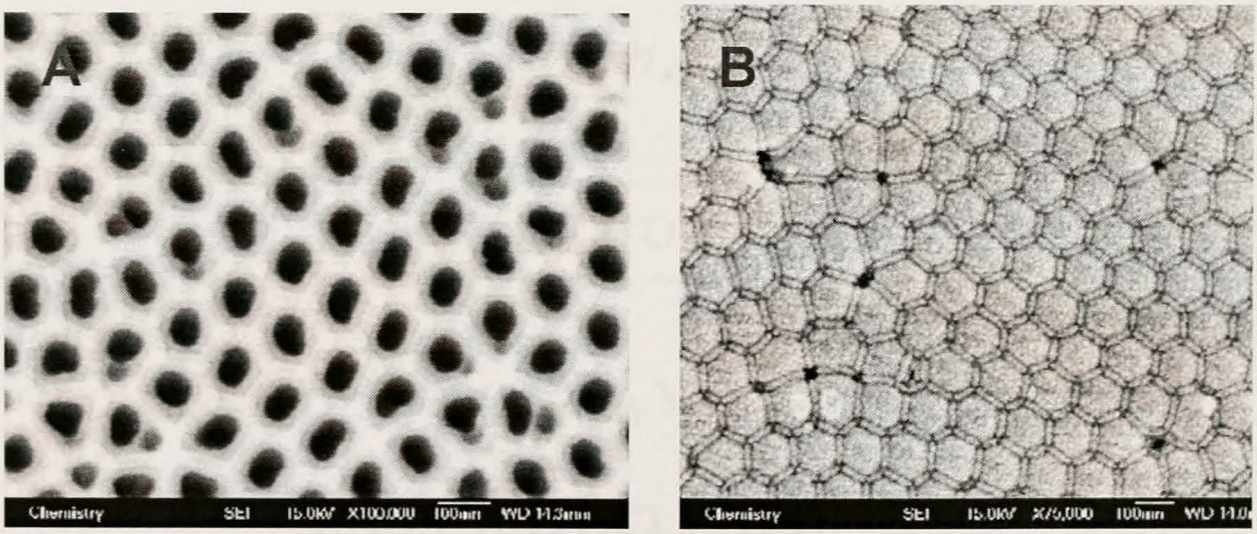


Figure 1-5. Scanning electron micrographs of (A) solution side and (B) barrier side of an alumina membrane formed at 50 V in 5% oxalic acid.

This barrier layer can be removed by etching of alumina films for very short time in dilute acid or basic solutions. The second method for detaching the alumina films is known as the "voltage reduction process" (61). This process uses a progressive reduction of the applied voltage until it reaches 4-5% from the initial value. Because the pore diameter is directly proportional to the voltage applied, the resulting pores branch down to smaller sizes. The anodization is then stopped and the aluminum/alumina system is placed into an etching solution, which can be a dilute acidic or basic solution. The thin barrier layer and the small pores dissolve faster, resulting in detachment of the alumina from the aluminum.

In our laboratory, using two-step anodization method, we obtained highly ordered, porous alumina membranes. The pores are very uniform throughout the whole thickness of the membrane, as can be seen in Figure 1-6.

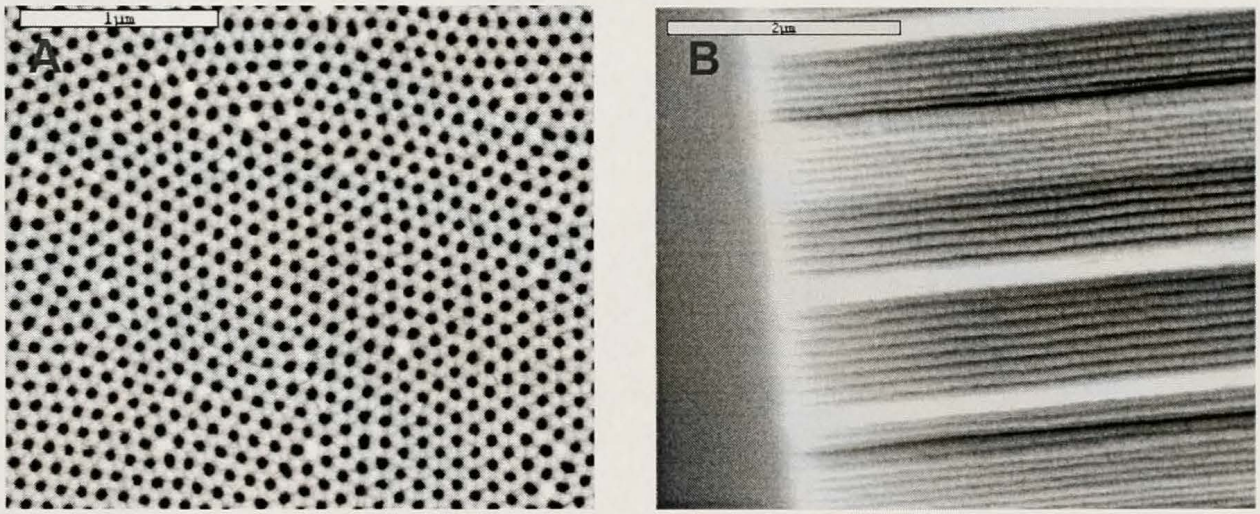


Figure 1-6. Scanning electron micrographs of (A) surface and (B) cross-section of an alumina membrane obtained at 50 V in 5% oxalic acid.

Alumina membranes with pore diameters of 200 nm are commercially available from Whatman International. Pores of 100 nm and 20 nm in diameter are also available, and all the membranes have a thickness of 60 μm. For diameters of 20 and 100 nm, only

on one side the pores have these diameters on a length of 200 nm; on the other side the membranes have pore with 200 nm in diameter. Figure 1-7 shows scanning electron micrographs of the (A) surface and (B) cross-section of a commercially available alumina membrane with a pore diameter of 200 nm. Compared to the home-grown membranes (Figure 1-6), these membranes have pores which are not uniformly distributed throughout the membrane and are characterized by much more heterogeneous diameter.

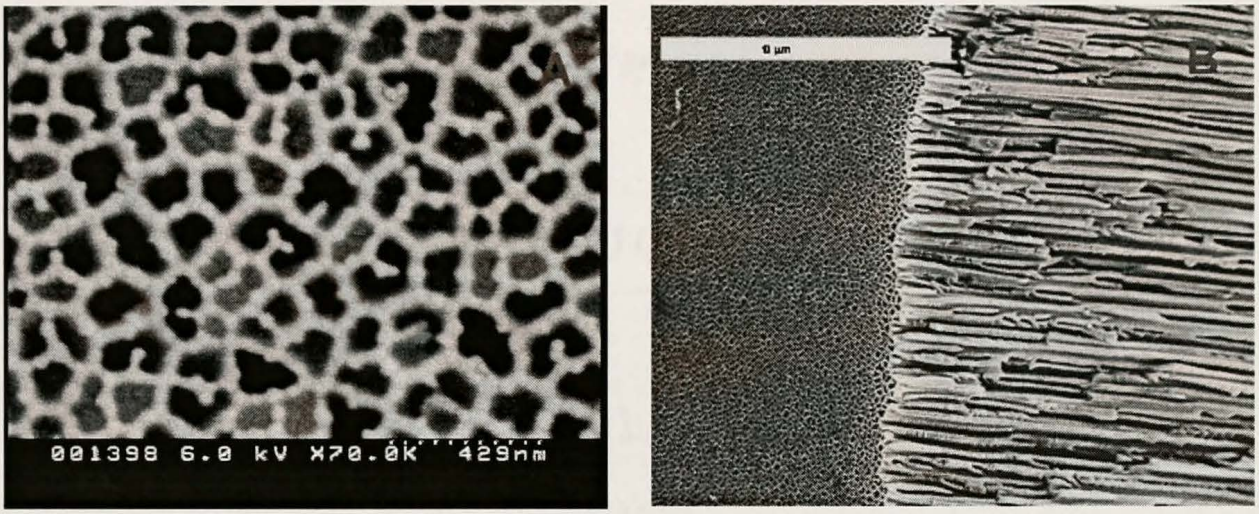


Figure 1-7. Scanning electron micrographs of (A) surface and (B) cross-section of a commercial alumina membrane (Whatman) with pore diameter of 200 nm.

**Mechanism**

The formation of a highly ordered pore array in the alumina membranes is the result of two competing processes: 1) the pore initiation process due to a geometric effect, which is called "field assisted dissolution process" (52) and 2) the self-organization of the pores which is thought to be driven by mechanical stress at the alumina/aluminum interface (62).

In the pore initiation process, the alumina film developed at the metal-film-electrolyte interface, at preferred sites (small pits or defects), undergoes dissolution, assisted by the electric field. At these sites, a local increase in field strength takes place. Interaction with the electrolyte results in the development of penetration paths from the

outer film surface, which are the precursors of the pores. Field-assisted dissolution effectively polarizes the Al-O bonds, allowing more $Al^{3+}$ dissolution than in the absence of the field. As a consequence of the pore development, the electric field and the ionic current become concentrated in the barrier layer beneath the major pores. This implies continued migration of the $O^{2-}/OH^-$ ions from the electrolyte to form a solid film at the metal-film interface and corresponding $Al^{3+}$ ejection at the pore base-electrolyte interface as well as field-assisted dissolution of $Al^{3+}$ ions (59). This mechanism of pore nucleation is illustrated schematically in Figure 1-8.

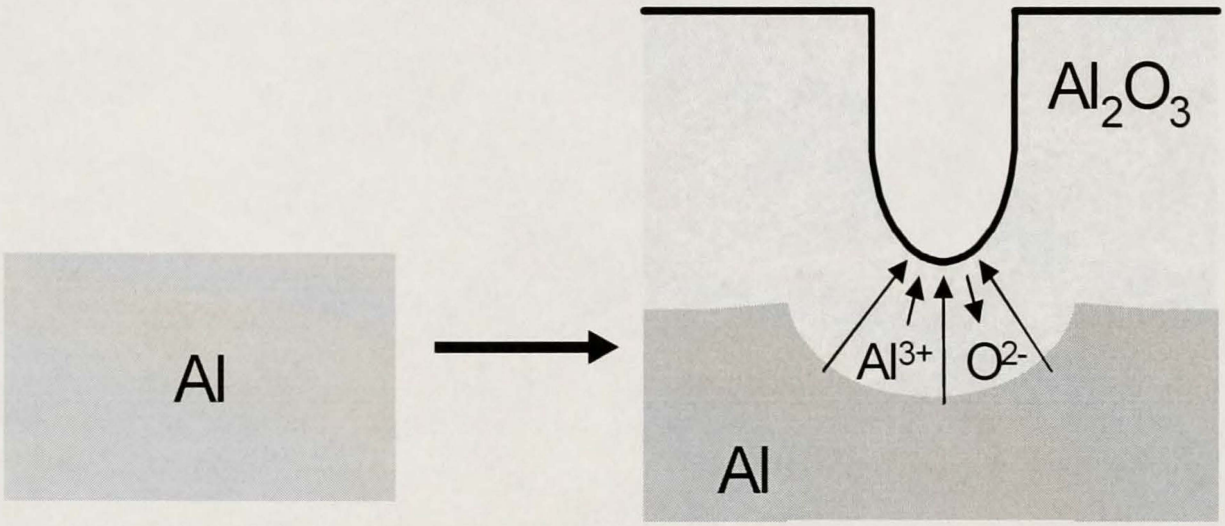


Figure 1-8. Schematic representation of the pore formation in the porous alumina film.

The pore initiation process is followed by a steady-state film formation. In this state, there is a dynamic equilibrium between film growth at the metal-film interface and field-assisted dissolution at the pore base-electrolyte. The mechanical stress, a possible origin of repulsive forces between neighboring pores, is associated with the expansion of the aluminum during oxide formation (62). This leads to the self-organization of the pores.

**Applications of alumina membranes**

Due to the packed array of columnar hexagonal cells with cylindrical, uniformly sized pores, porous alumina membranes have been used to fabricate many types of nanocomposites using the template synthesis method. For instance, template pores were filled with metals or semiconductors used for the preparation of magnetic recording media (63,64), optical devices (65), functional electrodes (66,67), electrochromic (68), and electroluminescence display devices (69,70). The outside diameter of the nanocomposites is determined by the pore diameter of the membranes, and the length of the nanocomposites is controlled by the thickness of the membranes. Natan and co-workers synthesized submicrometer metallic barcodes by alternating Au and Ag segments along the length of a nanowire (71). For sensing and nanoelectrode applications, the nanowires can remain in the template and function as an array. For single-nanowire applications, removing the template produces individual nanowires that can be isolated. Porous alumina has also been used as a template to make Au, Ni and Si nanoring arrays by a sputtering redeposition method (72).

The channels of alumina membranes were used to produce a new kind of artificial lipid membrane system. In this system, lipid bilayers were immobilized on the surface (73) and inside of the pores of the membranes (74), creating a platform with potential applications for biosensing.

Porous alumina membranes were also used as a support to incorporate metal clusters, or colloid particles (75). This opens the way to new applications, such as chemical complexation inside the membranes of radioactive organo-metallic compounds for possible clinical use or for catalytic studies.

Lahav et. al. reported a procedure to make metal "nanoparticles nanotubes" that combines nanotube geometry with nanoparticle morphology and properties (76).

When the alumina membranes are used as templates to make nanotubes, an important issue is controlling the inside diameter of the formed nanotubes. This problem has been approached by the layer-by-layer film deposition process. In this method, films of materials are deposited layer-by-layer on the pore walls of the membranes to make nanotubes. The resulting inner diameter of the nanotubes is dictated by the thickness and the number of film layers deposited. Using this method, Ai, et al. deposited layers of polyelectrolytes (77). Kovtyukhova et al. have also used a method based on alternate SiCl4/H20 deposition cycles to make silica nanotubes (78), and Hou, et al. used Mallouk's alternating α,ω-diorganophosphonate/Zr chemistry (79) to prepare nanotubes within the pores of alumina template membranes (80).

Highly selective silica nanotube membranes can be used as both sensors and as molecular filters (81,82,83). A sol-gel template method was used to prepare the silica nanotube membranes (84). In the next section, a detailed review of the chemistry involved is presented.

Two applications of the silica nanotube membranes are their use for biological extraction and for biocatalysis. In this procedure, silica nanotubes were removed from the membrane by dissolving the template, and collected by filtration. They were functionalized with octadecyl silane on the inside, resulting into a hydrophobic nanotube interior, while the outside was left unfunctionalized, giving an hydrophilic nanotube exterior. These hydrophilic/hydrophobic nanotubes were used successfully to extract lipophilic compounds from aqueous solution. The tubes were added to an aqueous

solution of 7,8-benzoquinoline, a lipophilic compound that preferentially entered the hydrophobic interior of the tubes. In this way, more than 90% of the compound was removed from the solution (81). In the same work, Mitchell et al. showed that enantiomers of a drug can be separated using a suspension of nanotubes (81). In this case the nanotubes were functionalized with an antibody that binds the RS isomer of the drug over the SR isomer. These nanotubes successfully extracted 75% of the RS isomer from a 20 μM racemic mixture, and all of the RS isomer from a 10μM racemic mixture.

Another application of the silica nanotube membranes is their use in bioseparation. Lee and co-workers also looked at the separation of RS and SR enantiomers of a drug (82). In this case, the membrane was not removed, and the silica nanotube membranes were modified again with an antibody that selectively binds the RS isomer. They found that these membranes facilitate the transport of the RS enantiomer, as the RS flux was twice the SR flux, for nanotubes with an inner diameter of 35 nm. It was also shown that the binding affinity of RS over SR could be tuned by addition of DMSO to the protein buffer solution, leading to an optimal DMSO concentration that maximized the selectivity. The selectivity could be further enhanced by decreasing the silica nanotube diameter, yielding a selectivity of 4.5 when the nanotube diameter was 20 nm.

Yamaguchi and co-workers have reported a method to form a hybrid membrane composed of silica–surfactant nanocomposites inside a porous alumina membrane, which functions as a nanometer-order size-exclusive separation (83). In this work, they added a precursor solution of TEOS (tetraethoxyortosilicate) and CTAB (cetyltrimethylammonium bromide) to the alumina membranes, resulting in the deposition of silica-surfactant nanocomposites into the porous alumina membranes. They

were able to separate two small protein molecules, myoglobin and bovine serum albumin, (diameter $\geq$ 4 nm) from two other smaller molecules, rhodamine B and vitamin B12, (diameter $\leq$ 2.4 nm).

Nanorods made in alumina membranes were used as gene delivery systems (85). Leong and co-workers fabricated nickel-gold nanorods by template electrodeposition in alumina membranes. Transferrin, an iron transport protein, was bound to the Au segments by a thiol linkage. They served to promote cellular uptake of the rods by a receptor mediated pathway. The Ni portions were functionalized with DNA plasmid that contained a fluorescent reporter gene. They showed that the nanorods were internalized by the cell, but they did not enter to the nucleus. These nanorods have two functions, one to target the cells and to deliver the DNA. In the nucleus, green fluorescence was observed, indicating the delivery of the reporter gene into the nucleus.

Porous alumina membranes in a tubular shape were made when the aluminum to be oxidized was purchased in the form of wires or cylinders. These porous alumina tubes were used in studies of catalysis (86), and as drug delivery systems (87).

**Sol-Gel Chemistry**

Sol-gel chemistry is a powerful method to generate inorganic materials. It originated in the 1970's, as scientists attempted to find low temperature routes to glass synthesis (88,89). The high temperatures (1300 to 2000$^0$C) needed to form glass are a result of the need to destroy the crystallinity of the precursors; that is, even the glass is an amorphous material, it is generally made from crystalline oxide precursors. As a result, a method to use noncrystalline precursors was searched for. It was found that liquid alkoxysilanes hydrolyze readily in the presence of water to form silanols by the following process:

$$R'_3Si-O-R+H_2O \rightarrow R'_3Si-O-H+R-OH \quad (1\text{-}3)$$

The silanols than can undergo further polymerization reactions with another silanols or other alkoxysilanes:

$$R'_3Si-O-H+H-O-SiR'_3 \rightarrow R'_3Si-O-SiR'_3+H_2O \quad (1\text{-}4)$$

$$R'_3Si-O-H+R-O-SiR'_3 \rightarrow R'_3Si-O-SiR'_3+R-OH \quad (1\text{-}5)$$

In both cases, the result is formation of a three-dimensional siloxane network. At the start of the polymerization, many small siloxanes particles are formed. They are very well dispersed in the liquid phase and form colloids. When the particles are well isolated from each other, the density of the suspension resembles that of the solvent. At this stage, the colloidal form is called a "sol". As polymerization continues, the particles increase in size and the viscosity of the solution increases. The particles develop a three-dimensional network throughout the solution, which is named a "gel" (90). Temperature, solution pH, water concentration and the type of the alkyl group are parameters that influence the rate of hydrolysis and polymerization (91). The rate of gelation increases with the temperature. The hydrolysis reaction is very slow and entails the replacement of alkoxy groups with hydroxyl groups. It is much faster when the reactions are either acid or base catalyzed (92). A larger, more sterically bulky alkyl group slows down the reaction rate (92).

There are two ways of converting gels to silica. In the first method, the gel is heated or placed under vacuum to remove the solvent phase. The open three-dimensional structure collapses, condensing it into a dense phase called a xerogel (91). In the second method, the liquid is eliminated by a critical-point drying procedure, forming a porous

material, called an aerogel (93). The maximum temperature for both processes can be kept below $100^0$C.

**Silane Chemistry**

Siliceous surfaces (e.g. silicates and aluminates) can be derivatized with a large variety of different functional groups using silane chemistry. Organosilanes form covalent bonding with these surfaces (94). The general formula of an organosilane is $R_nSiX_{(4-n)}$, where X is a hydrolyzable group capable of forming strong covalent bonds with the hydroxyl groups on silica surfaces such as halogen, alkoxy or aciloxy. The R group is a nonhydrolyzable group that may posses a desired functionality (95). The two most used types of organosilanes for surface modification are chlorosilanes and alkoxysilanes. The attachment chemistry of both types is equivalent because when the chlorosilanes are dissolved in alcohol, they react with the alcohol to form alkoxysilanes:

$$R_3^{'}Si-Cl+R\text{-}O\text{-}H \rightarrow R_3^{'}Si-O\text{-}R+HCl \qquad (1\text{-}6)$$

The extent of this reaction can be monitored by measuring the pH. Alkoxysilane chemistry is analogous to the sol-gel formation chemistry. Silanes with one hydrolyzable group can be utilized to produce monolayers on the surfaces. Because there is only one reactive group, the silanes can either bind to the surface or dimerize. Dimers cannot bind further and can be washed away. The silanes with one hydrolyzable group yield to hydrophobic surfaces (95). When surfaces with a higher degree of coverage are desired, silanes with two or three hydrolyzable groups are used. These are first allowed to oligomerize in a slightly aqueous alcohol solution (water content is typically 5% vol/vol) in order to initiate the formation of silanols (hydrolysis step) (94). The pH is adjusted between 5 and 5.5 with acetic acid to further facilitate the substitution reaction of the

alkoxysilanes (94). The surface to be modified is than added to this solution and the oligomers bind to the surface through the surface hydroxyl groups (coupling step). Figure 1-9 shows the reactions involved in the hydrolysis and coupling steps. Surface modification by this route requires only a few minutes of immersion. If a 2% of trialcoxy- or trichlorosilane solution is used, the resulting modified surface is normally 3-8 monolayers thick (95).

The silanized surfaces must be cured usually at $120^0$C for 30 minutes, or for 24 hours at room temperature.

Chlorosilanes can also be deposited from aprotic solvents, such as toluene and tetrahydrofuran (94). If these solvents are anhydrous (and the surface is free of water), then no alkoxysilane can be formed, and no polymerization of the silanes can take place. The reaction must proceed by the nucleophilic attack from surface hydroxyl sites, and as a result, only one monolayer can be formed (94). Surface modification in these cases takes longer time, usually 12-24 hours.

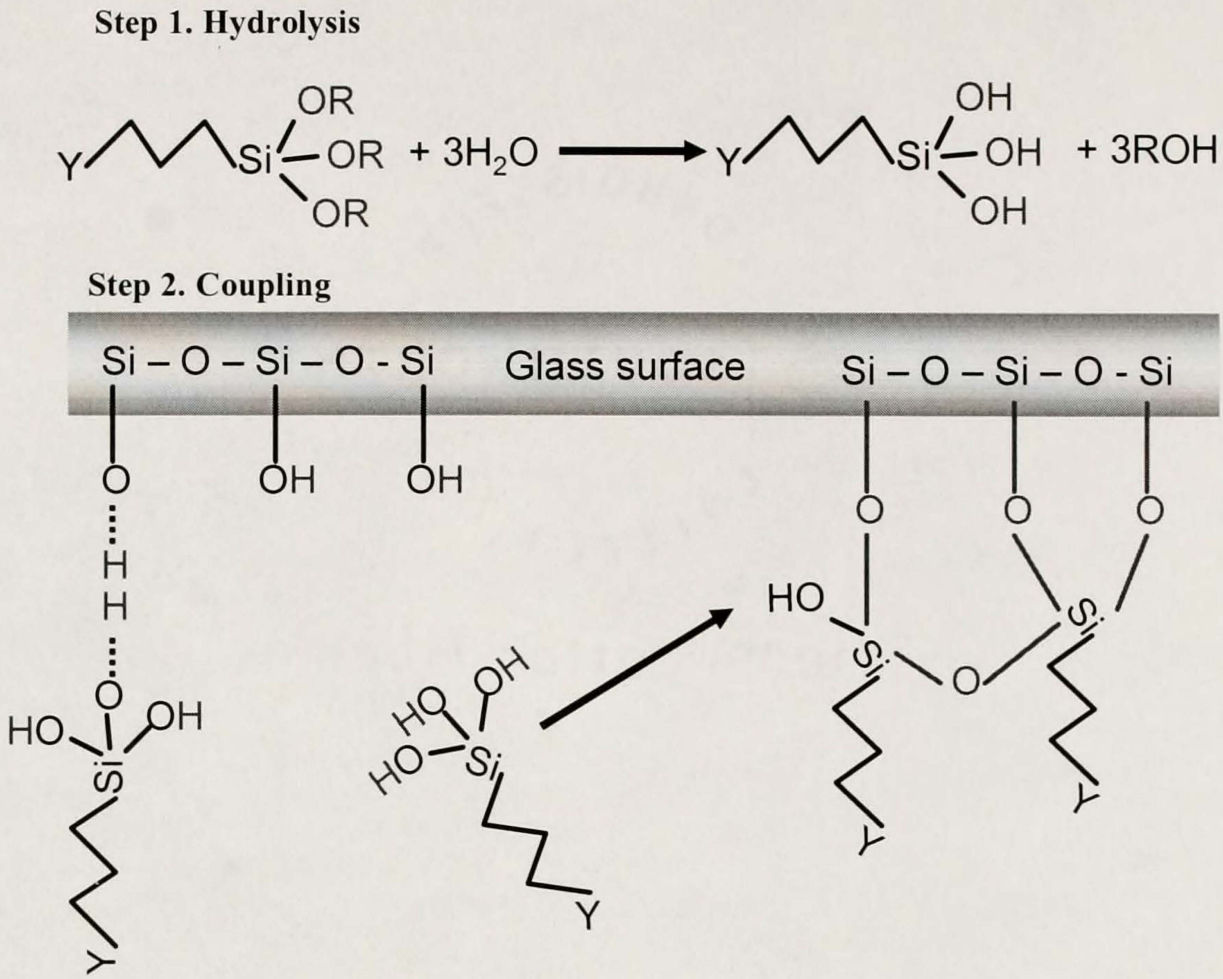


Figure 1-9 Steps involved in the silane chemistry.

**Carrier Facilitated Transport**

In biological systems, the simplest mechanism by which molecules pass through a plasma membrane is *passive diffusion* (116). During the passive diffusion, a molecule simply dissolves in the lipid bilayer, diffuses across it and passes to the other side of the membrane. Larger, uncharged, polar molecules, such as glucose, and charged molecules of any size, like small ions $K^+$, $Na^+$, $Cl^-$, are unable to cross the plasma membrane by passive diffusion. Their passage through the membrane is mediated by proteins that enable the transport of molecules and ions through the plasma membrane without interacting with its hydrophobic interior (116). There are two classes of proteins that mediate the facilitated diffusion of molecules: carrier proteins and channel proteins.

Carrier proteins bind specific some molecules that are transported. They then undergo conformational change that allows molecules to pass to the other side of the membrane. Channel proteins form open pores through the membrane, allowing free diffusion of any molecule of the appropriate size and charge. In biological systems, this phenomenon is called facilitated diffusion.

By the 1950's, scientists started to develop synthetic analogs of natural systems that function on the base of facilitated transport concept. Facilitated transport that uses a chemical complexing agent immobilized into a synthetic membrane has been the subject of numerous articles (96-104). Facilitated transport was accomplished in liquid membranes, in which two aqueous phases were separated by an organic solvent containing carrier molecules, such as crown ethers. Diffusion of metal ions in liquid membranes is governed by the complex formation with the carrier at the aqueous/organic interface and the selectivities are generally very high. The fluxes in the membranes are very low because they are limited by the convection of the carrier in the organic phase (104). The biggest disadvantages of using liquid membranes are the low fluxes, the leaching of the carrier and the poor physical stability. These problems have prevented wide-scale application of liquid membranes in industrial separations.

Polymeric facilitated transport has been applied more recently to eliminate liquid loss. Tsuchida and co-workers have published results based on various metalloporphyrins cast into polymer films for selective $O_2$ transport (105,106) and $N_2$ transport (107). Yoshikawa et al. described $CO_2$ transport in these fixed site carrier membranes (108). Polymeric facilitated membranes have been applied also to ion separations. For instance, polymer inclusion membranes containing crown ether carriers were used to separate

potassium from sodium and rubidium (97), and potassium from lithium (101). Facilitated transport of metal ions resulted in good selectivity with marked improvement in membrane stability as compared to liquid membranes. Some other applications include transport and separation of ethane and ethane through Nafion membranes (109), olefin (110) and small carbohydrate separation (111).

The first facilitated transport-based system described was that of Scholander (112), who showed that oxygen diffusion through a filter paper membrane containing a hemoglobin solution was enhanced. Oxygen diffusion through a membrane that has been soaked in methemoglobin, which has no carrier-oxygen binding capacity, showed the same low diffusion rate that would be expected for simple diffusion of oxygen through water. However, in the presence of hemoglobin an additional amount of oxygen is carried through the membrane due to the hemoglobin-oxygen complex formed in the membrane (113). The increase in oxygen transport due to the action of hemoglobin as a carrier is termed the "facilitation effect" (114). Figure 1-10 shows a typical nonlinear flux pattern for carrier-mediated facilitated diffusion.

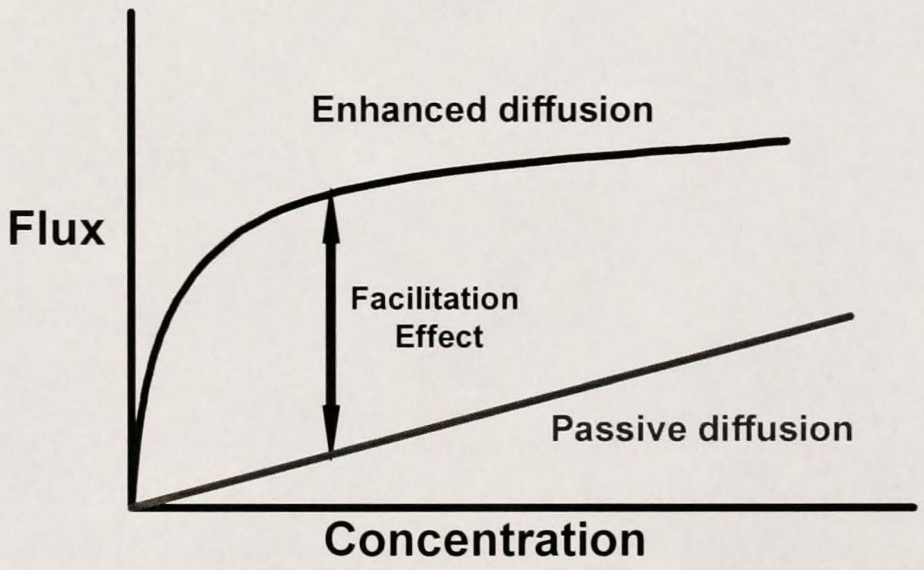


Figure 1-10. Typical nonlinear flux pattern for carrier-mediated diffusion.

As can be seen in Figure 1-10, facilitated diffusion occurs at low concentration of feed solution. Facilitation effect reaches a maximum value due to the saturation of carrier molecules which binds the analyte (115). The basic mechanism for this enhanced transport is a reversible reaction (see equation 1-7) between an analyte molecule A, which can enter the membrane phase, with a carrier B, which is immobilized on the membrane (114).

$$A + B \Leftrightarrow AB \qquad (1\text{-}7)$$

In this process, both the chemical reaction and diffusion occur simultaneously in the system, resulting in an accelerating transport of the permeate species, A, through the membrane.

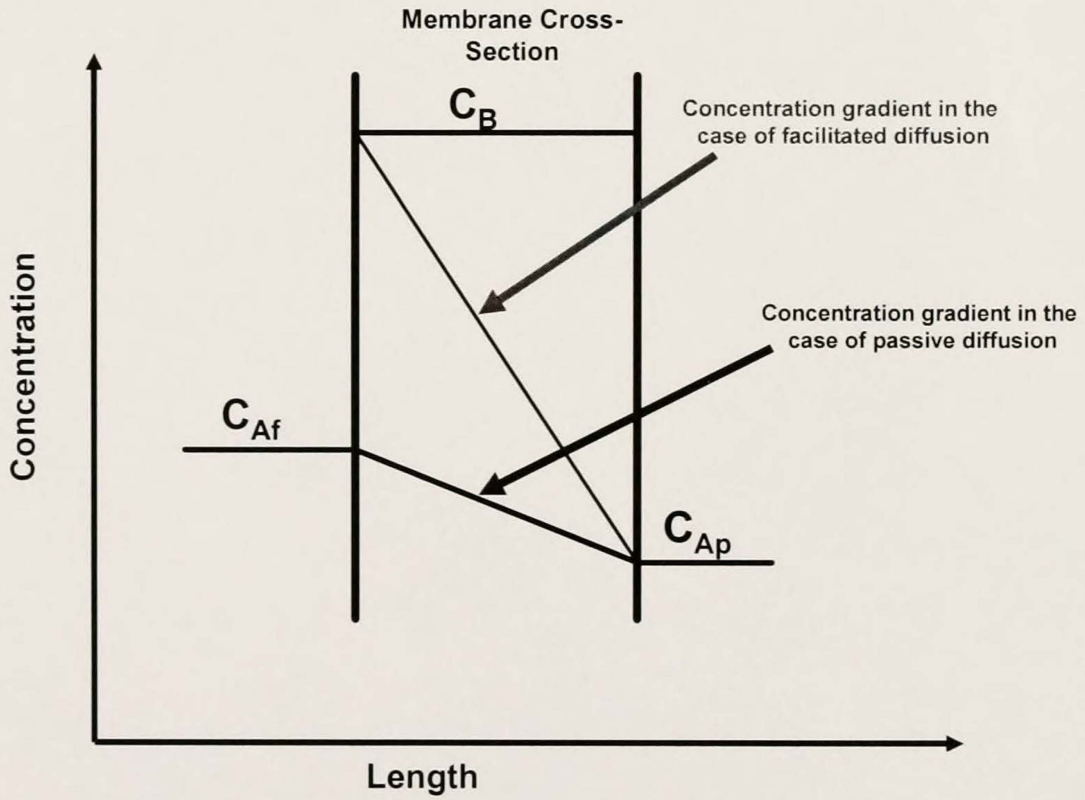


Figure 1-11. Schematic representation of how facilitated transport works.

A schematic explanation of how facilitated transport works is shown in Figure 1-11, where $C_{Af}$ represents the concentration of the permeant A in the feed side, $C_B$ is the

concentration of the immobilized carrier and $C_{Ap}$ is the concentration of the permeant A in the permeate side. According to Fick's first law of diffusion, the flux of a permeate molecule across a membrane is directly proportional to the concentration gradient across the membrane. One-dimensional representation of the Fick's law (see equation 1-8) has the following form:

$$J = -D\frac{\partial C}{\partial x} \qquad (1\text{-}8)$$

In equation 1-8, $J$ represents the flux, $D$ is diffusion coefficient and $\frac{\partial C}{\partial x}$ represents concentration gradient of a permeate molecule across the membrane. Inside the membrane the concentration of the immobilized carrier is higher than the concentration of the permeate molecule in the feed side. Due to that the concentration gradient for the permeate molecule that react with the carrier is higher than the concentration gradient of a permeate molecule that does not interact with the carrier and is transported by passive diffusion. This results in an enhanced flux of molecules that interact with the carrier, compared with those that do not interact.

**Single Pore Polymeric Membranes**

Ion channels and pores are crucial for functioning of a living organism (116,117). Channels and pores are the principal nanodevices mediating the communication of a cell with other cells where ion channels serve as extremely sensitive electromechanical devices that regulate electric potential, ionic flow, and molecular transport across cellular membranes (116). Emulating the function and structure of these natural nanodevices would be very helpful in designing new types of biosensors and understanding the ion transport through nanopores.

It has been shown that a protein nanopore (e.g.,the α-hemolysin channel), which is embedded into a lipid bilayer membrane, can function as a biosensor for biomolecules, for example, DNA (118). The sensing procedure is based on directing the biomolecule to the pore by means of an electric field. When passing through the pore, a biomolecule brings about its temporary blockage, which is observed as a change in the ion current signal. The ion current blockade depends on the structure and chemistry of the biomolecule (e.g., the DNA sequence) (118), which is the basis of its detection. This biological pore is however quite fragile. A more realistic approach to applying this idea on an industrial scale would involve replacing the protein channel with a durable, synthetic nanopore. Recent research has shown that a single conical-shaped pore generated in a polymeric foil presents similar transport properties to those of natural biological channels (119-123). In these studies, they have prepared model nanoporous systems of known geometry and chemistry to study the relationship between the structure and transport properties of nanopores, as well as, creating abiotic analogues of biological channels. Such an approach enables one to focus on the basic physical and chemical phenomena underlying biochannels function.

A special emphasize was given to the family of voltage-gated channels. Ion current rectification and the dependence of ion current fluctuations on voltage across the membrane are fingerprints of this type of channel (117). The synthetic pores studied were prepared by the track-etch technique. This technique is based on irradiation a polymer foil with swift heavy ions and subsequent chemical development of the latent tracks (37). What differentiates the track etching technique from conventional lithographic methods is the single-particle exposure. It is one swift heavy ion, which

penetrates the foil and produces one latent track (37). Subsequently, one latent track after chemical development results in the formation of one pore. Counting the number of ions, which penetrate the foil gives a possibility to prepare membranes with a designed number of pores. Controlling the irradiation down to one ion enables preparing a macroscopic sample containing just one pore. The Department of Materials Research, GSI Darmstadt, possesses a unique world wide facility suitable for single-ion irradiation (37). A membrane with a single pore creates an optimal system for fundamental studies of ion transport through nanopores, because averaging effects resulting from ion transport through many pores can be avoided.

To prepare voltage-gated nanopores, an asymmetric pore geometry has been used, because it was found that biological voltage-gated channels are asymmetric (124-126). The conically shaped nanopores in polymer membranes were shown to rectify ion current and exhibit ion current fluctuations of similar statistical properties as the ion current through biological voltage-gated channels (119,121).

The application of a single conical gold tube membrane to protein biosensing will be presented in chapter 5. The steps involved in preparing these membranes are presented here, and are as follows:

**Irradiation with heavy ions**

Polyethylene terephthalate (PET) (Hostaphan RN12, Hoechst) and polyimide (Kapton HN50, Du Pont) foils, having a thickness of 12 μm are irradiated with single swift heavy ions at normal incidence. Figure 1-12 shows the chemical formula of PET and Kapton.

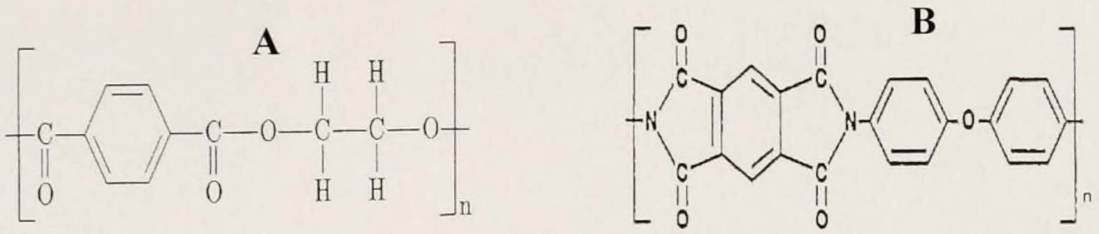


Figure 1-12. Chemical formula of the PET (A) and Kapton (B).

Gold, xenon and uranium ions of energy 11.4 MeV per nucleon are used at the linear accelerator UNILAC (GSI, Darmstadt). At this energy the penetration range of ions in PET foil is larger than the thickness of foils and the energy loss of ions along the track is well above the energy threshold, which assures a homogeneous etching (127). Single ion irradiation is performed by defocusing the ion beam and placing a metal mask with an aperture of 0.3 mm in front of the polymer foils. The ions pass through the aperture in a discrete way and as soon as one ion reaches the detector placed behind the sample, the beam is switched off by a beam chopper within several microseconds.

**Ion track etching**

Chemical etching of single-ion irradiated foils is performed in a conductivity cell, connected to a voltage source and picoamperometer (see Figure 1-13).

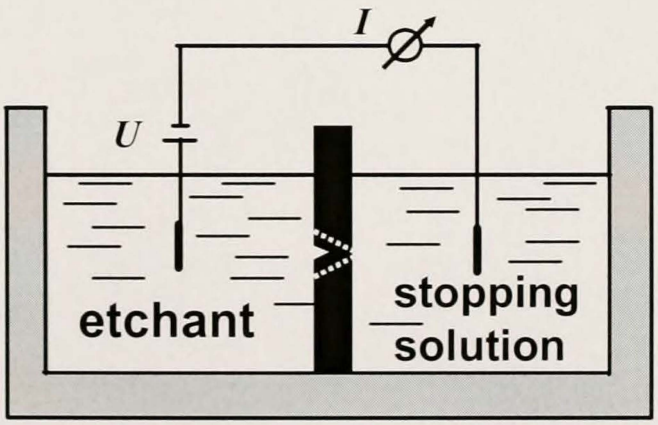


Figure 1-13. Schematic representation of a conductivity cell used for chemical etching.

To obtain conical pores, etching is performed only from one side. The other side of the membrane is protected against etching by a stopping medium, which neutralizes the etchant (121,122,128,129). For etching of PET, 9 M NaOH has been used, therefore an acidic solution plays the role of a stopping medium. Ion tracks in Kapton were developed in sodium hypochlorite with 13 % active chlorine content. A stopping medium of 1 M potassium iodide was used, which serves to reduce the $OCl^-$ ions, active in etching, to $Cl^-$ (122,129). The chemical stopping is supported by an electrical one. The platinum two electrode system is configured in a way that the anode is placed on the etching side, and the cathode is placed within the neutralizing side (128). At the very beginning of the etching process the two halves of the conductivity cell are not connected with each other and the ion current measured is zero. When the pore is etched through, the ion current increases gradually, indicating increase of the pore diameter. The etching process is stopped by washing the pore with a stopping medium and water.

The big opening of the pore, *D,* has been determined by scanning electron microscopy. For conical pores in PET, $D \sim 600$ nm and for pores in Kapton $D \sim 2$ μm. The difference in $D$ values results from difference in non-specific etching of the two polymers, the so-called bulk etch rate, which determines the big opening of the pores (129). The small opening of the conical pores is below scanning electron microscopy resolution and its diameter $d$ was estimated by measuring a current-voltage characteristic of a single nanopore in a standard solution of 1 M KCl. Assuming an ideal conical shape of the pore its small opening can be calculated using the following equation (128,122):

$$d = \frac{4\mathrm{LI}}{\kappa\pi D\mathrm{U}} \qquad (1\text{-}9)$$

where L is the length of the pore, κ stands for the specific conductivity of the electrolyte, U denotes the voltage applied across the membrane and I is the ion current measured. This etching process gives the possibility of producing pores with an effective diameter *d* as small as 2 nm.

**Gold electroless plating**

The single conical tube membranes are obtained using a template synthesis method. Single pore membranes are electroless plated with gold (40), as described before in this chapter.

**Dissertation Overview**

The aims of the research presented in this dissertation are to investigate potential applications of the nanotube membranes in chemical and biochemical sensing and transport.

Chapter 1 provides background information on the template synthesis method and two types of templates (porous alumina and polymeric membranes) that are used in this research.

Chapter 2 presents the preparation of a biomimetic ligand-gated ion channel membrane, based on a microbattery/nanoporous system. This membrane turns on the battery and attendant ion current in the presence of a targeted chemical stimulus (a surfactant in this case). This microbattery was prepared by depositing anode and cathode materials on either side of a nanoporous alumina membrane. The pores in the membrane were made hydrophobic by reaction with an 18-carbon ($C_{18}$) alkyl silane. When placed between two salt solutions, the pores in the $C_{18}$-modified membrane are not wetted by water, (the biomimetic gate is closed) and thus the microbattery is "off". When exposed to a surfactant solution, the surfactant molecules partition into the hydrophobic

membrane causing the biomimetic gate to open, which results in a high flux of ions through the nanoporous membrane, and consequently, the microbattery turns "on". Once "on", the microbattery discharges and the discharging current is collected in an external circuit.

Chapter 3 presents silica nanotube membranes are used to prepare highly selective membranes for protein separation. Two antibodies with different affinities for hevein have been immobilized on highly ordered porous alumina membranes. Hevein was labeled with green fluorescence protein (GFP). The transport of both GFP-Hevein and red fluorescence protein (RFP) - which was used as a control analyte- has been monitored. The transport of both proteins has been recorded simultaneously at two different emission/excitation wavelengths. As a control experiment, we used membranes with an immobilized antibody that does not have any affinity towards GFP-Hevein or RFP. The alumina membranes were prepared by two step anodization method, having pore diameters between 50 and 100 nm and thickness from 40 to 200 mm. Both the influence of pore diameter and the membrane thickness on the transport of GFP-Hevein and RFP were studied. These membranes selectively transport the protein (GFP-Hevein) that binds to the antibody, relative to the other protein (RFP) that has no affinity for the antibody.

Chapter 4 explores another application of the porous alumina membranes, in this case, serving as protein microarrays. Two methods of preparing alumina-based microarrays are presented. The first method implies growing alumina membranes on a pre-patterned aluminum surface. In the other approach, commercial alumina membranes are patterned by electrodeposition of silver in certain areas. The influence of the

thickness of the membranes on the fluorescence intensity, and also the capability of these microarrays to selectively recognize different analytes were studied.

Chapter 5 deals with a new class of artificial ion channels based on a synthetic membrane that contains a single conically shaped nanotube. These nanotube-based abiotic ion channels exhibit transport properties analogues to voltage-gated biological channels. The ion current through a single nanotube fluctuates in time in a voltage-dependent manner as well as it is rectified. The membrane with a single conically shaped gold nanotube was prepared by the template method. The nanotube has a large-diameter opening of ~ 600 nm and a small-diameter opening of 2 - 5 nm. In the biosensing application, the nanotube-containing membrane is placed between the two chambers of a conductivity cell filled with an electrolyte. Electrodes present in each half-cell solution are used to apply a transmembrane potential and measure the resulting ion current through the nanotube. The internal surfaces of the nanotube are modified with a specific biochemical molecular-recognition agent (the "capture" agent, e.g., an antibody) which interacts specifically with a given biomolecule (the analyte) present in one of the contacting solution phases. The binding interaction between the nanotube-bound capture agent and the solution-phase analyte is transduced as a change in the ion current that flows through the nanotube. This new biosensing technology was demonstrated using both biotin as the capture agent and streptavidin as the analyte, and protein G as the capture agent and IgG as the analyte. The detection of a biological warfare agent (ricin) is also presented.

The results and conclusions of this dissertation are summarized in Chapter 6.

# CHAPTER 2
# ION CHANNEL MIMETIC SENSOR WITH AN ON-BOARD MICROBATTERY

## Introduction

Ion channels are the heart of many biological processes including nerve activity and muscle contraction. Channels operate by being either open or closed. There are several aspects of the channel environment which affect the channel opening (gating) such as voltage, a molecular ligand, phosphorylation, or mechanical stimulus (116). Mimicking the principles of such natural sensor system is of great importance in sensor development (130,131). One example of a natural ligand-gated ion channel is the acetylcholine-gated ion channel (132), which is closed ("off" state) in the absence of acetylcholine but opens (and supports an ion current, "on" state) when acetylcholine binds to the channel. This concept of ion-channel mimetic sensing, originally proposed by Umezawa's group (133), has been of considerable interest in analytical chemistry (134-136). In the biological channel there are no electrodes, and the ion current is driven by an electrochemical potential difference across the cell membrane (137). That is, the cell membrane has its own built-in transmembrane power supply that drives the ion current when the channel opens. Whether this power supply can be utilized in this way depends on whether the channel is open or closed.

We describe here the preparation of a biomimetic ligand-gated ion channel membrane, based on a microbattery/nanoporous system. To explore this concept we prepared hydrophobic microporous alumina membranes as before, but we deposited a

thin-film battery anode onto one face, and a thin-film battery cathode onto the opposite face, of the membrane. Hence, in analogy to the naturally occurring channel case, we have an ion-channel mimetic membrane with a built in electrochemical potential difference across the membrane. We show here that in the absence of the ligand (again, a hydrophobic ionic surfactant), the membrane is in its "off" state, and the electrochemical potential difference cannot be utilized to drive a transmembrane ion current. In contrast, when the ligand is detected, the membrane switches to its "on" state and the transmembrane battery discharges producing a corresponding transmembrane ion current.

## Experimental

### Materials

Octadecyltrimethoxysilane was obtained from Aldrich. Dodecyltrimethylammonium chloride, hexadecyltrimethylammonium chloride, dodecylbenzenesulfonic acid, and the nonionic surfactant Triton X-100 were obtained from Acros Chemicals. Octyltrimethylammonium bromide was obtained from from Fluka and N-Dodecyl-N,N-dimethyl-3-ammonio-1-propanesulfonate from Sigma. Silver powder 99.9% was obtained from Strem Chemicals and zinc powder (99.33%) from Fisher Chemicals. All chemicals were used as received. MiliQ 18-MΩ water was used for preparing all aqueous solutions. Commercial porous alumina membranes (~200 nm-diameter pores, 60 μm thick) were obtained from Whatman Inc.

### Silanization of the Alumina Membranes

A solution that was 5% (v/v) in octadecyltrimethoxysilane ($C_{18}$-silane) was prepared in ethanol; to this solution was added acetate buffer (50mM, pH=5.1) to make the solution 5 % (v/v) in this buffer. The resulting solution was stirred for 30 minutes and the alumina membrane was then immersed. After 2 hours, the membrane was removed

from the solution and rinsed with ethanol. The membrane was sonicated for 10 minutes in ethanol to remove the physisorbed silanes from the surface. The modified membrane was cured at $150^0$C in air for 20 min. The performance of the coating was assessed by measuring a contact angle of $130^0$ ($\pm 8^0$).

**Microbattery Fabrication**

As shown schematically in Figure 2-1, the anode and cathode of the battery were deposited as thin films coating the faces of the $C_{18}$-modified membrane. These films were deposited by thermal evaporation of either Zn (anode material) or Ag (precursor to cathode material) from a tungsten boat. A Denton Vacuum DV-502 vapor-phase depositor was used. The pressure inside the deposition chamber was ~10-5 Torr. Deposition time was 10 minutes for both the silver and zinc films. The Ag film was deposited first, and then a portion at the surface of this film was converted to AgCl, which acted as the cathode for the microbattery. This was accomplished by immersing the silver-coated membrane in an aqueous solution that was 0.1M in $FeCl_3$ and 0.3M in HCl. The Zn film was then deposited on the opposite face of the membrane. It is important to point out that these films are porous and are thus permeable to ions and molecule present in solution phases that contact the membrane (*vide infra*).

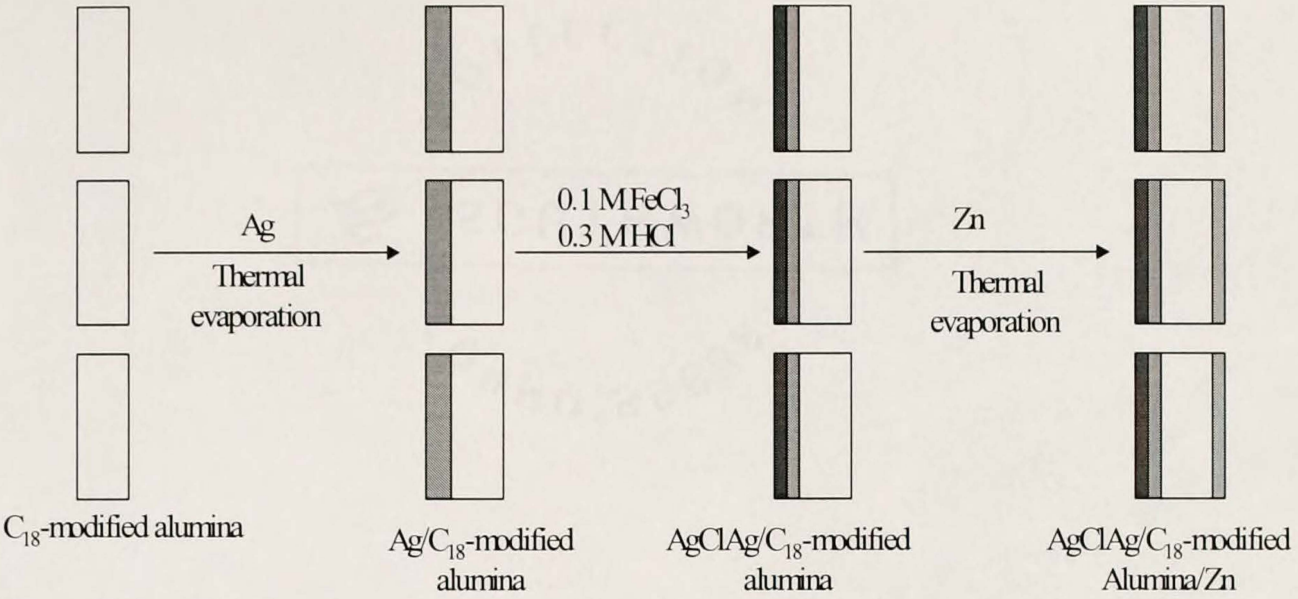


Figure 2-1. Schematic representation of the microbattery fabrication.

**Scanning Electron Microscopy (SEM)**

SEM was used to study the surface morphology of the anode and cathode films. Data were obtained using a JEOL 6400 microscope. Elemental compositions for the films were obtained using an Oxford energy dispersive spectrometer (EDS) attached to the JEOL microscope.

**Cell Assembly and Battery Discharge Measurements**

After deposition of the electrode films, the membrane was sandwiched between two pieces of Scotch tape that had 0.47 cm diameter holes punched through them. These holes defined the area of the membrane exposed to the contacting solution phases. In addition, the tape was used to attach a Pt foil lead to the surface of each battery electrode film in order to make electrical contact with the electrodes. The membrane was then mounted between the two halves of a U-tube permeation cell (31,40,43). Figure 2-2 shows a schematic representation of a U-tube permeation cell. The electrolyte solution used in both half-cells was 0.1 M NaCl. As noted above, surfactants were used as the ligand or chemical stimulus to turn the transmembrane microbattery from "off" to "on."

This was accomplished by injecting the desired volume of a stock surfactant solution into the 0.1 M NaCl in both half-cells. The surfactant solutions were also 0.1 M in NaCl. The battery discharge current was monitored using a potentiostat (EG&G model 273) interfaced to a PC running CorrView and CorrWare software packages (Scribner Associates, Inc., Southern Pines, North Carolina).

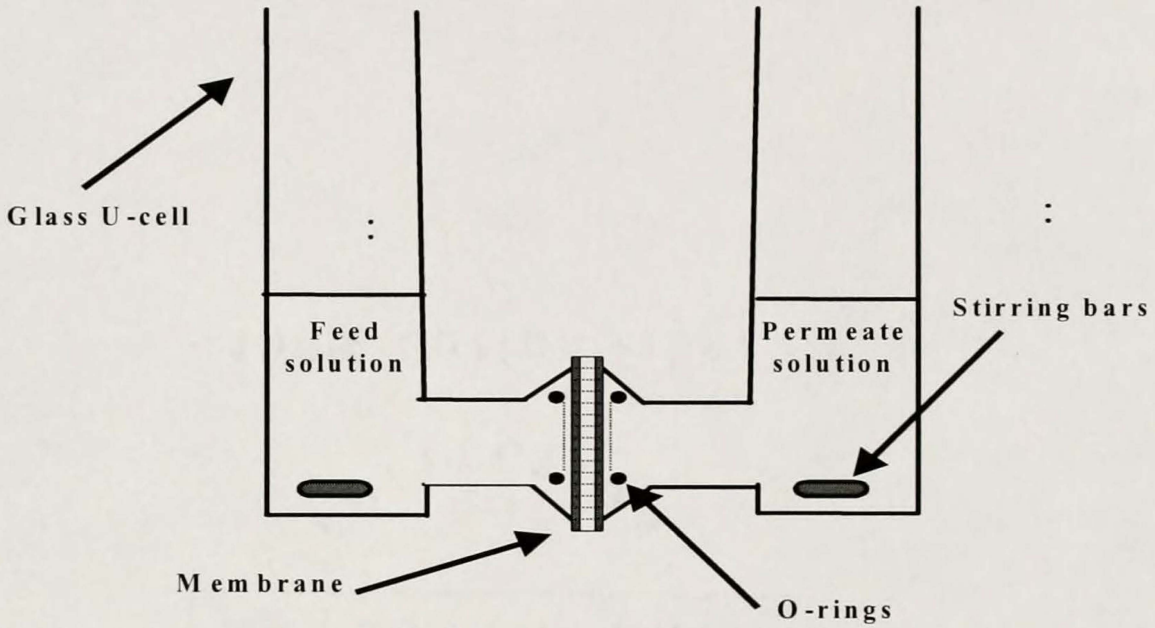


Figure 2-2. Schematic representation of a U-tube permeation cell.

## Results and Discussions

### Characterization of the Electrode Films

Surface and cross-sectional SEM images (Figure 2-3) show that both the Ag/AgCl and the Zn thin films are porous. This porosity results because the films are deposited as particles. The cross-sectional images indicate that these particulate films are ~500 nm thick, and that deposition does not propagate down into the pores. (The particles seen in the pores in the cross-sectional images were dislodged from the surface films during fracture of the membrane.)

EDS spectra for the Ag, Ag/AgCl and Zn films are shown in Figure 2-4. The Ag film (Figure 2-4 A) shows prominent peaks for Ag and Au; the Au peak results because the surface of the film was sputtered with Au prior to taking the SEM image. Much weaker signals are observed for Cu (from the Cu foil tape used to attach the sample to the SEM stub) and Al and O (from the underlying alumina membrane). The upper surface of the Ag film was chemically oxidized to AgCl, which served as the cathode for the transmembrane microbattery.

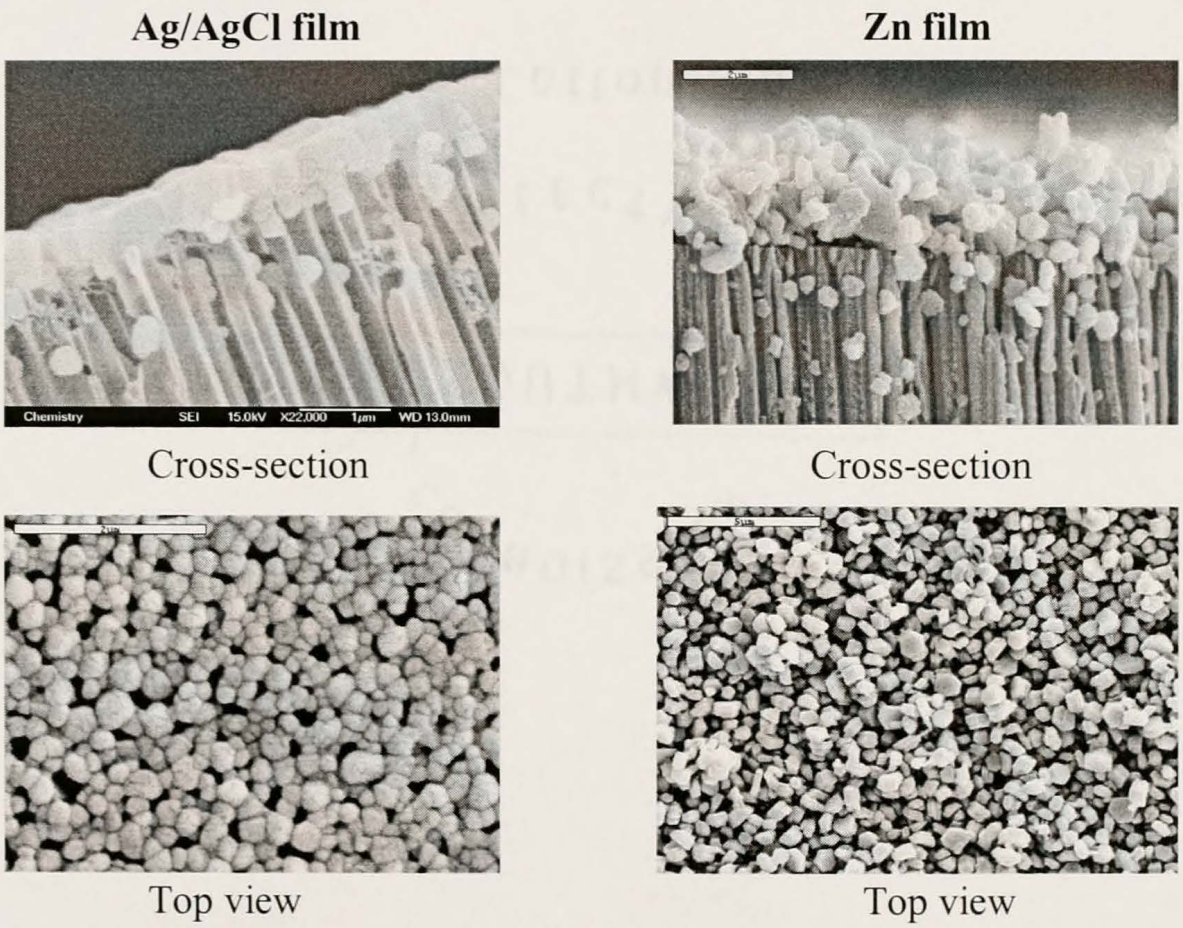


Figure 2-3. Cross-sectional (upper) and surface (lower) SEM images of the battery electrode films that coat the faces of the alumina membrane.

After oxidation a prominent Cl peak is observed in the EDS spectrum (Figure 2-4 B). The Zn film shows prominent peaks for Zn and Au and much weaker Al, Cu, and O (Figure 2-4 C).

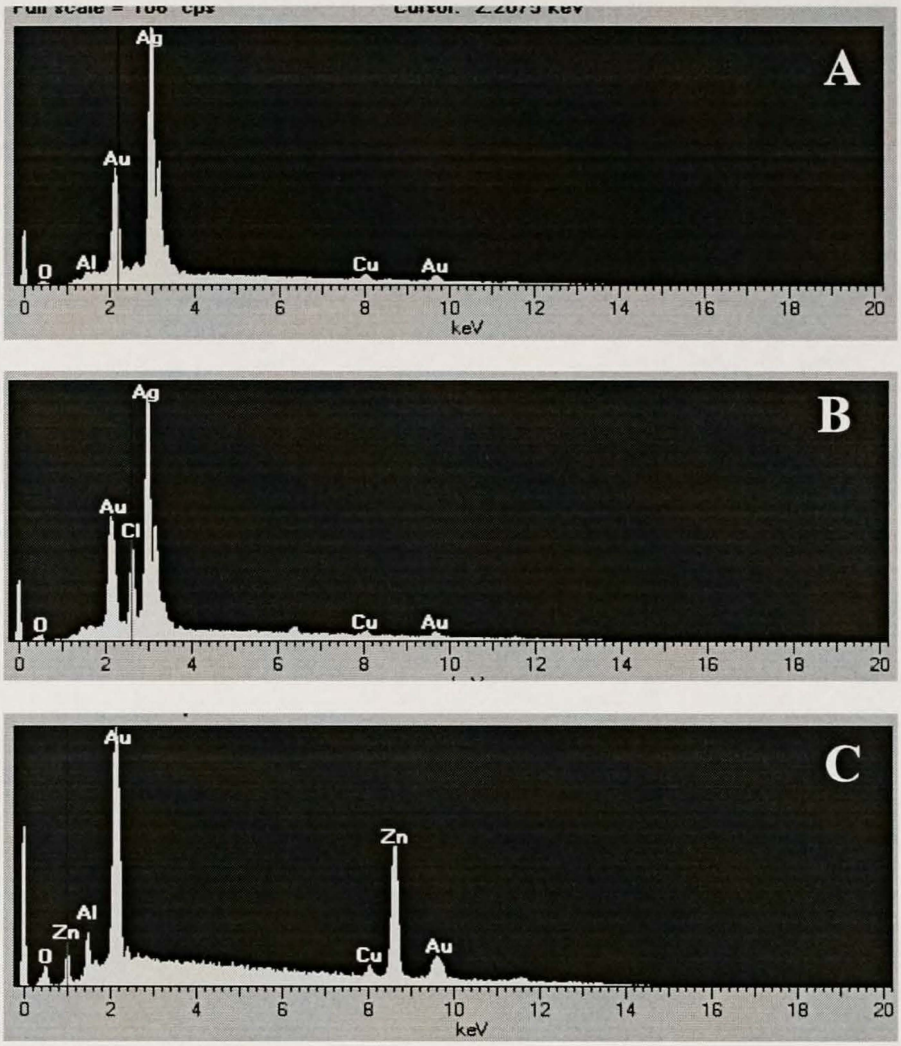


Figure 2-4. EDS spectra of the membrane surface after deposition of Ag (A) and after conversion of the Ag surface to AgCl (B). EDS spectrum of the opposite membrane surface that had been coated with Zn (C).

**Battery Discharge Experiments**

Control experiments were first conducted with membranes that were not modified with the hydrophobic $C_{18}$-silane. As described above, a Zn anode film was applied to one face of the membrane and a Ag/AgCl cathode film was applied to the opposite face. The membrane was mounted in the U-tube cell, and the electrode films were connected to the leads of the potentiostat. However, the half-cells were initially devoid of electrolyte solution, and as a result, there was no ionically conductive pathway through the membrane to link the anode and cathode films. This prevented battery discharge, and no current was detected ($t < 7$ min, Figure 2-5 A). At $t = 7$ minutes, electrolyte (0.1 M

NaCl) was added to both half-cells. Because the untreated alumina membrane is so hydrophilic, electrolyte immediately flooded the pores, allowing for ionic conduction between the anode and cathode films. This allowed the transmembrane microbattery to discharges via the following discharging half-reactions:

$$Zn \rightarrow Zn^{2+} + 2e^{-} \qquad E^0 = 0.763\ V \qquad (2\text{-}1)$$

$$2AgCl + 2e^{-} \rightarrow 2Ag + 2Cl^{-} \qquad E^0 = 0.222\ V \qquad (2\text{-}2)$$

As indicated by $E^0$ values, this battery delivers almost 1 V. As shown in Figure 2-5 A the current raises immediately to a peak value of ~250 μA and then decays away with time. Before this experiment, the face of the membrane coated with the AgCl cathode film was dark purple in color due to the AgCl. After this experiment this face of the membrane was white, indicating that all of the AgCl had been reduced during the battery discharge. This explains why the current ultimately decays to zero (Figure 2-5 A).

An analogous experiment was conducted with a $C_{18}$-modified membrane that had the Zn anode and AgCl cathode films on its surfaces (Figure 2-5 B). In this case, electrolyte was added to the half-cells at t = 0. However, the current obtained is at the noise level of the potentiostat, indicating that battery discharge is prevented. As shown in our prior work, this is because the hydrophobic pores are not water wetted (138), and as a result there is, again, no ionic-conduction pathway through the membrane. These results show that when the hydrophobic microbattery membrane is exposed to NaCl solution, the membrane is in its "off" state, and transmembrane battery discharge is prevented.

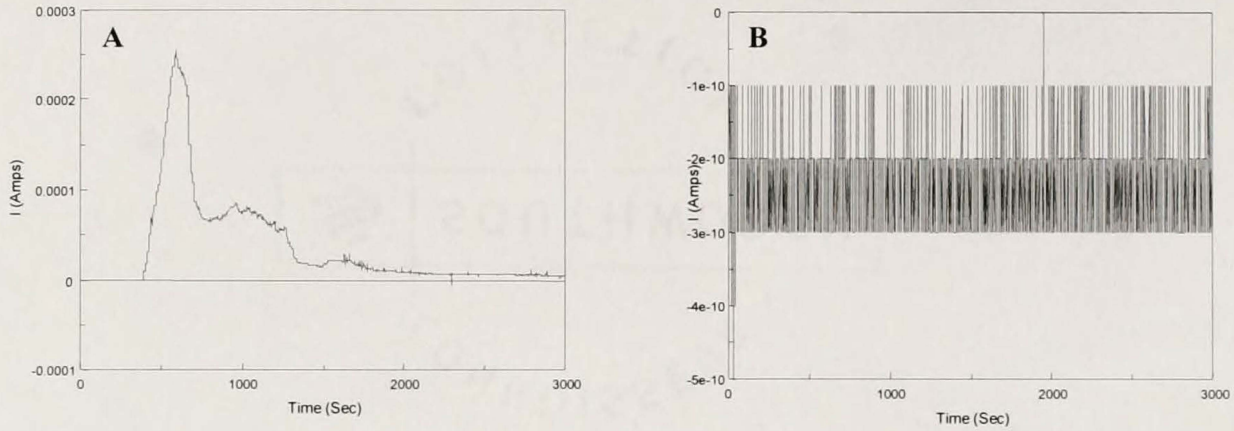


Figure 2-5. Current-vs.-time response for the transmembrane microbattery applied to an alumina membrane that was not rendered hydrophobic by silane functionalization (A). Analogous current-vs.-time response for the hydrophobic C18-modified membrane (B).

Figure 2-6 shows current-vs.-time data for the $C_{18}$-modified membrane before and after injection of dodecylbenzene sulfonate (DBS) into the half-cell solutions. Prior to injection of DBS, $t < 200$ s, the membrane was again in its "off" state, and battery discharge was prevented. At $t = 200$ s, DBS was injected to make the DBS concentration in both half-cells 1 mM. After injection there was an induction period followed by a time region in which a low-level discharge current (~1.5 μA) was observed (inset Figure 2-6). This low-level discharge current flowed for ~ 1300 s, after which a burst of current, at a much higher level was observed. Analogues results were obtained for $C_{18}$ membranes upon exposure to the cationic surfactant dodecyltrimethylammonium (DTA).

These results are in many ways similar to results obtained in our prior investigations of the effect of DBS on the ionic resistance of the $C_{18}$-modified alumina membrane (138). First, when 0.1 M KCl was present in both half-cells, without added DBS, the membrane resistance was very large (> 50 MΩ), again signaling the "off" state of the membrane. Addition of low levels of DBS to both half-cells (< 1 μM) caused the

membrane resistance to decrease, but still the resistance remained high (> 20 MΩ). When the DBS concentration reached 10 μM a precipitous 4-order of magnitude drop in resistance was observed. The key point is that two "on" states were observed – a high-resistance "on" state at low concentrations of DBS followed by a sharp transition to a low-resistance "on" state at higher concentrations of DBS.

We showed that the sharp transition from the high-resistance "on" state to the low resistance "on" state is associated with flooding of the pores with the electrolyte solution (138). That is, at some critical solution-phase concentration of DBS, the quantity of DBS partitioned into the membrane is sufficiently high that the pores are no longer hydrophobic, and water cannot be prevented from entering the pores. In this flooded state charge is carried through the membrane by migration of ions in the solution-filled pores. At lower DBS concentrations, the ionic current is presumably carried by surface migration of the DBS and attendant counterion along the pore walls in pores that are devoid of water (138). This accounts for the high resistance of this "on" state.

In the transmembrane microbattery experiments described here, after injection of DBS into the electrolyte solutions, DBS must diffuse through the porous electrode films (vide infra) and then into the hydrophobic pores. The two "on" states observed previously (138) are analogous to the two current-levels observed here. The low current "on" state (e.g., inset Figure 2-6) is associated with surface migration in pores devoid of water, and the sharp transition to the higher current "on" state is associated with flooding of the pores with water and electrolyte. As before, flooding occurs when diffusion brings some critical level of DBS into the membrane. Finally, the induction period prior to the low current "on" state is simply associated with achieving a high enough quantity of DBS

in the membrane such that a discharge current above the detection limit for the potentiostat can be supported.

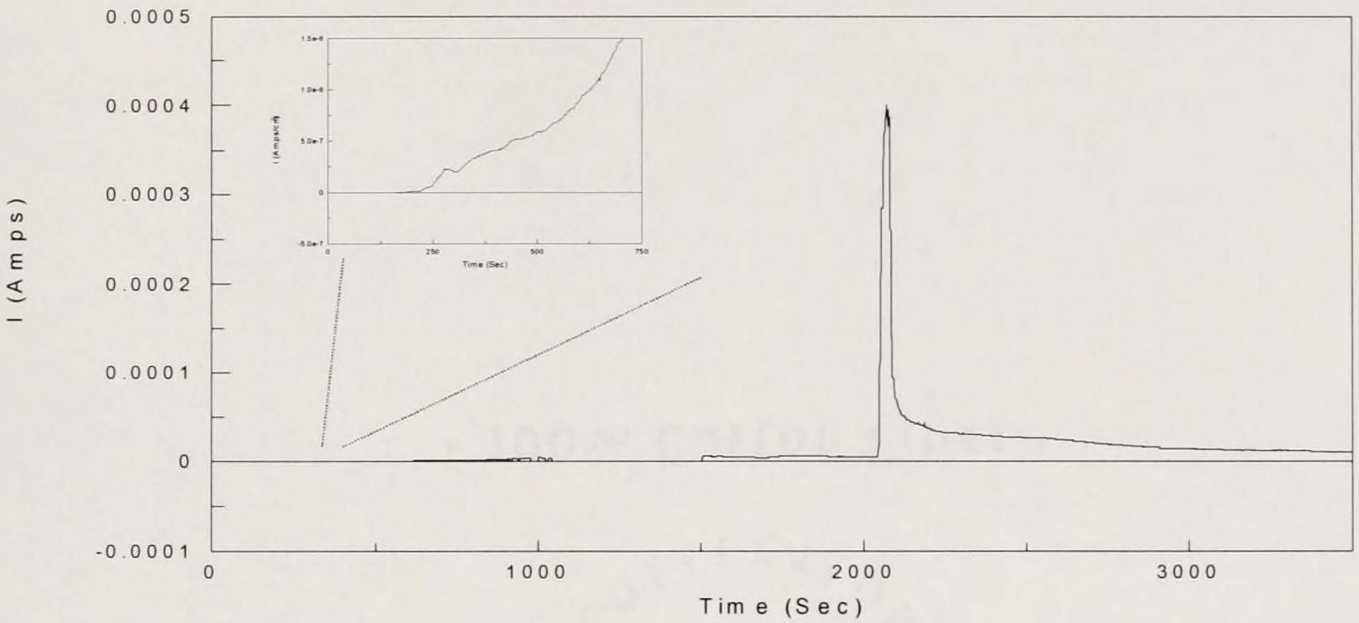


Figure 2-6. Current-vs.-time response for a hydrophobic membrane before and after injection of DBS surfactant solution.

After injection, the DBS concentration in both half-cells was 1 mM. The timescale of this induction process, however, seemed long; e.g., in Figure 2-6 it takes in excess of 1300 s before the critical membrane level of DBS is achieved. This suggests that there is some barrier to transport of DBS into the membrane. The most likely source of this barrier is diffusion of DBS through the battery electrode films on the surfaces of the membrane. To explore this issue we attempted to make thinner electrode films; however, because of the particulate nature of these films, the lateral electronic resistance of these thinner films was too high, and battery discharge was not observed.

To circumvent this problem, we first sputtered both faces of the membrane with a thin (25 nm) layer of Au. Thinner Ag and Zn films (400 nm as opposed to the 500 nm

used above) were then thermally evaporated onto these Au films. In essence, the Au films act as current-collectors for the overlying battery electrode films. We found that the induction times for these thinner battery electrode films were shorter than for thicker films. For example, with the 1 mM DTA solution a membrane with the thinner battery electrode films showed a response time of 400 s as opposed to 1000 s for the membrane with the thicker films. These results show that transport of surfactant through the battery electrode films is a kinetic barrier in this system.

**Effect of Surfactant Concentration on the Response Time**

The response time of this device is defined as the induction time period between injection of surfactant into the half-cell solutions and observation of the low current "on" state. Over the concentration range 0.01 mM to 1 mM, the response time is inversely proportional to the solution-phase DBS concentration (Table 2-1). This result is consistent with our model that the response time is associated with transport of DBS through the electrode films and into the pores of the membrane. Higher DBS concentrations yield higher concentrations at the membrane solution interface and thus higher net fluxes into the membrane. As a result, the time required to achieve a concentration of DBS in the membrane sufficient to support the low current "on" state decreases with increasing solution-phase DBS concentration.

Table 2-1. Effect of DBS concentration on the response time.

| DBS Concentration (mM) | Response time (s) |
|---|---|
| 2 | 350 |
| 1 | 1.5 |
| 0.1 | 52 |
| 0.01 | 70 |

Table 2-2 shows that analogous results are obtained for the cationic surfactant DTA; however, at both the 0.01 and 0.001 mM levels the response times for DTA are about a factor of three times higher than for DBS. These results also fit our diffusional-transport model because the diameter of the DTA head group is larger than the diameter of the DBS head group - ~3.7 nm vs. ~2.0 nm (139). The larger diameter for the DTA head group makes the surface diffusion coefficient smaller, and as a result the diffusional transport time longer.

Table 2-2. Effect of DTA concentration on the response time.

| DTA Concentration (mM) | Response time (s) |
|---|---|
| 1 | 1000 |
| 0.1 | 140 |
| 0.01 | 216 |
| 0.001 | 600 |

When the solution-phase DBS concentration is increased to 2 mM the response time goes up again, indeed, to a value higher than is observed for the lowest DBS concentration (Table 2-1). While analogous results are obtained for DTA, the concentration producing the longest response time (1 mM, Table 2-2) is lower than for DBS. Our initial hypothesis was that these longer response times at the highest surfactant concentrations were in some way associated with micelle formation; however, the critical micelle concentrations (CMCs) for DBS and DTA are 1.1 mM (140) and 4.4 mM (141), respectively. Hence, while the concentration that yields the longest response time for DBS (2 mM) is above the CMC, the concentration that yields the longest response time for DTA (1 mM) is below the CMC. It is not yet fully understood why the response time goes up again for the high concentrations of surfactant.

**Investigations of Alkyl Chain Length on the Response Time**

During the investigations of hydrophobic alkyl thiol-modified gold nanotube membranes it was shown that the transmembrane flux increases with the hydrophobicity of the permeate molecule (44). This is because the flux is directly proportional to the partition coefficient for the permeate molecule at the membrane/feed-solution interface (Equation 2 in reference 44). The same principle should apply for flux of hydrophobic surfactant molecules into the $C_{18}$-modified alumina membranes studied here. As a result, response time should decrease with increasing hydrophobicity of the surfactant. To explore this issue we investigated response times for three alkyl trimethylammonium surfactants (Table 2-3). In agreement with the above analysis, response decreases with increasing hydrophobicity (alkyl chain length) of the surfactant.

Table 2-3. Effect of alkyl chain length in alkyl trimethylammonium surfactants on the response time. Concentration in all cases = 1 mM. These results were obtained using the C18-modified membrane with thinner battery electrode films.

| Number of carbons in alkyl chain | Response time (s) |
|---|---|
| 8 | >3600 |
| 12 | 400 |
| 16 | 5 |

**Conclusions**

It has been shown in this work that a microbattery /nanoporous membrane acts as a biomimetic "smart membrane" in the sense of emulating the function of ligand-gated ion channels; i.e., they can be switched from an "off" state to an "on" state in response to the presence of a targeted chemical stimulus. Modifying the aluminum oxide with long chain alkylsilanes makes the membrane pores hydrophobic and the microbattery is "off". In the presence of surfactant, the pores became hydrophilic , which turns the microbattery "on". The results can be briefly summarized by pointing out three factors which influence the

response time of the system: the hydrophobicity of the analyte (shorter response time for more hydrophobic analytes), the nature of the polar head group of the analyte (anionic surfactants are sensed faster than the cationic ones) and the concentration of the analyte (shorter response time for lower concentration). This concept could ultimately lead to a remote sensing technology where the battery discharge current is use to drive a device (e.g., a buzzer) that signals to the outside world that the ligand has been detected.

# CHAPTER 3
# HIGHLY SELECTIVE ANTIBODY-BASED NANOTUBE MEMBRANES FOR PROTEIN SEPARATION

## Introduction

Many technically challenging and commercially attractive separation problems can not be solved with existing membranes because the typically achieved separations of complex mixtures are only fractionation into substance groups (142). Membranes with high selectivities for example for chiral drugs, toxins or complex biomolecules are required. The aim of current membrane development is preparing "tailored" membranes with high selectivity and/or high flux of the analytes of interest across the membranes; this can be achieved by developing membranes modified with molecular recognition elements, with high pore density and a narrow pore size distribution. Active research is devoted to highly specific membrane separations based on molecular recognition inside the nanoporous membranes (47,82,152).

We report here a protein separation method based on facilitated transport selectivity, that utilizes immobilized molecular recognition elements in a porous alumina membrane. We found that by modifying the walls of the alumina membrane pores with antibodies, proteins that have an affinity towards these antibodies are transported at a higher rate than proteins that do not interact with the antibodies. We used two Fab fragments (1C2 and 1A4) of antibodies that were grown against the protein hevein; 1A4 has higher affinity ($K_d \sim 10^{-8}$ M) towards hevein than 1C2 (143). Hevein is a latex protein which has been identified as an allergen; it is a defense protein of the rubber tree

*Hevea Brasiliensis* involved in the inhibition of several chitin-containing fungi (144,145). Hevein was produced as a green fluorescence protein (GFP) fusion protein (GFP-Hevein) in insect cells (143). In this way GFP-Hevein can be detected by fluorescence spectroscopy. Red fluorescence protein (RFP) was used as a control protein because it does not have any affinity towards any of the antibodies. Because their excitation and emission spectra do not overlap ($\lambda_{exGFP}$=395 nm, $\lambda_{emGFP}$=510 nm, $\lambda_{exRFP}$=563 nm, $\lambda_{emRFP}$=582 nm), GFP and RFP are very well suited for dual-label experiments (146).

## Experimental

### Materials

The antibodies ENA 11 His, 1A4 and 1C2 Fab fragments were provided by VTT Biotechnology, Finland. Red fluorescence protein (rDsRed2 protein) was purchased from BD Biosciences Clontech. High purity aluminum foils 100 mm x 500 mm x 0.2 mm, purity 99.9998%) were obtained from Alfa Aesar, tetraethyl orthosilicate (TEOS) from Sigma Aldrich and triethoxysilylaldehyde from Gelest.

### Fabrication of the Nanoporous Alumina Membranes

We used a two-step anodization method (52,53) to fabricate the porous alumina membranes. Briefly, the aluminum foils were first electropolished at 15 V in a solution with the following composition: 95 wt. % $H_3PO_4$, 5 wt. % $H_2SO_4$ and 20 g/L $CrO_3$. The solution was heated at 70 $^0$C. The polished aluminum foil was anodized at 40, 50 and 70 V to obtain membranes having 50, 70 and 100 nm pore diameter, respectively. We used 5% oxalic acid as the electrolyte solution and the anodization experiments have been done at 0 $^0$C. The first film of the membrane was dissolved away in an aqueous solution that was 0.2 M in $CrO_3$ and 0.4 M in $H_3PO_4$, at 60-70 $^0$C. The second anodization step was carried out in exactly the same conditions as the first step. This yields the desired

highly ordered nanoporous alumina membranes. The aluminum that was not oxidized was dissolved into a saturated $HgCl_2$ solution. Then the barrier layer of the alumina membranes was removed in 5% $H_3PO_4$ solution.

Scanning electron microscopy was used to measure the pore diameters and the thicknesses of the alumina membranes prepared. A JEOL FE-SEM 6438 was used. Alumina nanoporous membranes (Figure 3-1) were used as templates for immobilization of the antibodies.

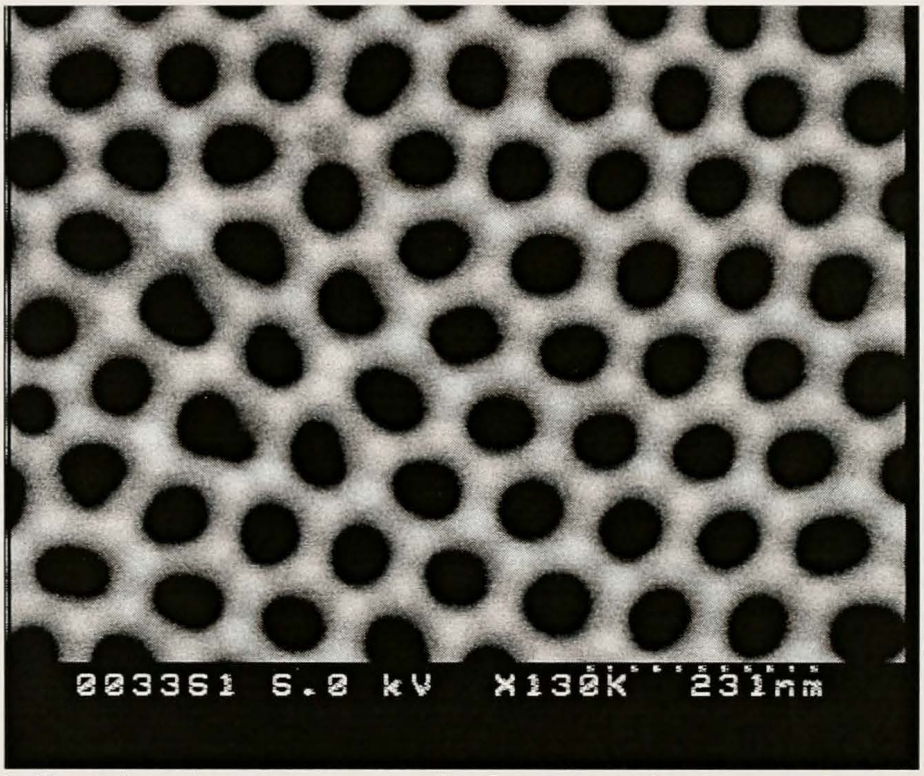


Figure 3-1. Scanning electron micrograph of a porous alumina membrane with pores of 50 nm in diameter and pore density of ~ $10^{10}$ pores/$cm^2$.

**Antibody Immobilization**

Figure 3-2 shows a schematic representation of the modification steps involved in antibody immobilization. Silica nanotubes were deposited inside the pores of the alumina membranes using a sol-gel method (81,84). Briefly, a sol-gel silica precursor was prepared by mixing absolute ethanol, TEOS and 1 M HCl (50:50:1). This solution

was allowed to hydrolyze for 30 minutes. Alumina membranes were than immersed into the sol-gel for 1 minute under sonication, after which they were air dried for 10 minutes at room temperature and cured in the oven for 12 hours at $150^0$C. Triethoxysilylaldehyde has been used to attach aldehyde terminal groups onto the pores of the membranes. The free amino sites of the antibody Fab fragments react with the aldehyde groups via a Schiff base chemistry (147,176,177). The aldehyde-modified silica nanotube membranes were incubated for 12 hours at 4 $^0$C in a solution containing 0.2 mg/ml antibody Fab fragments solutions. All solutions of the antibody Fab fragments, GFP-Hevein and RFP were made in phosphate buffer saline (PBS) solution having pH=7.4. After washing them with PBS, the antibody-modified membranes were incubated for 3 hours in a blocking solution containing 1% bovine serum albumin (BSA) and 1% Tween-20 in PBS. Blocking solution was used to block both the unreacted aldehyde groups and nonspecific adsorbtion. The membranes were washed copiously with PBS afterwards and stored in PBS at $4^0$C until used in transport experiments.

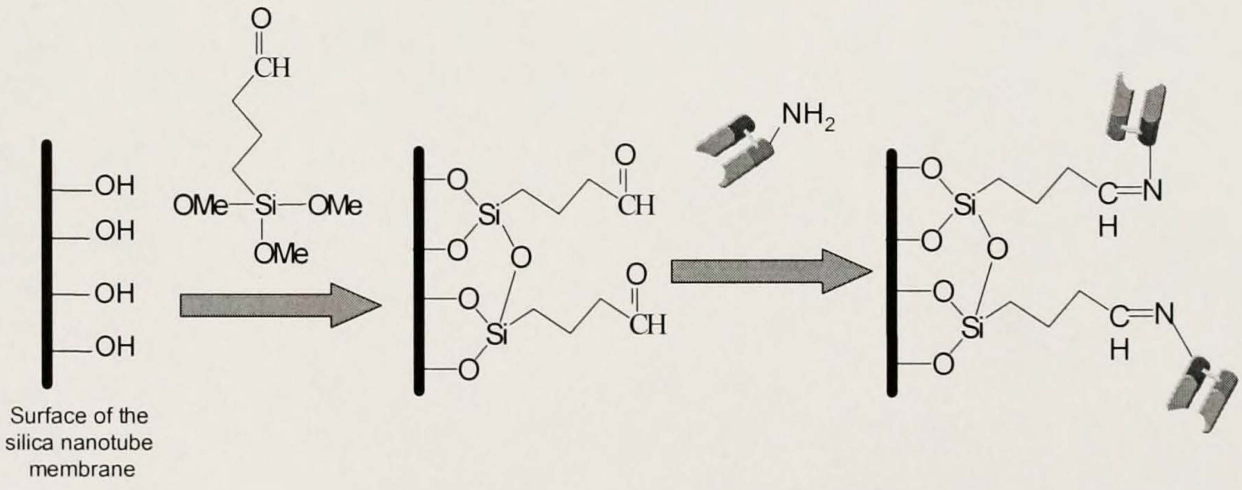


Figure 3-2. Modification steps involved in antibody immobilization.

**Transport Experiments**

The antibody-modified silica nanotube membranes were sandwiched between two pieces of Scotch tape that had 0.314 $cm^2$ area holes punched through them. These holes defined the area of the membrane in contact with the solution phases. The membranes were then mounted between two halves of a U-tube permeation cell (40,43,44,148). The feed solutions had equal concentrations in GFP-Hevein and RFP. A volume of 3 ml PBS was used on both halves of the permeation cell. The rate of transport (flux) was determined by periodically measuring the fluorescence intensity of the permeate solution using a Varian Cary Eclipse spectrofluorometer. GFP-Hevein and RFP were detected simultaneously.

## Results and Discussions

**Effect of Antibody Affinity on Selectivity Coefficient**

Transport plots in Figure 3-3 show the number of picomoles of GFP-Hevein and RFP transported through the nanotube membranes versus the permeation time. A single membrane was cut into three pieces and they were modified with ENA 11His Fab fragments (Figure 3-3A), 1C2 Fab fragments (Figure 3-3B) and 1A4 Fab fragments (Figure 3-3C) respectively. The membrane used for these experiments had pores 70 nm in diameter and a thickness of 90 μm. A concentration of 10 nM in both GFP-Hevein and RFP in PBS was used in feed side, with PBS only in the permeate side. Due to the fact that ENA 11His does not have affinity for either GFP-Hevein or RFP, membranes modified with this antibody were used for control experiments. As can be seen from Figure 3-3A RFP is transported by passive diffusion at a higher rate than GFP-Hevein, when the membrane is modified with ENA 11His. This is due to higher molecular weight of GFP-Hevein; GFP and RFP have approximately the same molecular weight of

28,000 Da (149,150) and Hevein has a molecular weight of 4,000 Da (151). When the antibody having an affinity towards Hevein (1A4 or 1C2 Fab fragments) was immobilized, the membranes transported GFP-Hevein at a much higher rate (Figure 3-3A and 3-3B) than they transported RFP.

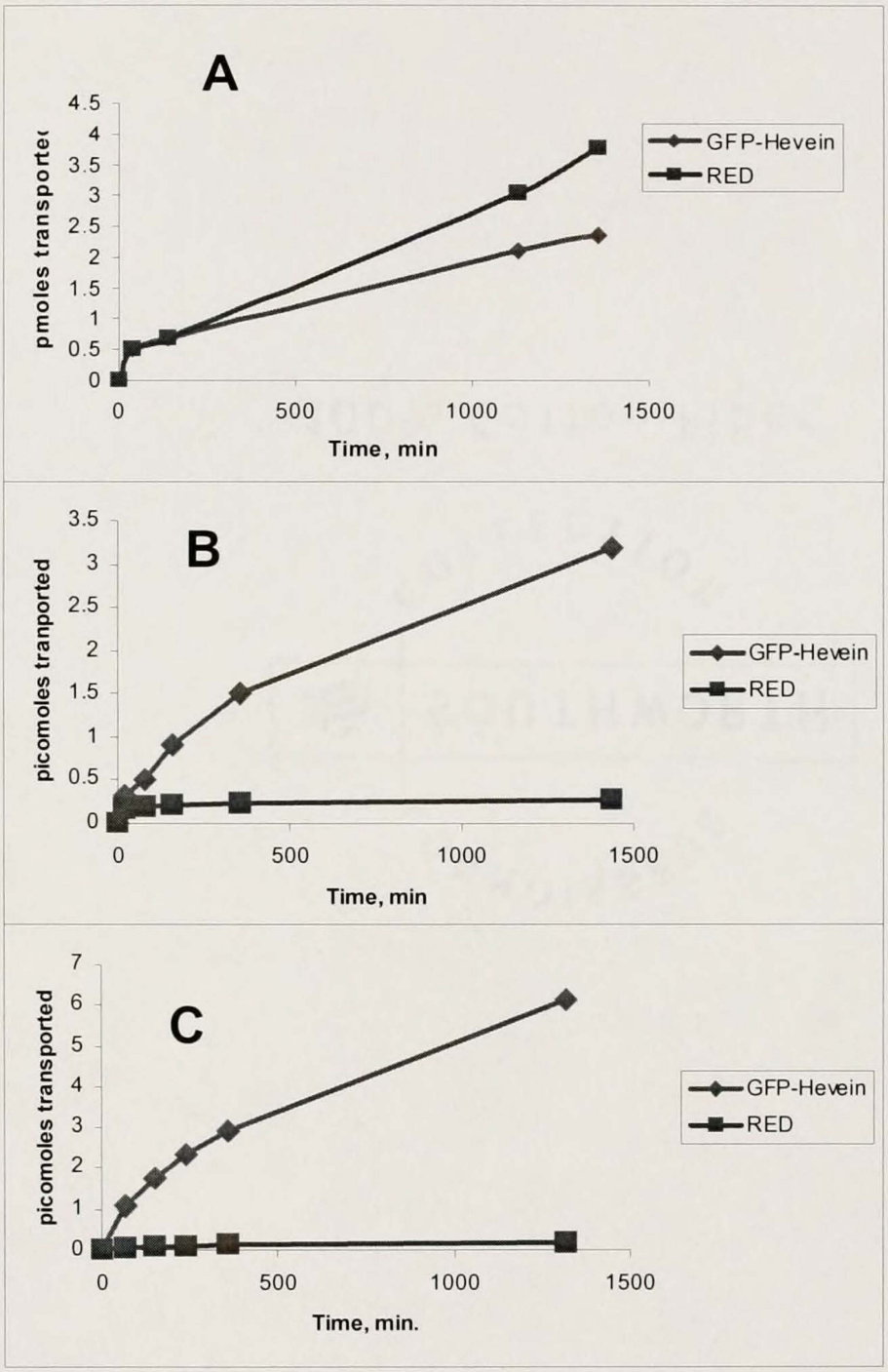


Figure 3-3. Transport plots of GFP-Hevein and RFP through ENA 11His (A), 1C2 (B) and 1A4 (C) modified nanotube membranes.

Because 1A4 and 1C2 Fab fragments bind hevein, these data suggest that immobilization of these antibodies facilitates the transport of GFP-Hevein versus RFP. The transport of GFP-Hevein through the membranes is not linear in time because the concentration gradient decays with time, so the driving force for diffusion decays as well. Due to that, the fluxes of GFP-Hevein and RFP through the membranes were calculated with respect to the linear part of the transport plots (the first two points of the plots). We defined a selectivity coefficient for a membrane, *s*, as the ratio between the flux of GFP-Hevein and the flux of RFP. Figure 3-4 shows the influence of the type of the antibody immobilized on the selectivity coefficient.

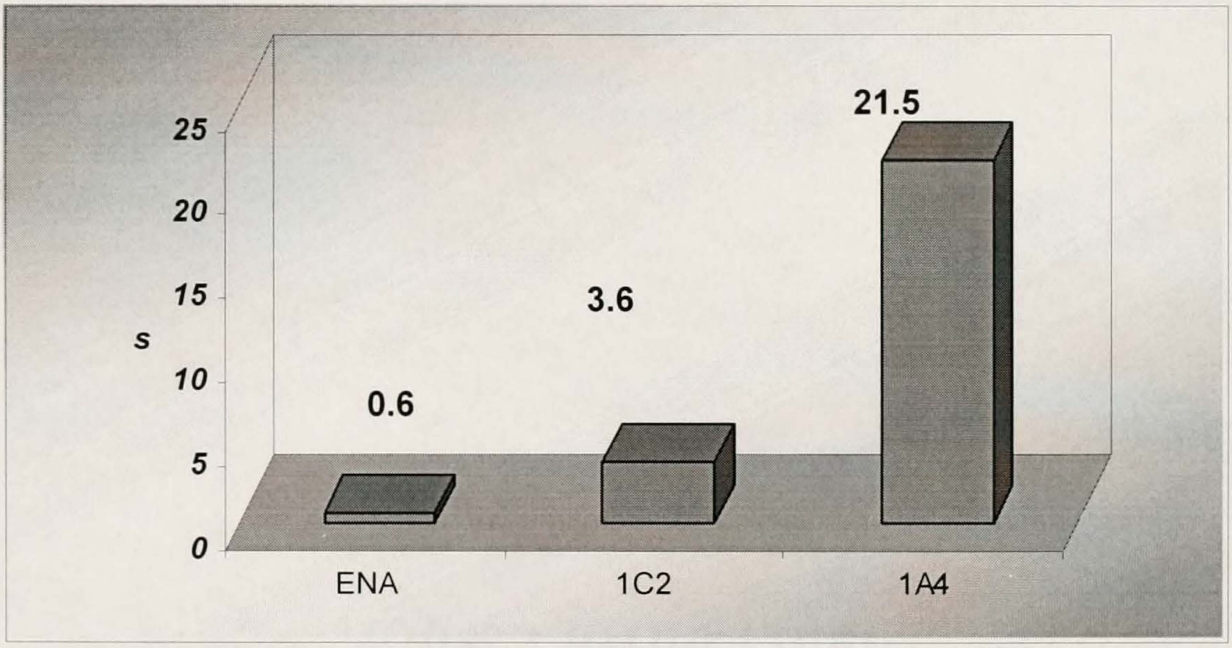


Figure 3-4. Effect of the antibody immobilized on the selectivity coefficient.

As can been observed from Figure 3-4, immobilization of an antibody with higher affinity towards the analyte yields a higher selectivity coefficient. Immobilization of an antibody of high binding affinity towards an analyte, results in increase of the analyte concentration inside the pore. Consequently it leads to creation of higher concentration gradients across the membranes and hence higher fluxes.

**Effect of the Feed Solution Concentration on the Flux and Selectivity Coefficient**

An important parameter in characterizing facilitated transport of the molecules through membranes is the feed solution concentration. A plot of flux versus feed concentration should have a "Langmuirian" shape (47,82,152). We investigated the effect of the feed solution concentration on fluxes of GFP-Hevein and RFP (Figure 3-5). In these experiments the membranes were modified with 1A4 Fab fragments and they had pores of 70 nm in diameter and 90 μm thickness.

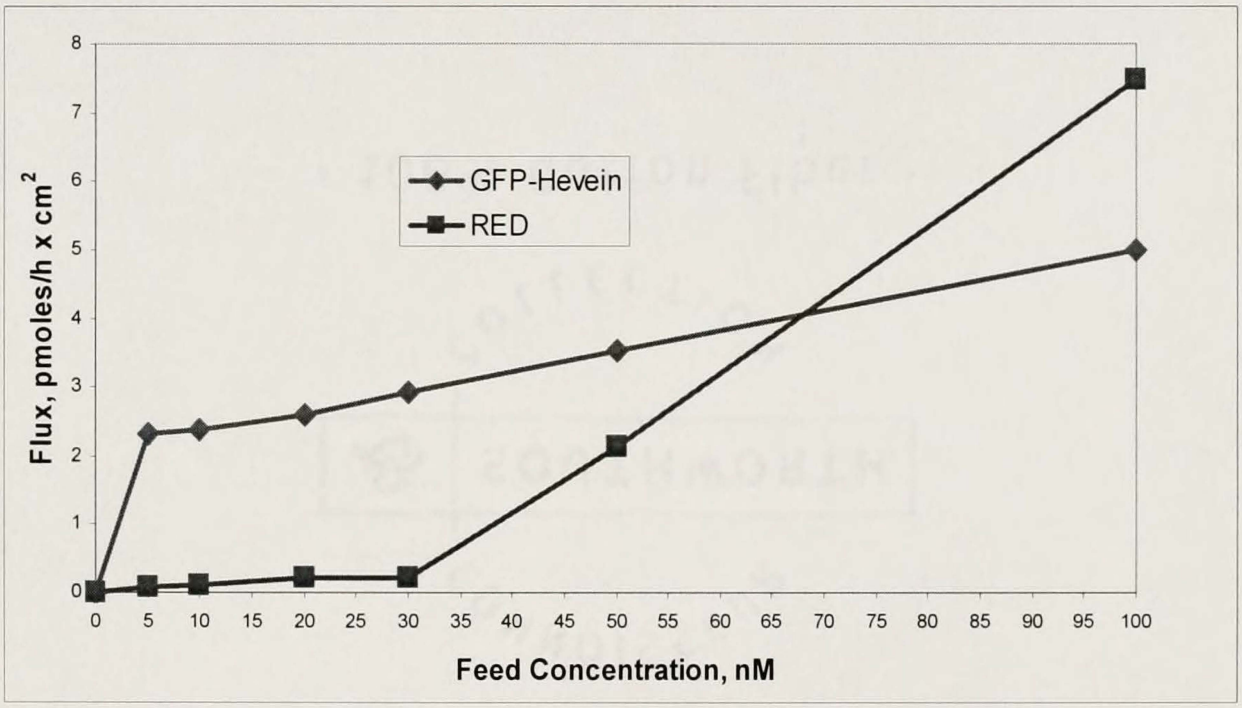


Figure 3-5. Plot of fluxes of GFP-Hevein and RFP versus feed solution concentration. The plot showed in Figure 3-5 has a Langmuirian shape for GFP-Hevein. It can be observed that at high feed concentration the membrane transports RFP at higher rates than GFP-Hevein. At high feed concentration (100 nM), passive diffusion is predominant. Facilitated transport theory also predicts that the highest selectivity coefficient should be obtained at low feed concentrations. Figure 3-6 shows the transport

plots of GFP-Hevein and RFP through a 1A4 antibody-modified membrane when using 5 nM (A), 20 nM (B), 50 nM (C) and 100 nM (D) feed solution concentration.

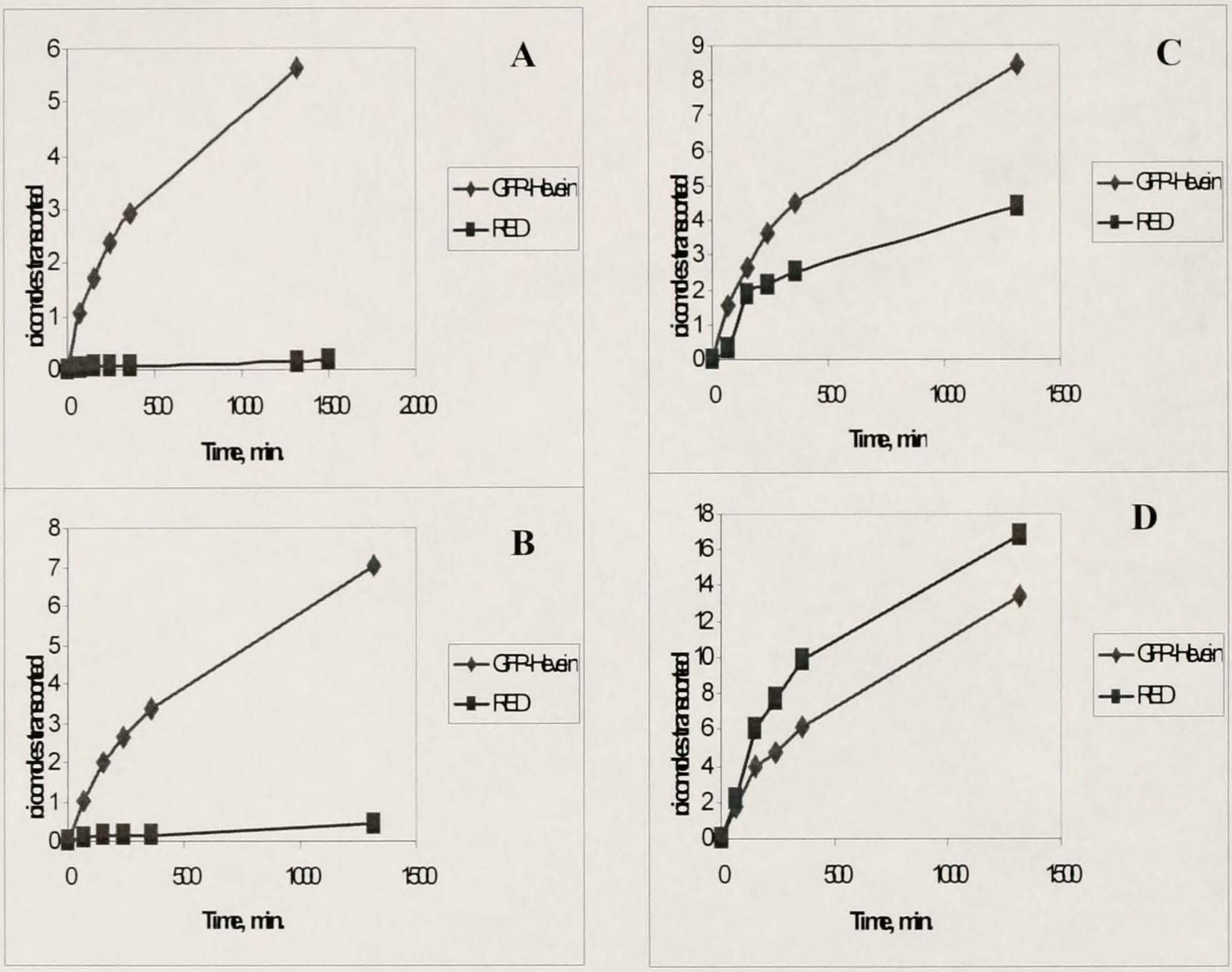


Figure 3-6. Transport plots of GFP-Hevein and RFP through a 1A4 antibody-modified membrane when using 5 nM (A), 20 nM (B), 50 nM (C) and 100 nM (D) feed solution concentration.

These transport plots were used to calculate the selectivity coefficient (Figure 3-7). Indeed the selectivity coefficient decreases as the feed solution increases. For 5 nM feed solution concentration a selectivity coefficient of 30.6 is obtained, and for 100 nM feed solution concentration we obtained a value of 0.7 of the selectivity coefficient, which corresponds to passive diffusion of the proteins.

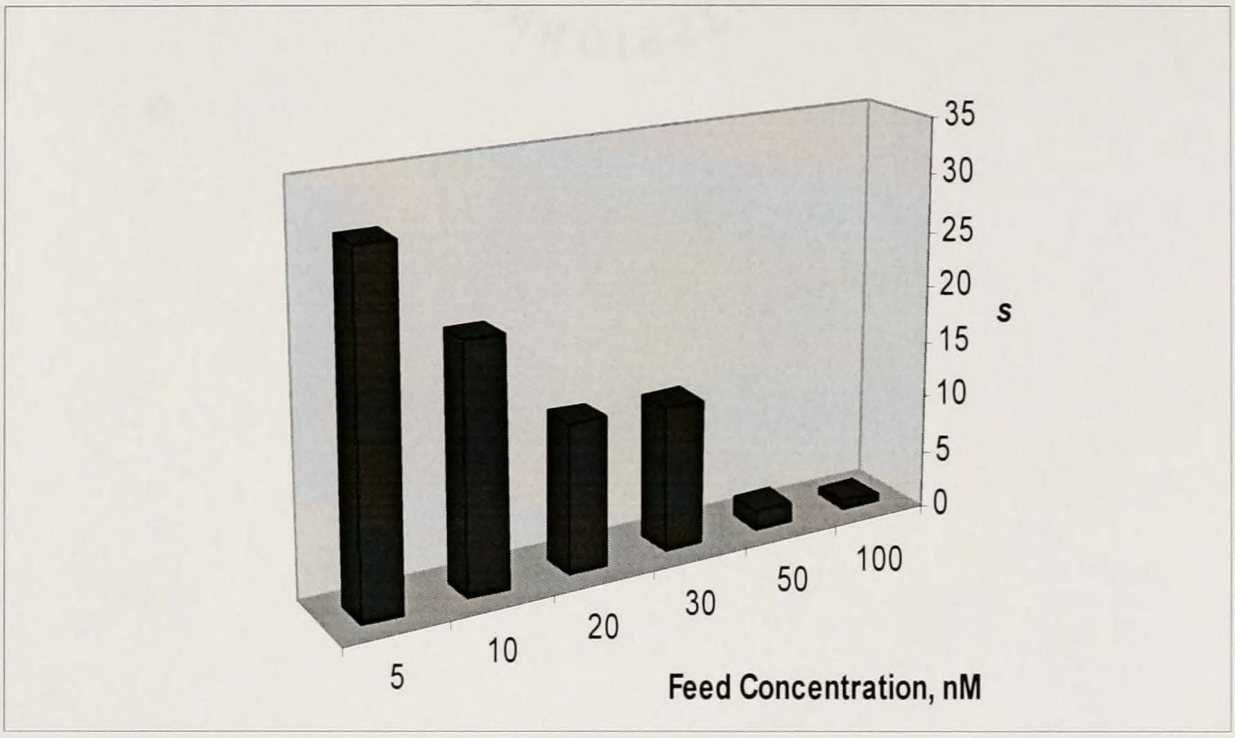


Figure 3-7. Variation of the selectivity coefficient with feed solution concentration.

**Effect of the Pore Diameter on the Flux and Selectivity Coefficient**

The diameter of the pores of the alumina membranes is another important parameter that influences the flux of the proteins and selectivity coefficient of a membrane. Figure 3-8 shows the transport plots obtained when membranes with pores of 50 nm (Figure 3-8A), 70 nm (Figure 3-8B) and 100 nm (Figure 3-8C) in diameter were used. The membranes with pores of 50 nm and 70 nm in diameter had thickness of 80 μm and 90 μm respectively, and were modified with 1C2 Fab fragments. The membrane with pores of 100 nm in diameter had a thickness of 50 μm and was modified with 1A4 Fab fragments. In all cases a feed solution concentration of 10 nM in GFP-Hevein and RFP has been used. The selectivity coefficient decreases as the pore diameter increases (Figure 3-9). The increase in selectivity coefficient is obtained at the cost of lowering the fluxes. For 100 nm pore diameter, the selectivity coefficient has a value of 0.7, which

means that when using membranes with this pore diameter, facilitated transport is not predominant; only passive diffusion is observed at high pore diameters.

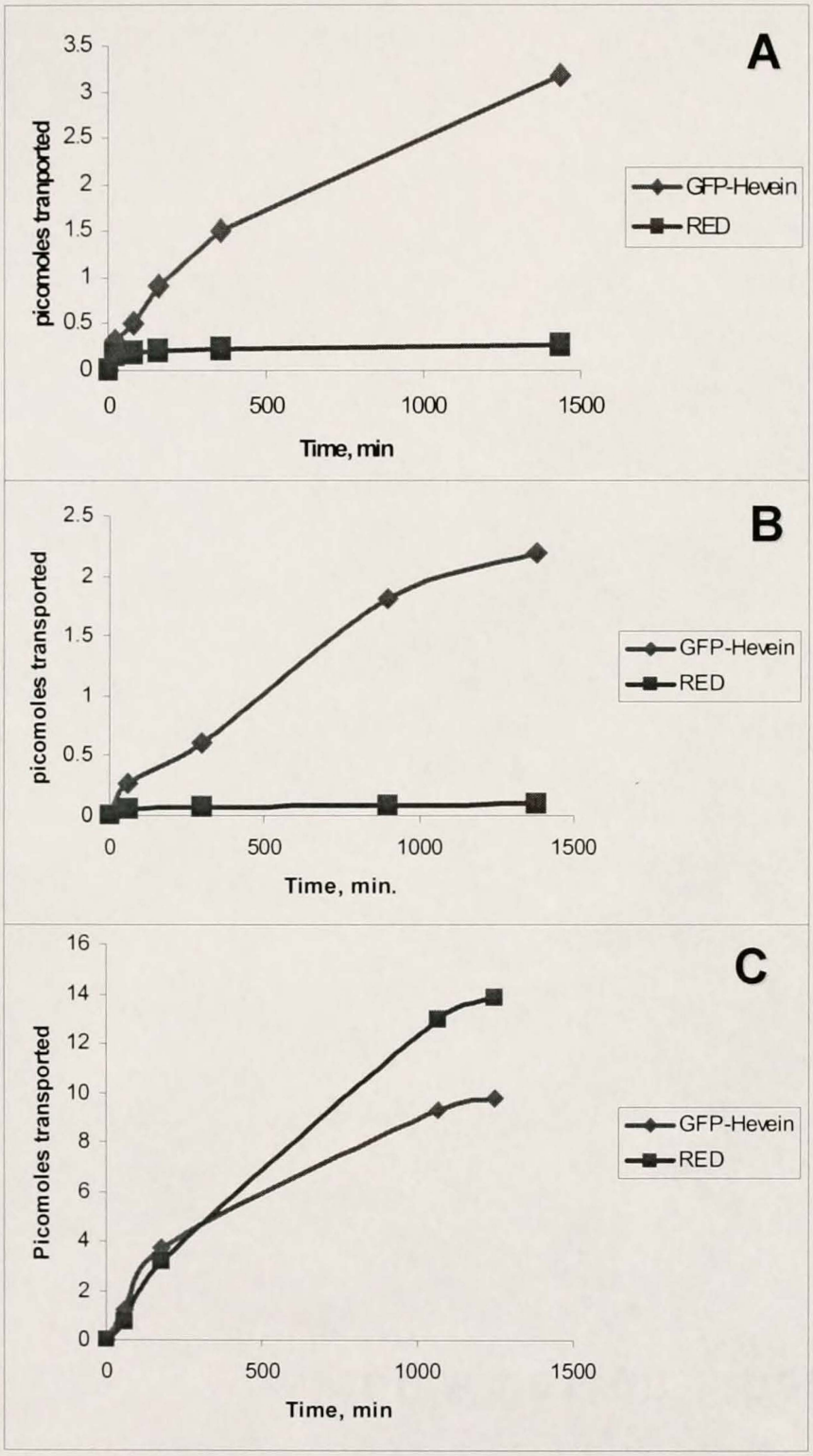


Figure 3-8. Transport plots obtained when used membranes with pores of 50 nm (A), 70 nm (B) and 100 nm (C) in diameter.

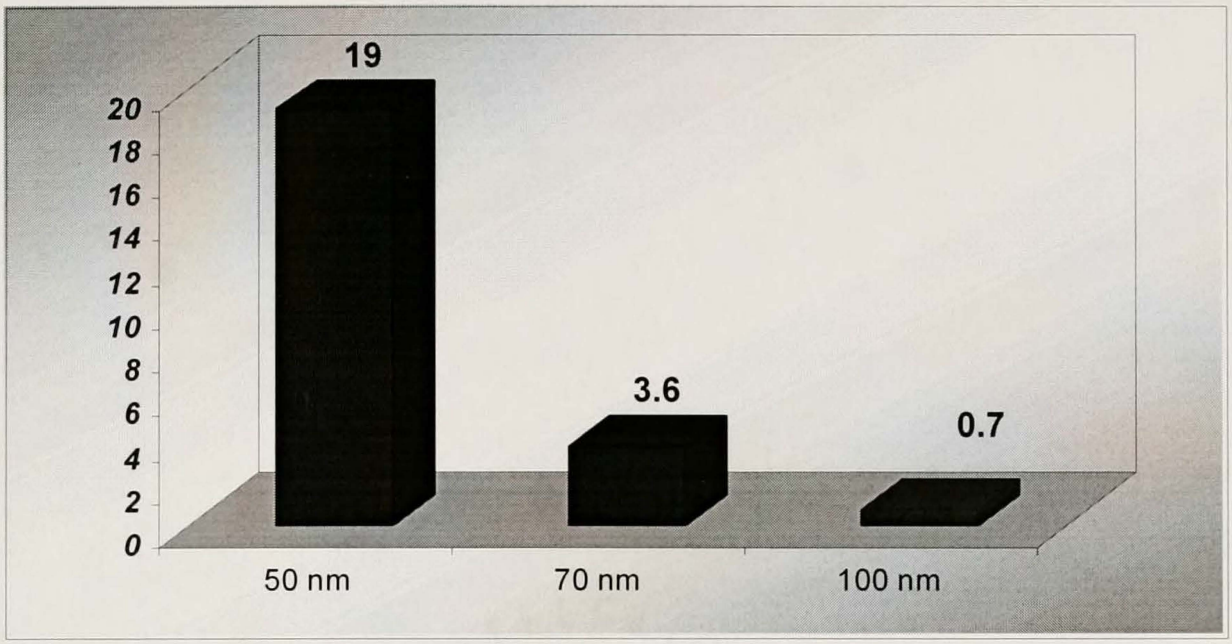


Figure 3-9. Selectivity coefficient variation with the pore diameter.

## Conclusions

Highly selective nanotube membranes for protein separations have been prepared. The separation is based on molecular recognition inside the nanopores of alumina membranes. We have used antibody Fab fragments which as molecular recognition elements selectively bind and transport proteins. There are important parameters that should be taken into account in obtaining a desired protein separation with certain fluxes and selectivity coefficients. These parameters are: binding affinity between the antibody and the antigen, feed solution concentration, pore diameter of the membrane and membrane thickness. A higher binding affinity is desired because it leads to a higher selectivity; although a very high binding affinity is not appropriate because the analyte should be released from the antibody and transported through the membrane. Higher selectivity coefficients are obtained at lower feed solution concentration and when using membranes with small pore diameters. Using membranes with small pore diameters,

however, lower fluxes are obtained. High fluxes are important in separation processes; higher fluxes can possibly be obtained by decreasing the membrane thickness, by applying pressure (153) or by applying an electric field across the membrane (154).

# CHAPTER 4
# 3-D POROUS ALUMINA-BASED MICROARRAYS

## Introduction

Microarray technology is an emerging technology which is having a considerable impact in proteomic research. Protein microarrays allow the identification and quantification of a large number of target proteins using a small amount of sample within one single experiment (155 ). This technology requires rapid, high throughput protein assays. Recent studies showed that protein microarrays can be used to screen for protein-protein interaction (156,157), antibody specificity profiling (158,159 ), immune profiling (160), and protein-small molecule interactions (161).

Significant challenges exist for protein microarrays which do not exist for gene arrays (155,162,163,164). The initial challenge is developing a system capable of detecting a broad range of concentrations; proteins can exist in a very broad dynamic range (up to $10^{10}$) in any cell. The second challenge is detecting very low abundance proteins; for DNA, PCR methods exists for amplification, while for proteins no amplification method is available yet. DNA is a very uniform and stable molecule (it does not lose its activity when stored dry), with a well defined activity prediction based on primary nucleotide sequence. These factors are different for proteins. Proteins exhibit very diverse individual tertiary molecular structures; further, their 3D structure is important for their activity, they should always be kept wet to avoid denaturation. Protein binding interaction takes place by different means such as electrostatic forces,

hydrogen bonds, hydrophobic or Van der Waals interactions. In addition proteins may have multiple binding sites and can possibly interact with different molecules in the same time.

Because of these challenges, substrate requirements are more demanding for protein microarray technology. Various types of substrate have been explored (165,166) and the search for new supports with superior performances is still a challenge. There have been reports on the spotting of protein microarrays using a variety of surfaces and immobilization chemistries, including but not limited to agarose (167), polyvinylidene difluoride (168), and polyacrylamide gel pads (169). Proteins arrays on glass surfaces coated with aldehyde (161), poly-L-lysine, and gold surfaces derivatized with SAMs (170) have been reported also. Application of nanoporous silicon as support for protein microarrays has been recently reported (171). Three dimensional porous surfaces offer several advantages over the flat surfaces, including higher sensitivity due to the higher sample loading capacity, broader dynamic range of concentrations and a 3-D environment that preserves protein activity and accessibility.

Here we report two methods of fabrication of 3-D porous alumina-based microarrays and show their applications in antibody specificity screening. Besides the advantages offered by a 3-D support for microarrays, alumina membranes present a very well defined morphology, which is important for uniform immobilization of the proteins and providing reproducible detection of the ligand-binding events.

## Experimental

### Materials

High purity aluminum foils 100 mm x 500 mm x 0.2 mm, (purity 99.9998%) were obtained from Alfa Aesar, 3-aminopropyltrimethoxysilane (APTES) from United

Chemical Technologies, and triethoxysilylbutyl aldehyde from Gelest. Triton X-100, tetraethylorthosilicate (TEOS), rhodamine B isothiocyanate, human and mouse IgG, anti-human IgG labeled with Alexa 488 and anti-mouse IgG labeled with Alexa 594 were purchased from Sigma Aldrich. Surface coating polymer FSC-M was obtained from Shipley and polymer remover (remover 1165, Shipley) was purchased from MicroChem. All the materials were used as received. The TEM copper grids (400 mesh, PELCO) that were used as masks were purchased from Ted Pella. The porous alumina membranes that were used for the second method were bought from Whatman, and they had a nominal pore diameter of 200 nm. Silver plating solution (Ag 1025) was purchased from Technic (Cranston, RI). Silver wire (2 mm thick) were purchased from Alfa Aesar (Ward Hill, MA).

**Fabrication of porous alumina microarrays**

**Method 1**

High purity aluminum foil was first glued to a glass by using an epoxy glue. Then the Al foil/glass plate was electropolished into a solution composed of 95 wt. % $H_3PO_4$, 5 wt. % $H_2SO_4$ and 20 g/L $CrO_3$, heated at 70 $^0$C. Al foil/glass was washed with distilled water and dried under vacuum at room temperature.

Figure 4-1 shows a schematic representation of the first method of fabrication of the porous alumina microarrays. There are four steps involved in this procedure and they are as follow:

**Step 1.** The electropolished Al foil/glass was first spin-coated with a surface coating polymer (FSC-M). From the SEM measurements we found that the thickness of the polymer film was 3 μm.

**Step 2.** The polymer/Al foil was then inserted into a reactive ion etching apparatus (Samco Plasma Ion Etching System, model RIE-1C). The polymer surface was etched for 5 seconds in order to make the surface hydrophilic. This was accomplished using oxygen plasma with radio frequency (13.56 MHz) of 140 W. The plasma pressure was 20 Pa oxygen and oxygen flow rate was 30 sccm. Copper grids (400 mesh) were placed on top of the polymer with a dilute Triton X solution, which is a wetting agent, and ensures the copper grid was stick flat to the surface after drying.

**Step 3.** The plate with copper grids was etched for 4.5 minutes and then the copper grids were blown away. In this way, we obtained Al surfaces patterned with the coated polymer.

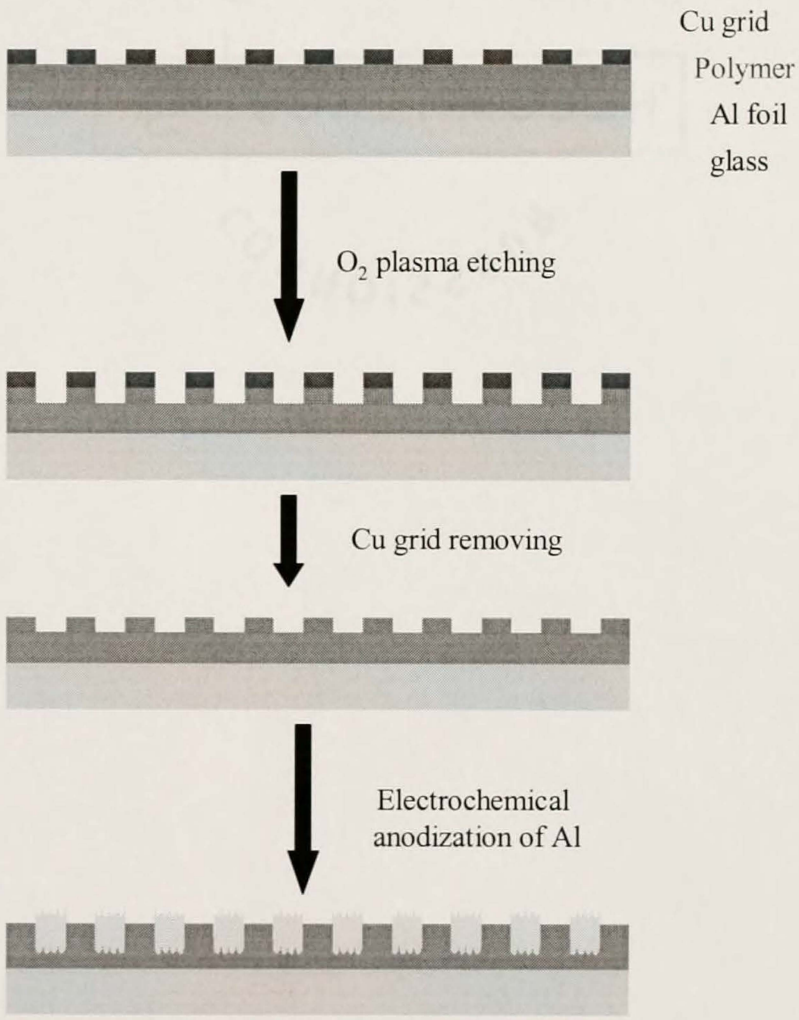


Figure 4-1. Schematic representation of the microarray fabrication by method 1.

**Step 4.** The patterned Al/glass system was electrochemically oxidized to form porous alumina films, only in the areas where the Al was exposed. The anodization was carried out in 5% oxalic acid as electrolyte, at $0^0$C, under a constant voltage of 50 V.

In a similar way, patterning of anodic alumina into aluminum was reported ( 172). In this case, the aluminum was patterned with silica either by a sol-gel process or by dielectric evaporation. In the first case they reported the presence of cracks at the interface between aluminum and alumina, and in the second case they observed the growth of tilted pores underneath the silica layer.

**Method 2**

Figure 4-2 shows a schematic representation of the steps involved in fabrication of the alumina microarrays by method 2. A thin Au-Pd layer (approximately 90 nm in thickness) was sputtered on one side of the alumina membrane. Au-Pd sputtering was performed using a Denton Vacuum Desk II Cold Sputter. The Au-Pd layer was used as a seed layer for electroplating. Commercial alumina membranes having 60 μm in thickness and 200 nm pore diameter were used. A copper TEM grid was placed on top of Au-Pd sputtered alumina membrane. Another mask (aluminum foil) was placed on top of the copper grid just to have enough Au-Pd material for making the electrical contact. This assembly was then inserted into the center of the vacuum chamber of a reactive ion etching apparatus (Samco Plasma Ion Etching System, model RIE-1C) and Ar plasma was used to etch the Au-Pd seed layer. The Ar plasma parameters were as follows: 10 mins, 13.56 MHz, 140 W, 10 Pa Ar, Ar flow rate = 12 sccm. After etching, an Au-Pd replica of copper grid was transferred to the membrane.

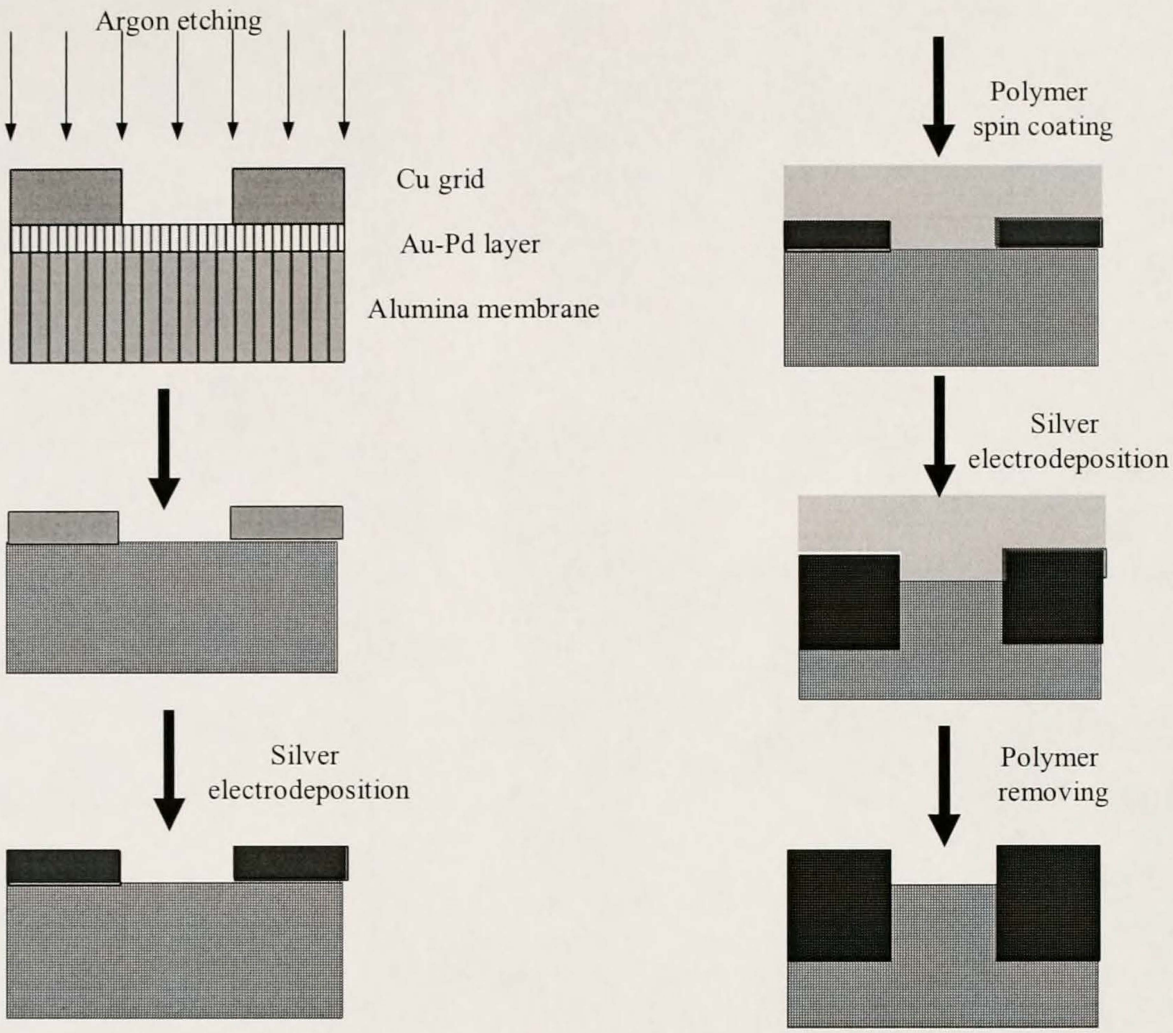


Figure 4-2. Schematic representation of the microarray fabrication by method 2.

Electroplating was accomplished using a EG&G PAR Model 273 galvanostat/potentiostat which was controlled using a CorrWare software package (Scribner Associates, Inc., Southern Pines, North Carolina). Electrochemical cells were prepared from a Teflon cell (17 mm inner diameter) and stainless still plate, which were held together using screws and o-rings (see Figure 4-3). To electrodeposit Ag into the membrane, the membrane was placed on Teflon tape, Au-Pd sputtered layer side up. Electrical contact was made to the membrane using copper adhesive tape. A silver wire was used as the counter electrode. Ag was then deposited at $-2$ mA $cm^{-2}$ for 8 minutes, resulting in a 1 μm thick of Ag on the Au-Pd layer. The cell was then disassembled. The spin coated polymer layer (ca. 3.5 μm thick) was added on the top of the electroplating

layer to prevent the leakage of plating solution through the membrane and suppress the lateral growth of the electrodeposits. The spin-coated membrane was place into the electrochemical cell again. In this case, the Ag electroplated layer was side down so that the open pores faced up. Additional Ag was then plated into the membrane at −0.50 mA $cm^{-2}$ for 90 minutes. After electroplating, the membrane was immersed into spin coating polymer remover for 10 minutes, rinsed with ethanol, and dried at room temperature.

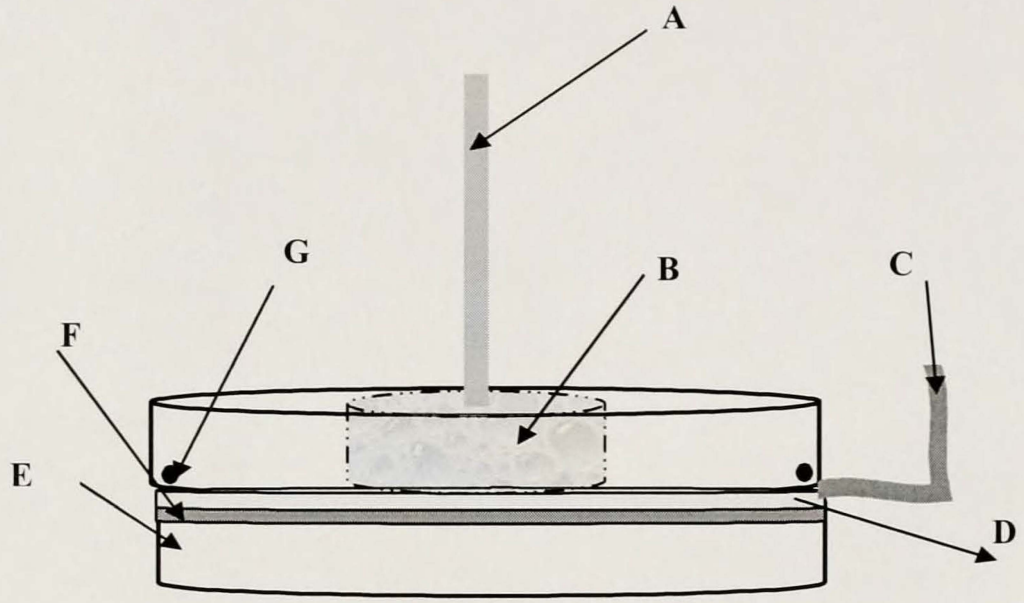


Figure 4-3. Electrochemical cell setup for silver electrodeposition: A, Ag wire counter and reference electrode; B, Ag plating solution; C, Cu foil; D, Au-Pd modified alumina membrane as working electrode; E, stainless steel plate; F, teflon tape; G, O-ring seal.

**Membrane modification for sensitivity studies**

For sensitivity experiments, five membranes with 0.5, 1.2, 50, 60 and 90 μm thickness have been prepared. They were prepared by electrochemically oxidation of aluminum, using the two step anodization method (52). Briefly, high purity (99.9998%) aluminum foils were electropolished at 15 V in a solution with the following composition: 95 wt. % $H_3PO_4$, 5 wt. % $H_2SO_4$ and 20 g/L $CrO_3$,at 70 $^0$C and for 10 minutes. The electropolished aluminum foils were then anodized at 50 V using 5%

oxalic acid as the electrolyte. The anodization was conducted at $0^0$C, for 15 hours. The first film of the membrane was dissolved away in an aqueous solution that was 0.2 M in $CrO_3$ and 0.4 M in $H_3PO_4$, at 60-70 $^0$C. The second anodization step was carried out in exactly the same conditions (referring to the voltage applied and the electrolyte solution used) as the first step. The time of the anodization in the second step varied for the five membranes from 20 minutes to 16 hours, resulting in formation of highly ordered nanoporous alumina membranes having pore diameter of 75 nm and thicknesses between 0.5 and 90 μm. The aluminum that was not oxidized was dissolved into a saturated $HgCl_2$ solution, except for the case of 0.5 and 1.2 μm thick membranes due to their more susceptibility to fragment into the small pieces.

A sol-gel template synthesis method was used to deposit silica nanotubes (with a wall thickness ~ 3 nm) within the pores of the alumina films (173,174 ). First, a sol-gel silica precursor was prepared by mixing absolute ethanol, TEOS and 1 M HCl (50:50:1). This solution was allowed to hydrolyze for 30 minutes. Alumina template membranes were than immersed into the sol-gel for 1 minute under sonication, after which they were air dried for 10 minutes at room temperature and cured in the oven for 12 hours at $150^0$C. The inside walls of the silica nanotubes were reacted then with APTES, a silane with an amino terminal group. The silica nanotube membranes were immersed into an ethanol-based solution which contained 6% APTES and 6% pH 5.1 acetate buffer solution. The membranes were kept in solution for 10 minutes under vacuum followed by 20 minutes in ambient air at room temperature. They were dried under nitrogen and cured at 120-$130^0$ C under vacuum. Amino groups react with the isothiocyanate (175). This approach was used to covalently bind rhodamine B to the silica nanotube membranes (see Figure 4-

4). The amino modified silica nanotube membranes were immersed in a solution of 1 % (wt) rhodamine B isothiocyanate in DMF for 16 hours in the vacuum, under nitrogen. The rhodamine B modified membranes were washed in DMF, chloroform and ethanol. The washing was performed for 10 minutes under sonication in each solvent.

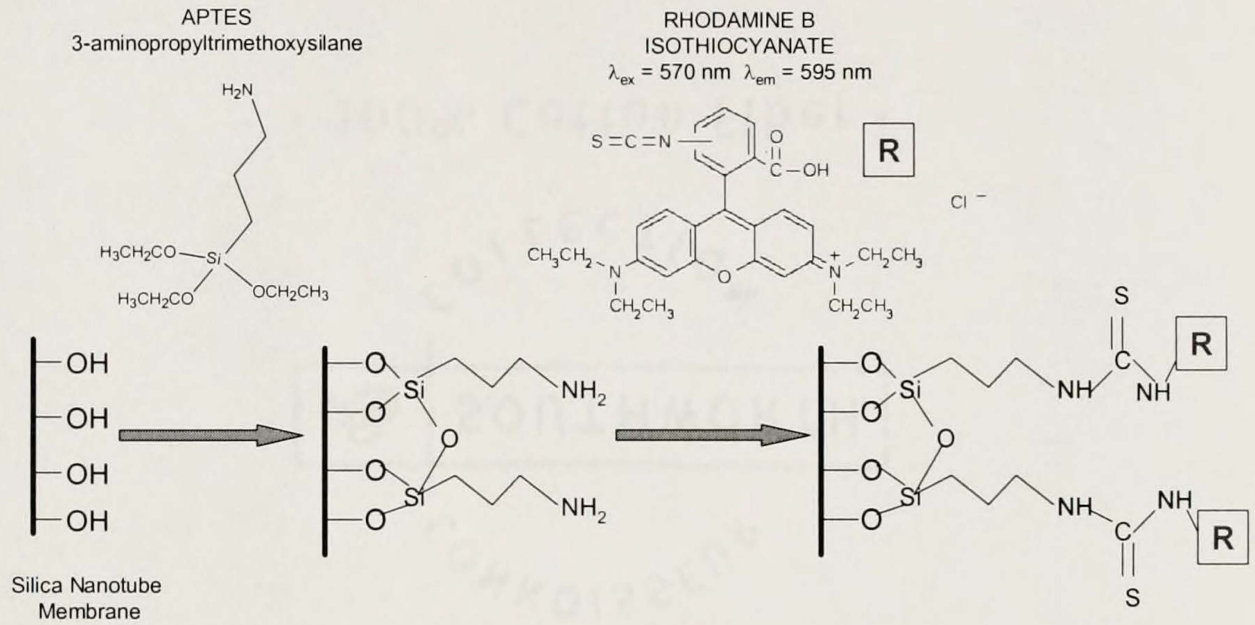


Figure 4-4. Modification steps for sensitivity studies.

As a control experiment we modified a piece of glass with rhodamine B in the same conditions as the alumina membranes. The glass was initially cleaned in a piranha solution (3:1 $H_2SO_4$:30% $H_2O_2$) at $90^0$C and washed copiously with deionized water.

Fluorescence spectra of the alumina membranes and glass modified with rhodamine B were taken using a Zeiss fluorescence microscope. The Rhodamine B dye was excited using 570 nm light and the emission was monitored using a 590 nm band pass filter. The dye was excited while simultaneously monitoring the emission with a fluorescence detector for 30 ms.

**Microarray modification for selectivity studies**

The alumina microarrays made by method 2 were used to investigate their selectivity, in terms of screening for antibody specificity. Again, a silica thin film was deposited on the pore walls of alumina membrane-based microarrays. These were immersed into a ethanolic solution that was 5% in an aqueous acetate buffer with a pH of 5.1, and 5% in triethoxysilylbutyl aldehyde. The aldehyde groups react readily with the primary amines on the proteins to form a Schiff's base linkage (176,177 ). This approach was used to covalently attach the capture proteins, which in this case were human and mouse IgG's.

The proteins were spotted on the alumina microarrays using a 10 X microscope connected to a monitor, and a manual microinjection system (Brinkman, Westbury, NY). A volume of 10 μL of protein solution (0.2 mg/ml in PBS pH=7.4) was back loaded into a femtotip (Fisher Scientific, Pittsburgh, PA) and a compensation pressure of 50 psi applied. The tip was positioned using a micromanipulator until the tip touches the alumina surface. Due to the porous nature of the alumina, the dye is pulled into the islands through capillary action without the need for addition pressures. Once the surface was saturated with protein solution the tip was reposition to another spot and filled in a similar manner. After 12 hours incubation at $4^0$C, the arrays were immersed into a blocking PBS buffer solution that contained 1% BSA and 0.1 % Tween-20 for 3 hours. This step is necessary not only for blocking the unreacted aldehyde groups, but also for reducing the non-specific adsorption of the proteins (161). After washing thoroughly with PBS, the arrays were incubated in a solution containing the target proteins (a mixture of anti-human IgG labeled with Alexa 488 dye and anti-mouse IgG labeled with

Alexa 594 dye, both having a concentration of 1mg/ml in PBS). After 12 hours of incubation, the arrays were washed three times with PBS and then twice with deionized water.

Fluorescence microscope imaging was performed in order to evaluate the selectivity of the alumina-based microarrays. The Alexa 488 dye was excited with 495 nm light and the emission monitored using 515 nm band pass filter. The Alexa 594 dye was excited using 590 nm light and the emission monitored using a 590 nm band pass filter. After individual image acquisition, the fluorescence images for each dye were overlaid. Also an optical image of the surface was acquired using reflected light from the surface.

## Results and Discussions

### Microarrays fabricated by method 1

Figure 4-5 shows scanning electron micrographs (SEM) of the porous alumina microarrays fabricated by method 1 at a low (A) and higher (B) magnification. As can be seen in the SEM image, the porous alumina films are very distinct areas on the polymer/Al surface. The pores of the alumina film are not highly ordered in this case, due to the fact that the anodization process took place only in one step and for a very short period of time (20 minutes). Uniformly cylindrically pores can be obtained by using a two-step anodization method (52).

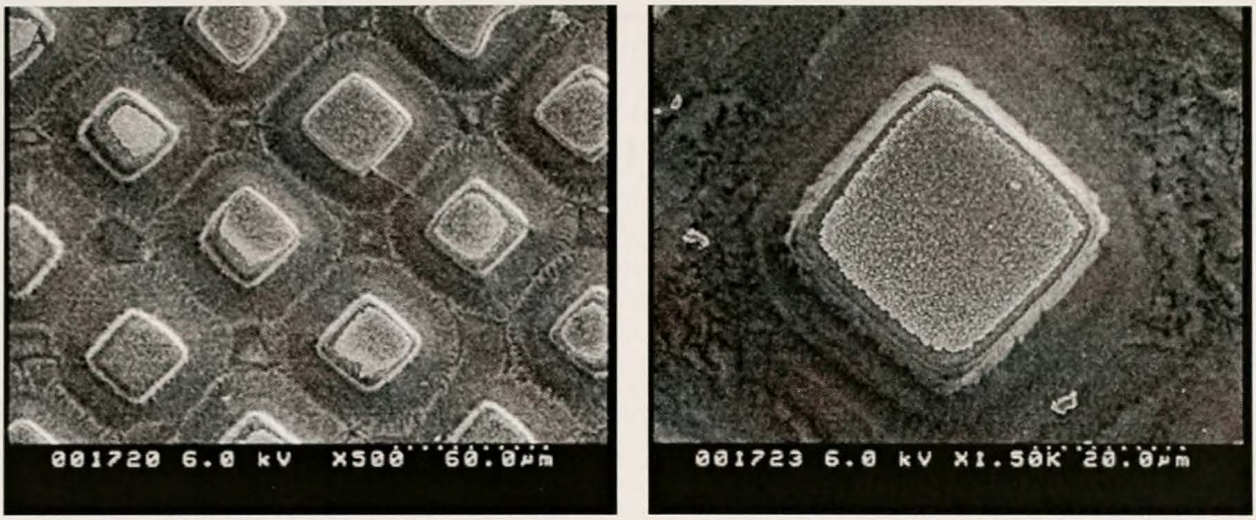


Figure 4-5. Scanning electron micrographs of the porous alumina microarrays fabricated by method 1 at a low (A) and higher (B) magnification.

**Microarrays made by method 2**

Figure 4-6 A shows the SEM image of the silver patterned porous membrane. The silver metal was not electrodeposited throughout the whole length of the membrane; it was deposited only along on a distance that represents 5% of the membrane thickness (see Figure 4-6 B). The possibility of using commercially available alumina membranes presents an advantage of this method. For quantitative studies, however, because of poor homogeneity of the pores diameter in these alumina membranes, one will have to use membranes prepared in house with highly ordered pores. These membranes will have to be patterned by method 2.

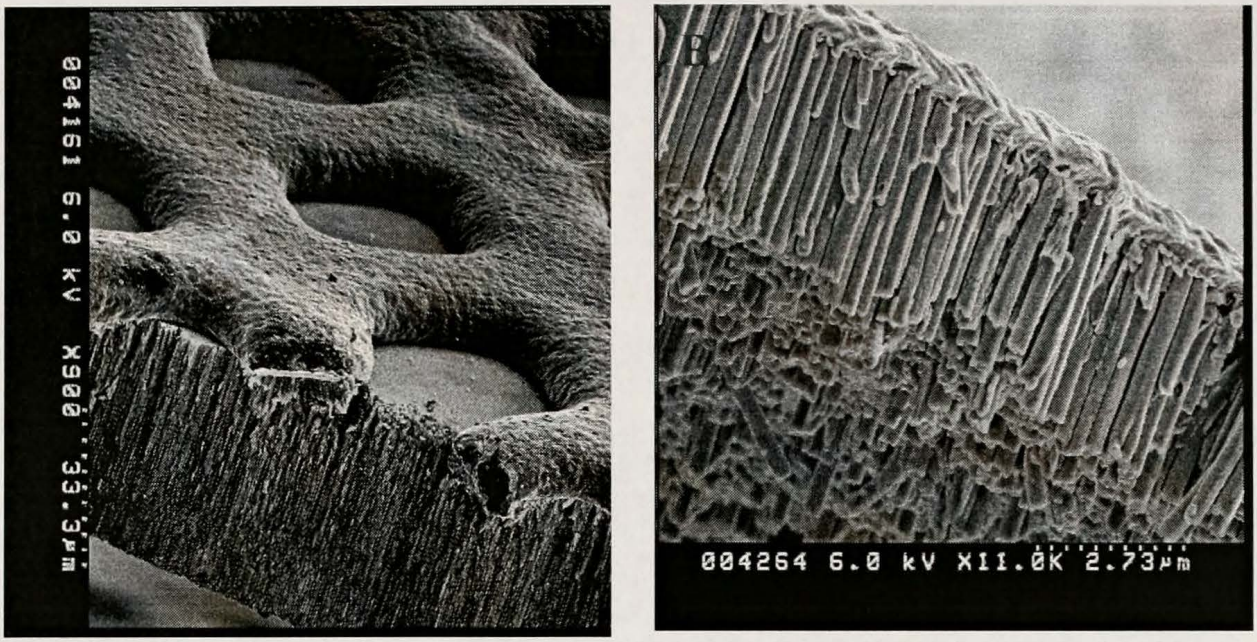


Figure 4-6. Scanning electron micrographs of the porous alumina microarrays fabricated by method 2: A, Ag patterned on porous alumina and B, Ag rods after dissolving the membrane

**Effect of the silica on the sensitivity measurements**

Although silanes can be attached directly on the alumina surfaces, we found that the fluorescence signal is enhanced if a thin film of silica is deposited primarily on the pore walls of the membrane (Figure 4-7). The silica film introduces a higher density of hydroxyl groups on the surfaces, which provides a higher reactive surface area for further modification. The fluorescence spectra in Figure 4-7 show that for samples modified with silica, the fluorescence signal is approximately 7 times higher than for samples modified initially only with the silanes.

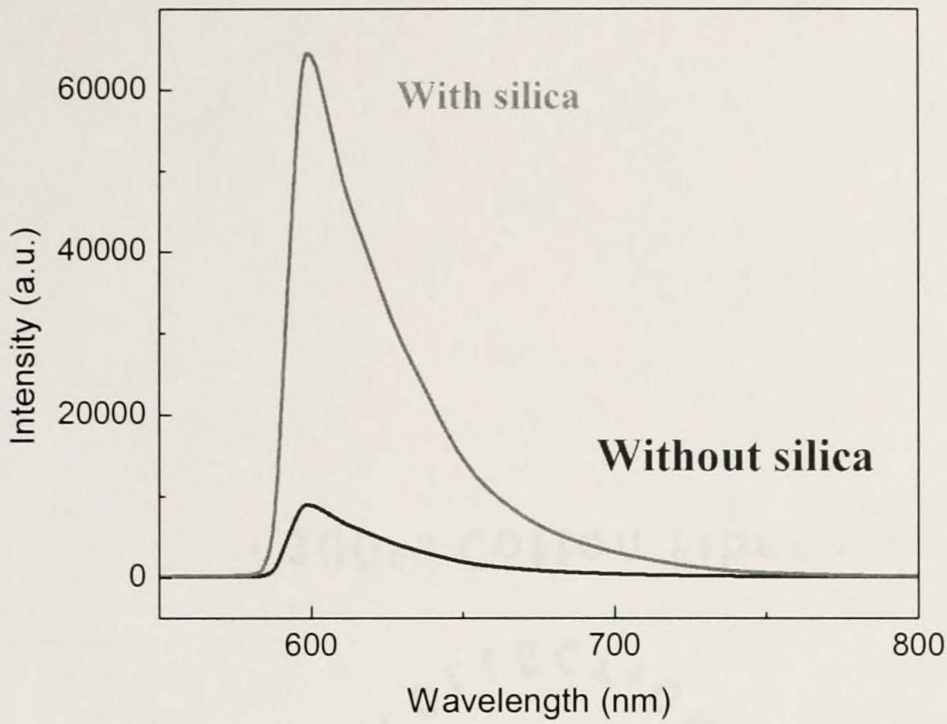


Figure 4-7. Fluorescence spectra for a rhodamine B-APTES-alumina sample with (green) and without (red) silica.

**Sensitivity**

The graph in Figure 4-8 shows the relative fluorescence coefficient for rhodamine B-modified membranes of 0.5, 1.2, 50, 60 and 90 μm thickness. We defined the relative fluorescence coefficient, α, as the ratio between the fluorescence intensity of the dye modified membrane and the glass slide modified in the same way. As we expected, the 3D structure of the alumina membranes leads to a higher sample loading capacity, yielding an enhanced signal. Depending on the thickness of the membrane, the signal can be enhanced as much as 416 times for a 90 μm thick membrane.

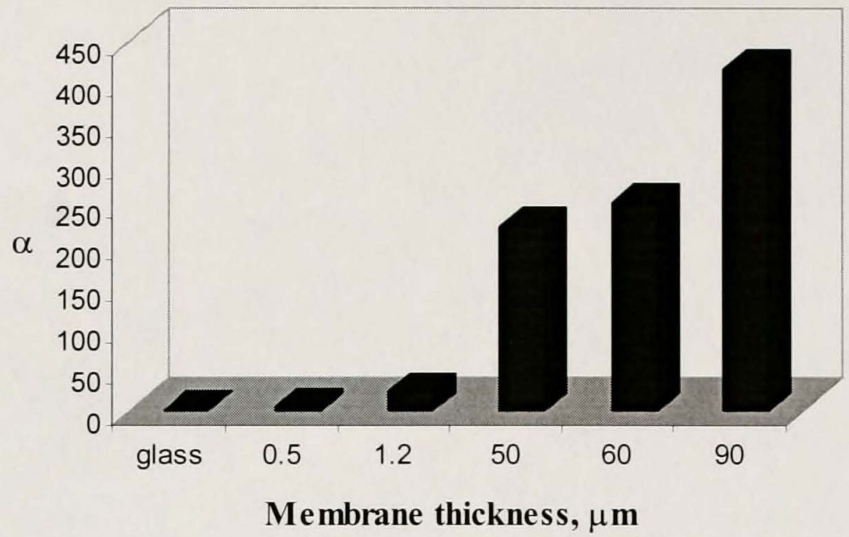


Figure 4-8. Relative fluorescence coefficient for rhodamine B-modified membranes of different thicknes.

**Selectivity**

As an application for the porous alumina-based microarrays we have screened the arrays for antibody specificity. After capture proteins were immobilized (human and mouse IgG's), the arrays were probed with a mixture of the target proteins (anti-human IgG-Alexa 488 and anti-mouse IgG-Alexa 594). The left side image of Figure 4-9 represents an optical image of a 350 μm x 350 μm section of the microarrays showing the spots where we immobilized the capture proteins, and the right side image shows the fluorescence image acquired after the imobilization of the target proteins. It can be seen from these images only the spots containing the capture proteins were highly fluorescent, indicating that the proteins were immobilized and able to retain their functional properties on the porous surfaces. The spots where no capture proteins were immobilized are lightly visible, indicating some nonspecific binding on the alumina surface.

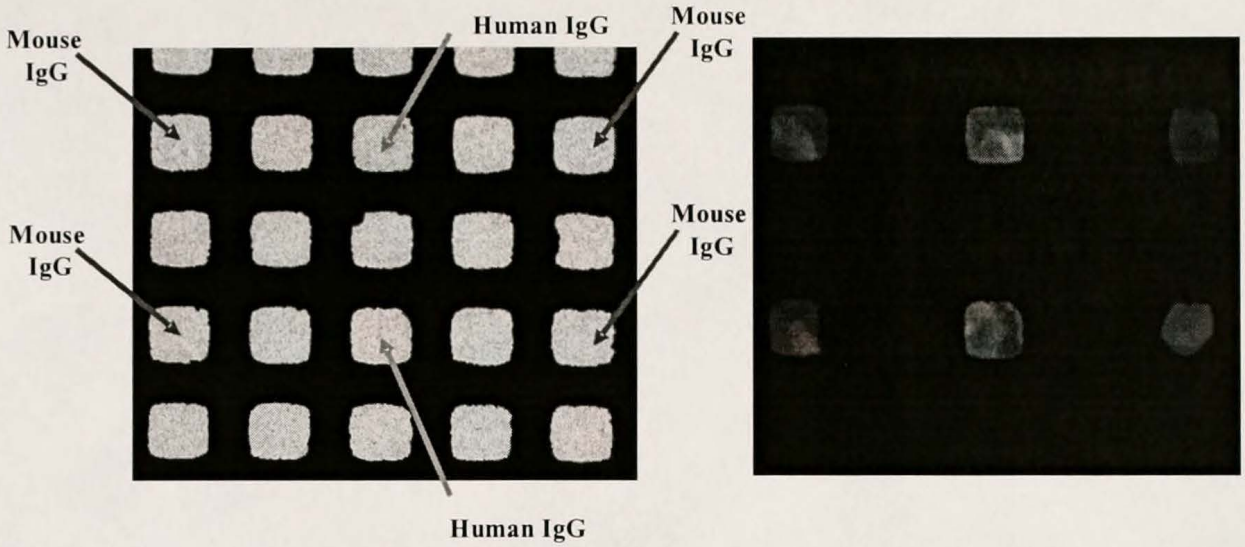


Figure 4-9: Optical (left) and fluorescence (right) image of a 350 μm x 350 μm area of the microarrays after immobilization of the target proteins.

Investigations of the fluorescence intensity profile (Figures 4-10 and 4-11) denoted cross-reactivity between the human and anti-mouse IgG, and mouse and anti-human IgG respectively. The uneven peaks in the intensity profile graphs are the results of both an inhomogeneous delivery of capture proteins using the manual injection system and the disordered structure of porous alumina. These drawbacks can easily be overcome by using a automatic injection system and a very highly ordered pore alumina support. That is, high uniformity of the porous support is one general demand for quantitative protein immobilization; both geometry (pore size) and morphology (pore shape, level of branching) affect the physical properties of the protein microarrays and thus their performances and characteristics (171).

One important feature of our microarrays is that the arrays are very well defined on the platform. They are separated from each other by either Al (method 1) or Ag (method 2). This eliminates the tendency of the samples to spread out, which is a main issue in the microarray technology.

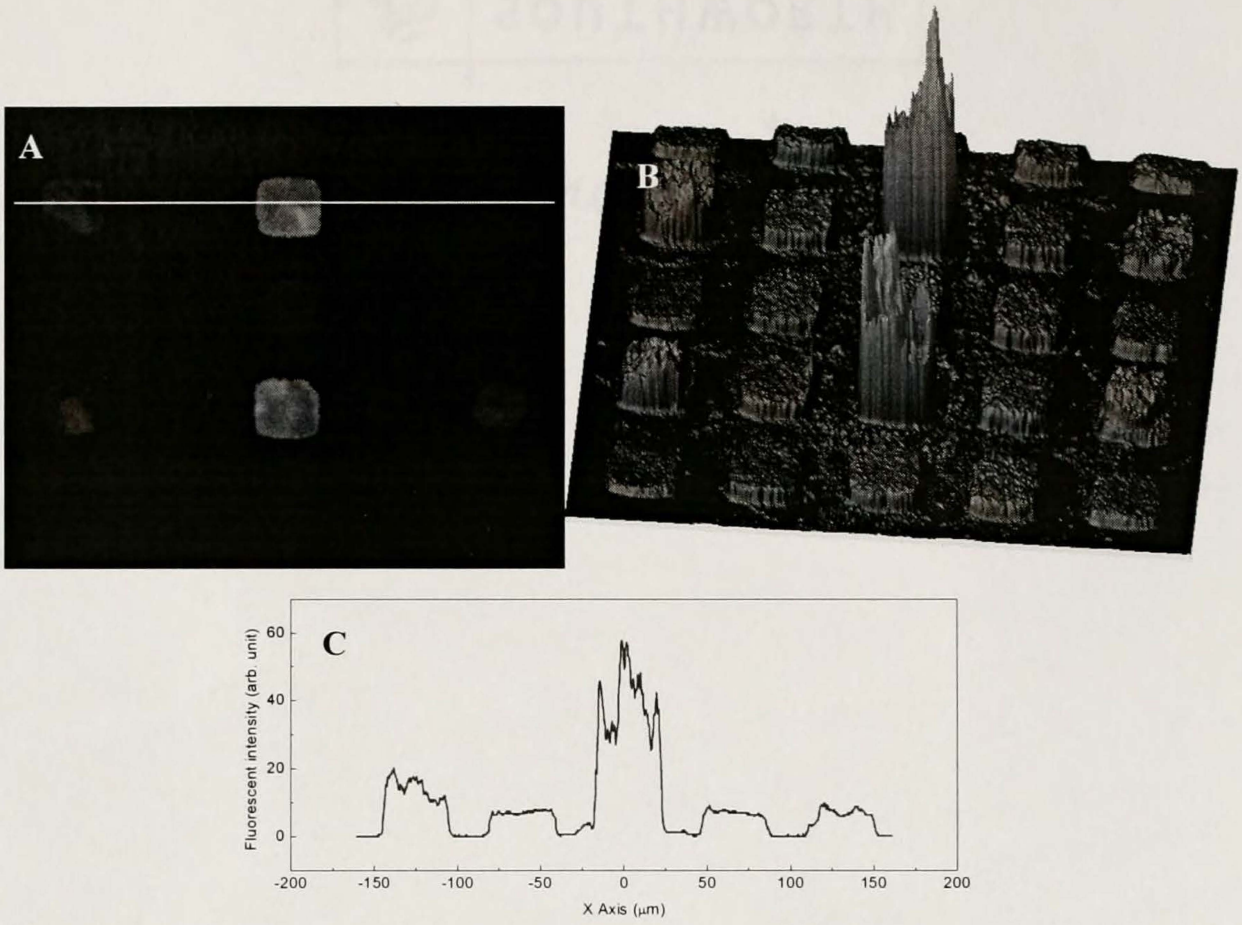


Figure 4-10. Excitation with 495 nm light: A, 2D fluorescence image; B. 3D fluorescence image; C, fluorescence intensity profile.

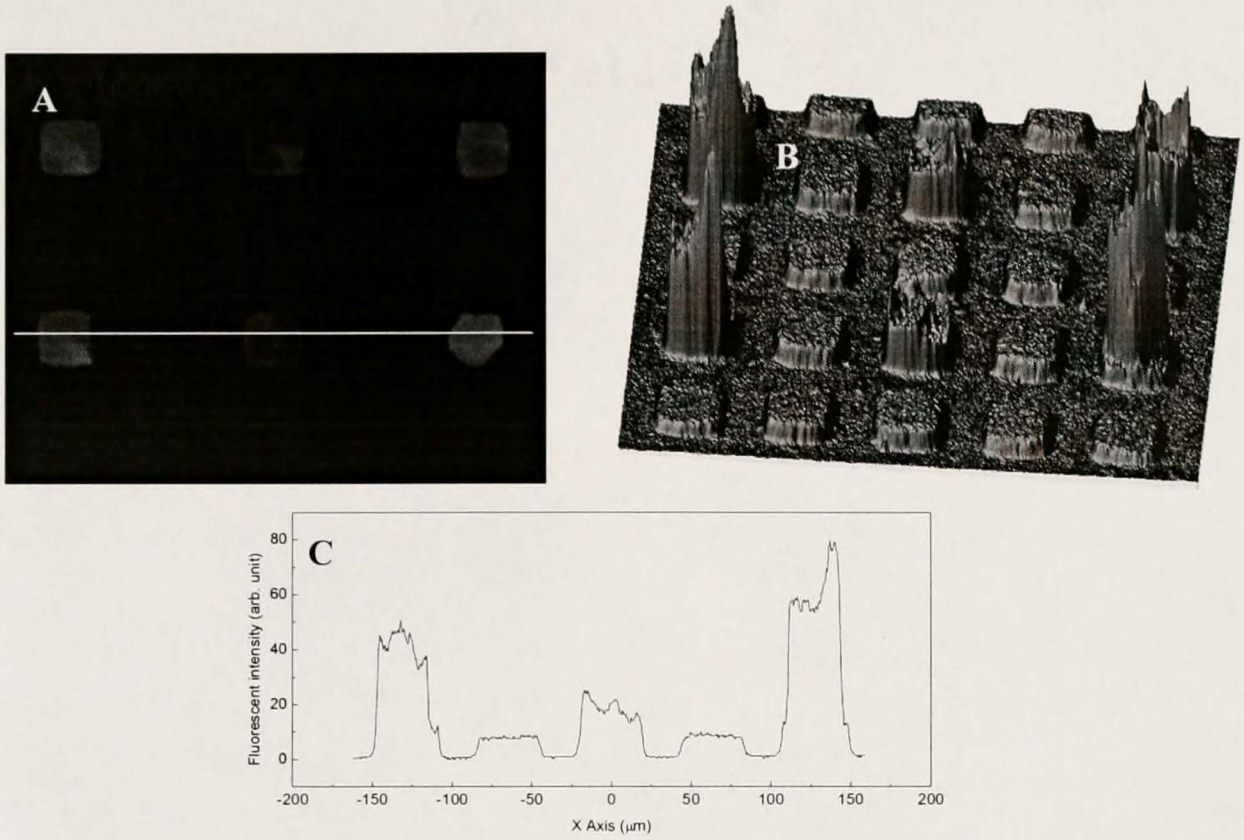


Figure 4-11. Excitation with 590 nm light: A, 2D fluorescence image; B. 3D fluorescence image; C, fluorescence intensity profile.

## Conclusions

In summary, we report here two methods of fabrication of 3-D porous alumina-based microarrays. We showed the advantages of using these arrays in terms of sensitivity and the importance of using silica nanotubes for signal enhacement. The application of these microarrays in antibody specificity screening has been shown also. The arrays obtained by method 2 being opened at both sides, can be incorporated into microfluidic devices. The electrodeposited Ag rods confer to the membrane a greater mechanical stability.

The shape and the dimensions of the arrays can be varied by choosing different grids (with different shapes and sizes) as masks. Once we have a grid with features of nanosize dimensions, the microarrays will become nanoarrays, and a greater number of

samples can be spotted on the same surface. Furthermore, the sample loading capacity can be controlled by varying the thickness and the pore diameter of the alumina membranes. The uniformity of the spot intensity profile can be improved by using alumina membranes with very highly ordered pore diameter distribution.

The ability to make protein arrays on a surface with very well defined features and morphology should increase the capabilities of researchers to study protein interactions on a whole proteome scale using the array technology.

CHAPTER 5
PROTEIN SENSING WITH SINGLE NANOPORE MEMBRANES

## Introduction

There has been a big interest in constructing single molecule sensors based on nanopores. The principle of the sensor operation is based on the nanometer opening of the pore which is comparable to the size of molecules to be detected (178). When a molecule enters the pore, the pore is temporarily blocked, which can be observed as a significant temporary reduction in the ion current passing through the pore. The device operates therefore as a Coulter counter on a single molecule level (178). This type of sensor has been constructed on the basis of a protein α-hemolysin and its functioning was demonstrated for DNA analysis (118,179, 180). The nanopore sensor enabled determination of the length distribution as well as chemical composition of DNA strands in a solution, which built hopes for single-nanopore super fast DNA sequencing (181,182). A further major advance was made in the group of Hagan Bayley in engineering a biosensor that is capable of identifying individual DNA strands with single-base resolution. Each biosensor element consists of an individual DNA oligonucleotide covalently attached within the lumen of the α-hemolysin pore to form a "DNA-nanopore". The other single strand — the analyte — is in the electrolyte solution. This system could distinguish between complementary and non-complementary DNA strands, making it specific for a given DNA sequence. This biological pore-bilayer system is however very fragile (178). A more realistic approach to applying this idea on an

industrial scale would involve replacing the protein channel with a durable, robust, synthetic nanopore. Detecting single DNA molecules and characterizing their distribution was demonstrated with several types of solid state nanopores but none of them was equipped with recognition sites specific for a given biomolecule (183-187).

Here we present a 3-dimensional nano-immunoassay based on a single pore system, capable of probing protein-protein interactions and detecting warfare agents. The principle of operation of this device is very simple and based on an intuitive and checked experimentally fact that transport properties of a nanopore depend very strongly on the pore walls surface characteristic (119, 188,189). If an analyte to be detected binds to the recognition sites placed on the pore walls and the pore has an opening of several nanometers, the transport characteristic of a nanopore, expressed for example in a form of current-voltage (I-V) characteristic, will be significantly changed. Basing the detection signal on I-V curves rather than time series will significantly simplify the recording as well as data analysis process. I-V curve represents average transport properties and as such is much less demanding concerning the noise-free environment for recording than time series, which is the main detecting signal for Coulter counter based devices (178).

As a base for the 3-dimensional nano-immunoassay we chose polymeric membranes covered electrolessly with gold. Gold surface enables easy modification of chemistry of the pore walls by application of a thiol chemistry (44,190). The pores in polymer membranes were prepared by the track etching technique, which is based on irradiation of polymer films with heavy ions and subsequent development of the latent tracks by chemical etching (37). The technique gives amazing freedom in preparation of pores of various shapes and as small diameters as several nanometers. For preparation of

our 3-dimensional nano-immunoassay we chose asymmetric, conical shape of the pore (120-128). A conical pore has a much lower resistance than an equivalent cylindrical pore of the same limiting diameter. Additional advantage of using asymmetric pores is that we limit the interactions zone in the pore, which makes the sensor's response faster and is expected to lower the detection limit. The pores were subsequently covered electrolessly with gold (40), which resulted in formation of gold tubes (123). The principles of the nanodevice operation were shown first with the system biotin-streptavidin, which is known to have a very high binding constant, and the binding is regarded as practically irreversible (191). We also checked applicability of the device for sensing protein-protein interactions on the example of protein G modified Au tubes. Protein G is a cell surface-associated protein isolated from Goward Group G Streptococci and binds with high affinity immunoglobulins (IgG's) (192,193). In our experiments we have used cat IgG which has no affinity for protein G, and horse IgG which has a strong affinity to the protein G (194,195). It is also shown the potential of this nanopore system in building sensors for warfare agents, on the example of ricin.

## Experimental

### Materials

We used 12 μm thick polyethylene terephthalate (Hostaphan RN 12, Hoechst) foils, irradiated with single swift heavy ions (e.g. Au, Xe, U) (196) of 2.2 GeV kinetic energy (UNILAC, GSI Darmstadt). To obtain conical pores, the single ion irradiated polymer foils were mounted between two chambers of a conductivity cell and etched from one side in 9 M NaOH, as described elsewhere (120,122,128). The chemical etching was monitored by applying a voltage of 1 V across the membrane. It allowed detecting of the breakthrough moment, when the pore was etched through. Etching for a longer time

resulted in increase of the pore diameter. The diameter of the large pore opening was estimated on the basis of the so called bulk etch rate, which for PET at 9 M NaOH and room temperature is 2.13 nm/min (120). For example, 2 hours etching results in 520 nm pore diameter. The diameter of the small opening was obtained on the basis of conductivity measurements assuming a conical shape of the pore (37). The pores we prepared had a diameter of ~40 nm. Plating the nanopores with gold resulted in final diameters varying between 5 and 20 nm, function of the gold deposition time. The big diameter of the pores did not change significantly.

**Electroless plating of PET membranes**

The electroless plating was performed according to the procedure described elsewhere (40). The plating process was performed at 3.6 $^{0}$C, and pH 9.9. Tipically, after 2.5 hours of plating, the gold layer has an approximative thickness of 4 nm.

**Proteins**

Lysozyme, streptavidin, bovine serum albumin (BSA), protein G - biotin labeled, cat IgG and horse IgG were purchased from Sigma Aldrich. EZ-Link Biotin-HPDP or (N-(6-(Biotinamido)hexyl)-3'-(2'-pyridyldithio)-propionamide was bought from Pierce. Ricin Toxoid and Biotinylated Anti-Ricin IgG were bought from Toxin Technology, Inc., Sarasota, FL. Ricin Toxoid has been toxoided using glutaraldehyde crosslinking and has less than 1% of the original toxicity.

**Experimental Setup**

The single conical-Au-nanotube membrane was mounted between two halves of a conductivity cell (128), and a Ag/AgCl electrode was inserted into each half-cell solution. Current-voltage (I-V) curves associated with ion transport through single nanotubes and transient time series were obtained using an Axopatch 200B (Axon Instruments). The

working Ag/AgCl electrode was in the half-cell solution facing the large-diameter opening, and the potential of this electrode was controlled relative to the counter Ag/AgCl electrode in the opposite solution. The potential was stepped in 100 mV steps through the desired potential range, and the resulting transmembrane ion current was measured. Ion current time series were recorded at 10 kHz sampling frequency and filtered with a Bessel filter at 2 kHz.

**Results and Discussions**

In investigation the biotin/streptavidin system, the Au tubes were modified with biotin by incubating them in ~ 0.2 mM EZ-Link Biotin-HPDP in ethanol (1% DMSO) at room temperature for 24 hours. The tubes, which we used for that series of experiments had the small opening typically of ~5 nm, while the big opening of conical pores was kept ~ 0.6 μm. With that size of the pores, binding of streptavidin was expected to block the current totally. Streptavidin would "cap" the pore and prevent the ion flow. Figure 5-1 shows the results obtained for sensing lysozyme with a single conical gold nanotube. The I-V characteristic of a single Au tube before and after modification with biotin are showed in Figure 5-1 A. As expected, the biotin modification did not change the I-V curve very strongly – the low molecular weight biotin did not diminish the size of the pore in a significant way. Before subjecting the pore to a streptavidin solution we checked how the pore "reacts" and "sees" other proteins, which do not bind to biotin. Figure 5-1 B and 5-C shows ion current in time through a biotin modified Au tube in the absence (B) and in the presence of 100 nM of lysozyme (C). The protein was added to the chamber facing the small opening of the pore. The experiments were performed at pH 7 where lysozyme is positively charged (pI ~ 11) (46). The net electric charge allows the protein to follow the direction of external electric field resulting in translocation

through the pore. As the pore diameter is comparable with the protein size we observe transient blockages of the pore, which we attribute to single lysozyme molecules passing through the pore.

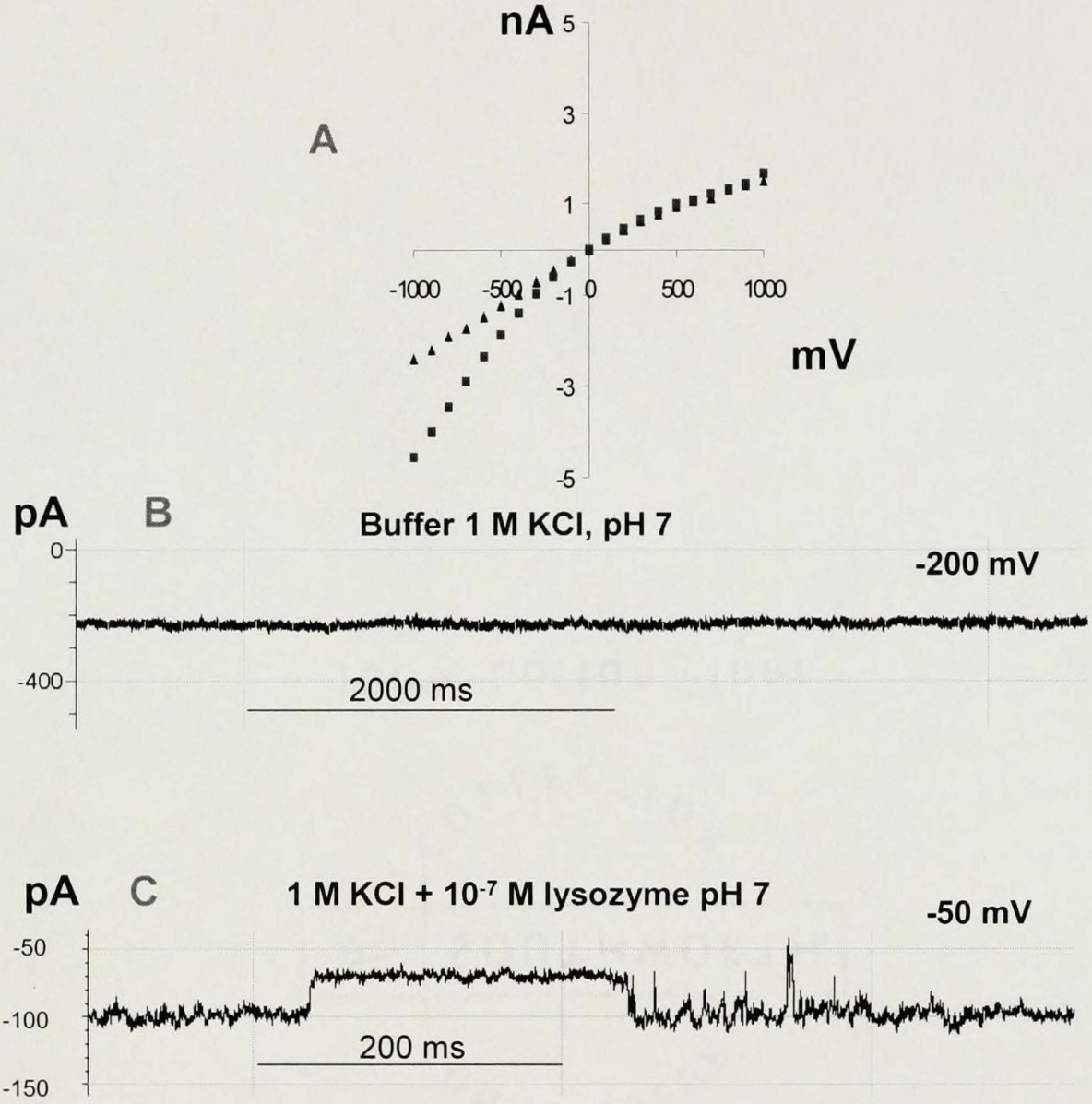


Figure 5-1. Sensing lysozyme with a single conical gold nanotube. (A) Current-voltage characteristic of the Au nanotube before (red points) and after modification with thiolated biotin (blue points). The diameters of the pore opening are 5 nm and 0.6 μm, respectively. (B) Ion current versus time through the Au nanotube modified with biotin recorded at 1 M KCl, pH 7. (C) Ion current versus time as in (B) at presence of 100 nM lysozyme in contact with the small opening of the pore.

It is important to notice that our sensor also functions as the Coulter Counter for molecules and can be used for stochastic sensing in case when the analyte does not interact with the pore walls. Identical results were obtained for the another un-binding protein - bovine serum albumin - as the analyte.

After washing the chamber with a buffer solution, we exposed the membrane to a streptavidin solution. The protein was again added only on one side of the membrane with the small opening. Figure 5-2 shows ion current recorded before and directly after exposure of the membrane to 180 pM streptavidin.

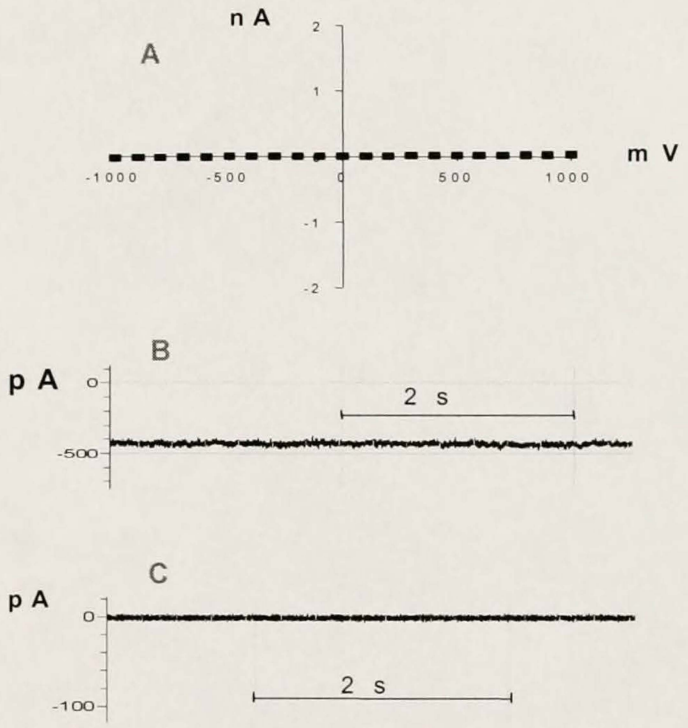


Figure 5-2. Sensing streptavidin with a single conical gold nanotube. (A) Current-voltage characteristics of a single conical Au tube modified with SH-biotin at presence of 180 pM streptavidin added on the small side of the conical nanotube. (B) Ion current in time through a single Au nanotube modified with biotin, recorded at 1 M KCl, pH 4.5, recorded at -1000 mV. (C) Ion current in time as in (B), at presence of 180 pM streptavidin.

As can be seen in Figure 5-2 A and C the current shut off totally, and was not recovered after washing with buffer solution or lowering pH to strongly acidic conditions (it is known from affinity chromatography that acidic conditions weaken the protein-protein bonding (197)). The membrane recovered only after exposure to UV light for 24 hours, which resulted in breaking the thiol bonds and washing out biotin and streptavidin.

We prepared a series of pores with the small diameter ~ 5 nm and exposed them to solutions of different concentration of streptavidin. The questions we asked are (i) what is the detection limit and (ii) whether the response time of our sensor is streptavidin concentration dependent. In order to be detected, the analyte streptavidin must randomly walk through the solution until it encounters, and binds to, a biotin at the mouth of the nanotube. As such, the time required for blockage, $\tau_b$, should be inversely related to the concentration of streptavidin (198), and Figure 5-3 shows that this is the case. While the $\tau_b$ values for the lowest concentrations are long, $\tau_b$ can be shortened by convectively transporting the analyte to the nanotube mouth. For charged analytes, electrophoresis provides a particular powerful way to apply convective transport (46,198). Indeed, Lee, et al. have shown that the time required to drive charged particles to the mouth of a nanopore can be controlled at will in this way (198).

The error bars in Figure 5-3 are associated with three measurements made with three different nanotube sensors. The error in $\tau_b$ increases with decreasing analyte concentration, which is not surprising given the random-walk nature of the response. However, since $\tau_b$ can be decreased by eletrophoretically driving the analyte to the nanotube (198), and since the error in $\tau_b$ is less for smaller $\tau_b$ values, it should be possible to obtain better reproducibilty at low concentrations if convective transport is used.

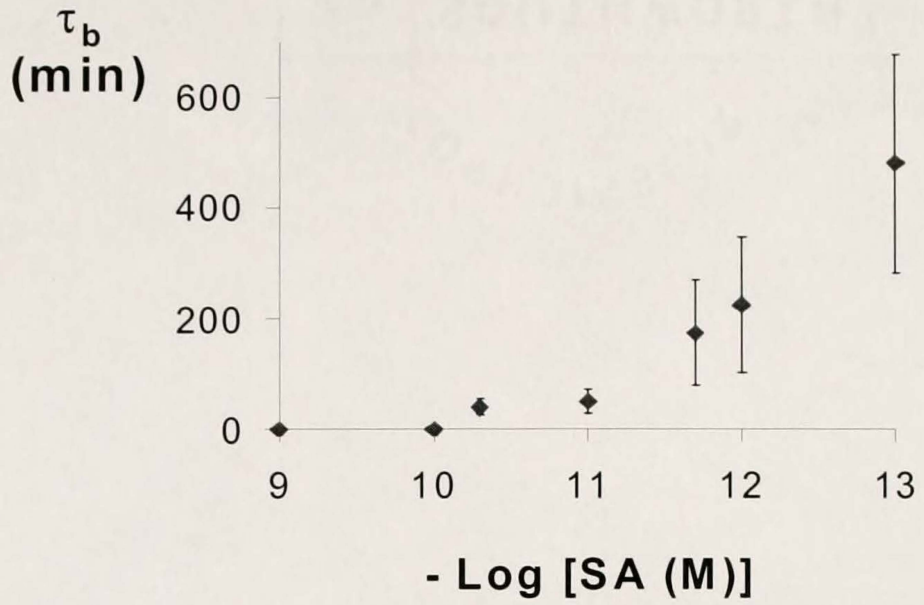


Figure 5-3. Blockage time vs. –log of the molar streptavidin concentration.

The well-studied system of biotin-streptavidin enabled us to show the potential of our nanoporous system, which subsequently was applied for building real nano-immunoassays on the pore wall. Nano-immunoassay requires normally performing a series of modifications, to expose the recognition site of interest. For example, if we want to immobilize protein G and subsequently study its affinity to various IgGs, we needed to develop as assay for a non-destructive attaching the protein to the pore wall. Figure 5-4 shows the modification steps we performed together with I-V curves recorded after every modification. Transport properties of the nanopores served as a probe for successful modifications. In the first modification step we again covered the Au tubes with biotin via EZ-Link Biotin-HPDP. Subsequently, the membranes were immersed in 2mg/ml streptavidin in PBS pH=7.4 solution for 24 hours at $4^0$C. The last modification step was the attachment of protein G onto the membrane using biotin-streptavidin chemistry. We immersed the membranes into 1mg/ml protein G-biotin labeled in PBS pH=7.4 solution at $4^0$C for 24 hours. Au tubes modified in this way enabled us to probe interactions of the protein G with cat IgG, which is known to have no affinity towards

protein G and of horse IgG with very strong binding affinities to protein G. The first case resembled our biotin modified tubes through which lysozyme was translocating (Figure 5-1). The experiments were again performed at the pH which assured a non-zero surface charge of IgG (pI of IgG is ~ 7.0).

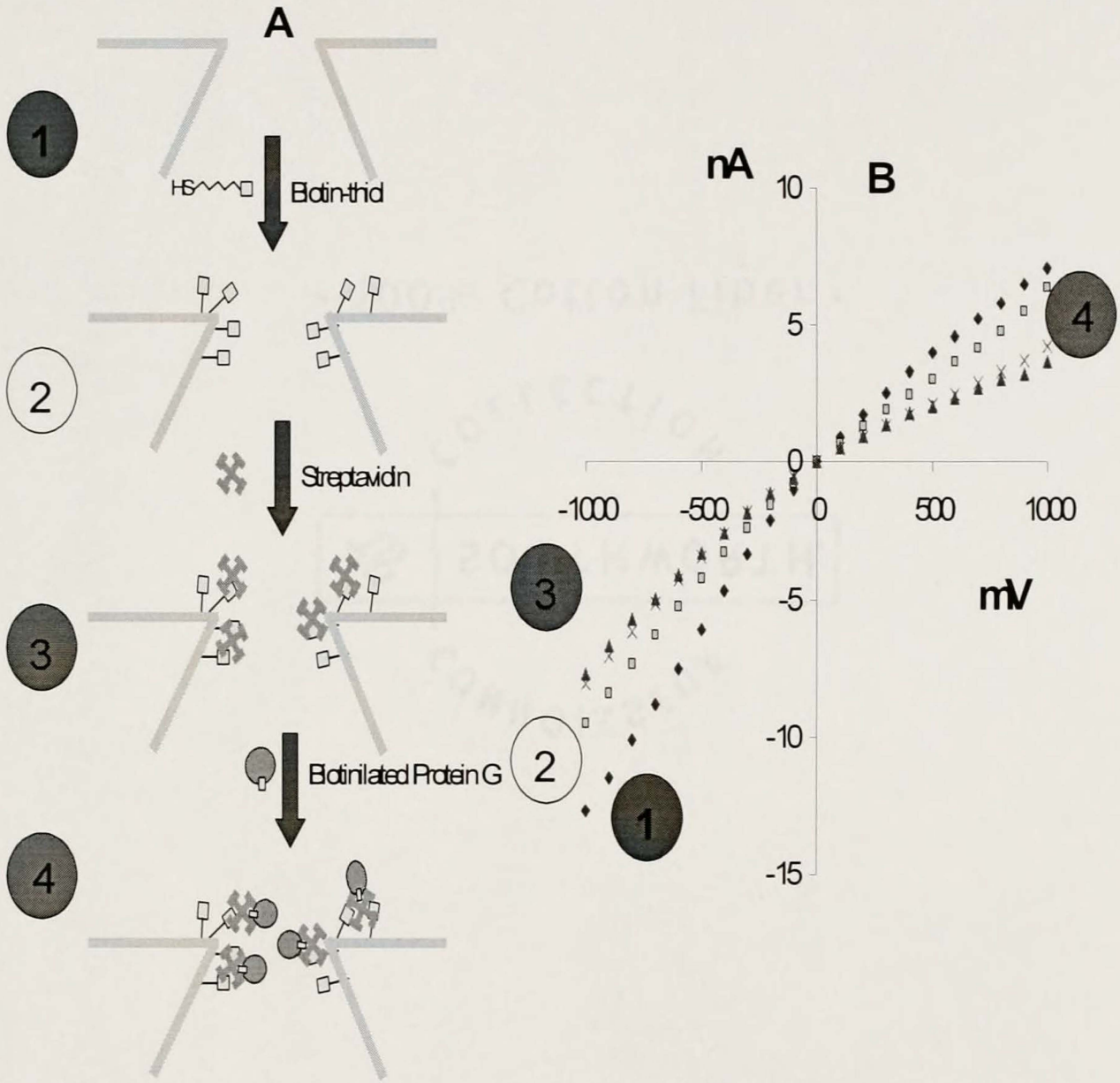


Figure 5-4. Chemical modifications of a single Au tube leading to preparations of 3 dimensional nanoimmunoassay for detection of IgGs and probing their interactions with protein G. (A) Schematic representation of the subsequent modifications of a single Au tube. (B) Current-voltage characteristics recorded at 1 M KCl, pH 7, performed after each modification step. The gold tube after modifications has diameters of ~15 nm and 0.6 μm, respectively.

Figure 5-5 A shows an I-V characteristic of a single Au tube with protein G, exposed to 100 nM cat IgG at pH 8.7. The cat IgG does not bind to protein G and the I-V curves remains the same. If one looks however at the time series of ion current at constant transmembrane potential, temporary blockages of ion current are observed. They correspond to cat IgG molecules passing through the tube (Figure. 5-5 B and C).

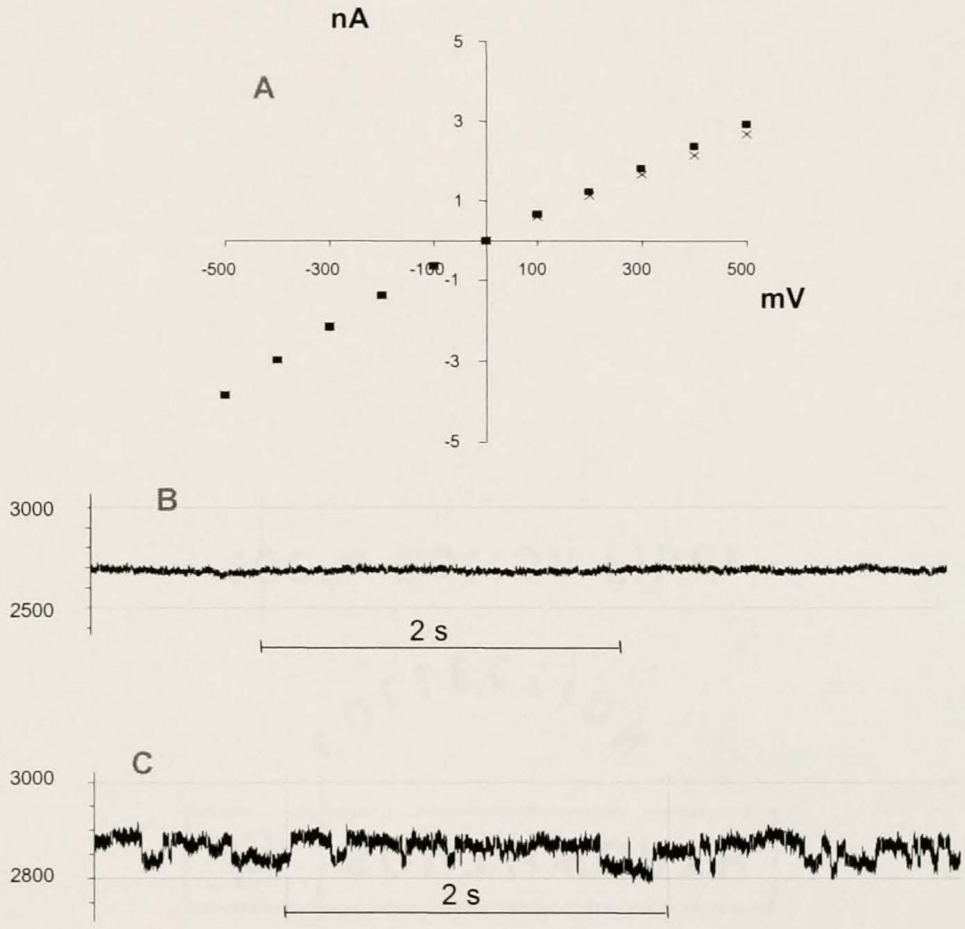


Figure 5-5. Sensing of cat IgG with a single conical Au nanotube modified with protein G as shown in Fig. 4. (A) Current-voltage characteristic of a single Au tube recorded at 1 M KCl, pH 8.7. Ion current in time recorded at 500 mV transmembrane potential before (B) and after (C) adding 100 nM cat IgG. The gold tube after modifications has diameters of ~15 nm and 0.6 μm, respectively.

On the other hand, after exposure the nanotubes to horse IgG, even at 10 times lower concentration that cat IgG, the pore was totally blocked (Figure 5-6). For 10 nM horse IgG concentration we waited 40 minutes to observe the blockage. A longer response time of this sensor, compared to the streptavidin shown before, results most probably from a higher molecular weight of the IgG and lower diffusion constant.

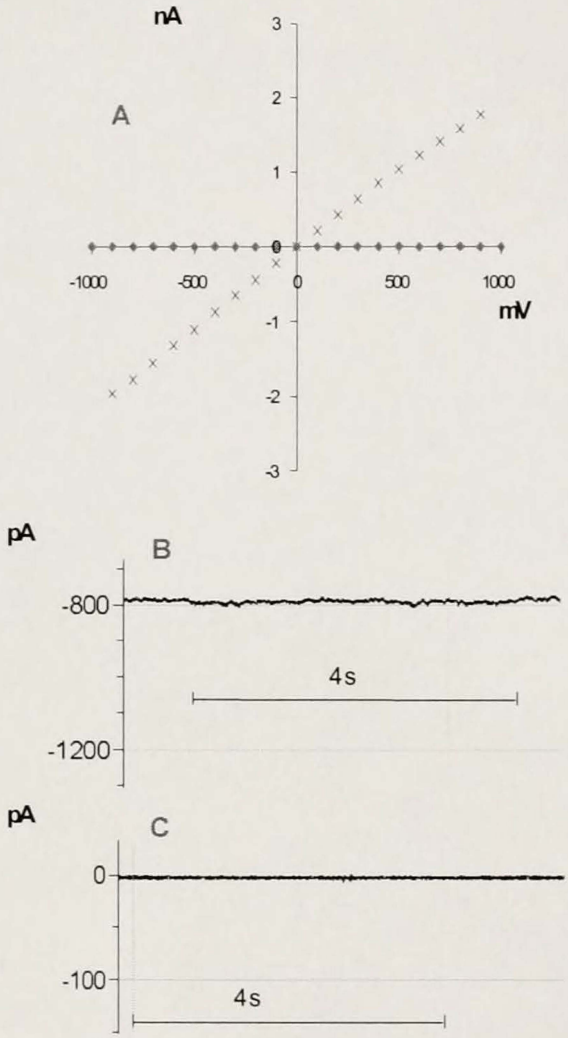


Figure 5-6. Sensing of horse IgG with a single conical Au nanotube modified with protein G as shown in Fig. 4. (A) Current-voltage characteristics of a single gold tube recorded at pH 4.4, 1 M KCl before (x) and after (•) adding 10 nM horse IgG. The gold tube after modifications has diameters of ~5 nm and 0.6 μm, respectively.

Finally, ricin (199) (molecular weight = 60 kDa) is a highly toxic protein and has been used as bioterror agent. However, the protein that we used had <1% of the toxicity

of the wild-type protein. Exposure of the anti-ricin-based sensor to ricin shuts down the ion current, whereas exposure to non-binding bovine serum albumin has no effect on the I-V curve. Figure 5-7 shows a set of I-V curves of an Au tube with anti-ricin on the walls before and after exposure to BSA and ricin. BSA and ricin have the same molecular weight of ~60 kDa, therefore, BSA served as a control for the ricin detection.

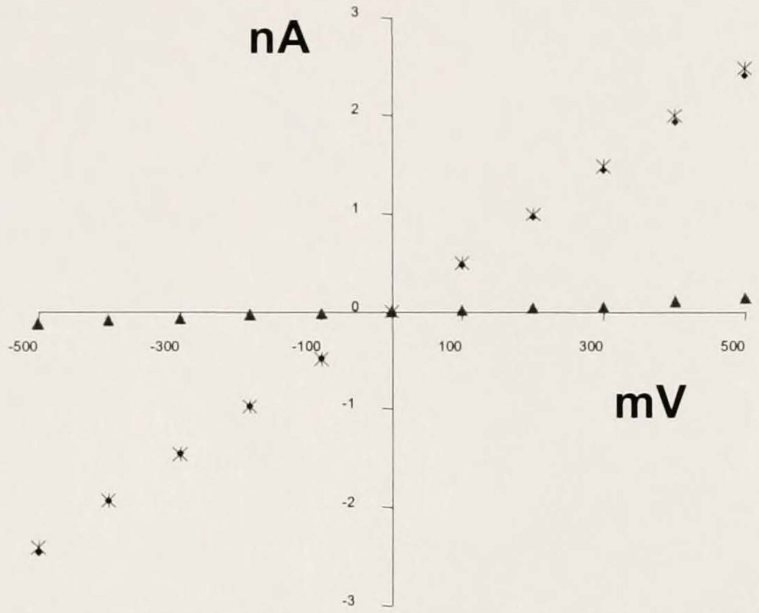


Figure 5-7. I-V curves for the ricin sensor in the presence of no protein (x), 100 nM BSA(♦), and ~100 nM ricin (•).

## Conclusions

We have demonstrated a new class of protein biosensors based on biofunctionalized conical Au nanotubes. The results reported here indicate that these biosensors can be both highly sensitive and highly selective. This sensor can be used for detection of any protein for which a nano-immunoassay can be developed. An important feature of the system is that it is no need for chemical pretreatment or labeling of the analyte to be detected. A nanotube with controlled surface chemistry can also be treated as a special 'probe' for surface properties of nanopores, not accessible by any other techniques.

# CHAPTER 6
# CONCLUSIONS

The main aim of the research presented in this dissertation has been the development of new nanostructures based on nanoporous membranes, and investigation of their applications as sensors and separation devices. A template synthesis method was used to produce nanotubes inside the pores of both aluminum oxide and polymeric membranes. After an introduction in the template synthesis method and the processes of fabrication of the porous membranes, the dissertation was centered on investigating new applications of these nanotube membranes. There were three applications of the nanotube alumina membranes explored, and one application of the single nanotube polymeric membranes was also examined.

Chapter 1 presents the development of alumina nanopore membranes that mimic the function of ligand-gated ion channels. In biological channels there are no electrodes, and the ion current is driven by an electrochemical potential difference across the cell membrane. This function of the ligand-gated ion channel is mimicked by applying a porous battery cathode film to one face of the hydrophobic alumina membrane and a porous battery anode film to the other face. Hence, in analogy to the naturally occurring channel case, this is a membrane with a built in electrochemical potential difference across the membrane. In the absence of the ligand (again, a hydrophobic ionic surfactant), the membrane is in its "off" state, and the electrochemical potential difference cannot be utilized to drive a transmembrane ion current. In contrast, when the ligand is detected, the membrane switches to its "on" state and the transmembrane battery discharges,

producing a corresponding transmembrane ion current. This concept could ultimately lead to a remote sensing technology where the battery discharge current is used to drive a device that signals that the ligand has been detected.

The application of silica nanotube membranes in selective separation of proteins is presented in chapter 2. A new separation method for protein separation via membrane facilitated transport selectivity is developed, based on introduction of the molecular recognition elements into the nanotube membranes. Two antibodies with different affinities for a protein (hevein in this case) are immobilized on silica nanotube membranes. The aldehyde silane is used as a linker for antibodies attachment. Hevein is labeled with green fluorescence protein (GFP). The rates of transport of the GFP-Hevein and red fluorescence protein (RFP) that was used as a control analyte are monitored. The transport of both proteins is recorded simultaneously at two different emission/excitation wavelengths. As a control experiment, membranes with immobilized antibody that does not have any affinity towards GFP-Hevein or RFP are used. Both the influence of pore diameter and the membrane thickness on the transport of GFP-Hevein and RFP are studied. These membranes selectively transport the protein (GFP-Hevein) that specifically binds to the antibody, relative to the other protein (RFP) that has no affinity for the antibody.

In Chapter 3 the silica nanotube membranes are investigated as a support used in the protein microarray technology. Two methods of fabrication of 3-D alumina-based microarrays are presented. These membranes represent distinct microfeatures on a robust platform, and they have cylindrical pores with monodisperse nanoscopic diameters. A

potential application in antibody specificity screening is explored, along with the studies of the sensitivity of the system.

Chapter 5 deals with a new class of artificial ion channels based on a synthetic membrane that contains a single conically shaped nanotube. These nanotube-based ion channels show a voltage-gating, or ion-current rectification, function completely analogous to biological voltage-gated ion channels. The membrane with a single conically shaped gold nanotube was prepared by the template method. The nanotube has a large-diameter opening of ~ 600 nm and a small-diameter opening of 2-3 nm. In the biosensing application, the nanotube-containing membrane is placed between the two chambers of a conductivity cell filled with an electrolyte. Electrodes present in each half-cell solution are used to apply a transmembrane potential and measure the resulting ion current through the nanotube. The internal surfaces of the nanotube are modified with a specific biochemical molecular-recognition agent (the "capture" agent, e.g., an antibody) which interacts specifically with a given biomolecule (the analyte) present in one of the contacting solution phases. The binding interaction between the nanotube-bound capture agent and the solution-phase analyte is transduced as a change in the ion current that flows through the nanotube. This new biosensing technology was demonstrated using biotin as the capture agent and streptavidin as the analyte and protein G as the capture agent and IgG as the analyte. The detection of a biological warfare agent (ricin) is also presented.

LIST OF REFERENCES


1. Bushah, B. In *Springer Handbook of Nanotechnology*; Bushah, B., Ed.; Berlin; New York: Springer-Verlag, 2004; p 2.

2. Freeman, R. G; Grabar, K. C.; Allison, K. J.; Bright, R. M; Davis, J. A.; Guthrie, A. P.; Hommer, M. B.; Jackson, M. A.; Smith, P. C.; Walter, D. G.; Natan, M. J.; *Science* **1995**, *267*, 1629.

3. Shipway, A. N.; Katz, E.; Willner, I. *Chemphyschem* **2000**, *1*, 18.

4. Rao, C. N. R.; Nath, M. *J. Chem. Soc. Dalton Trans*. **2003**, *1*, 1.

5. Tenne, R.; Zettl, A. K. Top. *Appl. Phys*. **2001**, *80*, 81.

6. Polysciences, Inc. 2001, *www.polysciences.com*. 04/15/2004.

7. R&D Systems 2004, *www.rndsystems.com*. 10/05/2004.

8. Dubertret, B.; Skouridid, P.; Norris, D. J.; Noireaux, V.; Brivanlou, A. H.; Libchaber, A. *Science* **2002**, *298*, 1759.

9. BioRad Laboratories, Helios Gene Gun, www.biorad.com. 11/02/2004.

10. Iijima, S. *Nature* **1991**, *354*, 56.

11. Ajayan, P. M. *Chem. Rev*. **1999**, *99*, 1287.

12. McEuen, P. L. *Nature* **1998**, *393*, 15.

13. Tans, S., J.; Verschueren, R., M.; Dekker, C. *Nature* **1998**, *393*, 49.

14. Ouyang, M.; Huang, J-L.; Lieber, C. M. *Science* **2001**, *292*, 702.

15. Rueckes, T.; Kim, K.; Joselevich, E.; Tseng, G. Y.; Cheung, C-L.; Lieber, C. M. *Science* **2000**, *289*, 94.

16. Ajayan, M.; Stephan, O.; Redlich, P.; Colliex, C. *Nature* **1995**, *375*, 564.

17. Jung, J. H.; Kobayashi, H.;van Bommel, K. J. C.; Shinkai, S.; Shimizu T. *Chem. Mater*. **2002**, *14*, 1445.

18. Rao, C. N. R.; Satishkumar, B. C.; Govindaraj, A. *Chem. Commun*. **1997**, 1581.

19. Chen, P.; Wu, X.; Lin, J.; Tan, K. L. *Science* **1999**, *285*, 91.

20. Dai, H.; Rinzler, A. G.; Nikolaev, P.; Thess, A.; Colbert, D. T.; Smalley, R. E. *Chem. Phys. Lett.* **1996**, *260*, 471.

21. Shim, M.; Kam, N.W. S.; Chen, R. J.; Li, Y.; Dai, H. *Nano Lett.* **2002**, *2*, 285.

22. Chen, P.; Wu, X.; Lin, J.; Tan, K. L. *Science* **1999**, *285*, 91.

23. Langer, R. *Science* **2001**, *293*, 58.

24. Baker, R. W. *Membrane Technology and Applications*; John Wiley & Sons, Ltd. 2004, p 7.

25. Giorno, L.; De Bartolo, L.; Drioli, E. In *New Insights into Membrane Science and Technology: Polymeric and Biofunctional Membranes*; Bhattacharyya, D.; Butterfield, D. A. Ed. Elsevier, 2003, p187.

26. Gavalas, V.; G.; Wang, J.; Bachas, L. G. In *New Insights into Membrane Science and Technology: Polymeric and Biofunctional Membranes*; Bhattacharyya; D.; Butterfield, D. A. Ed. Elsevier, 2003, p 379.

27. Kasianowicz, J. J.; Brandin, E.; Branton, D.; Deamer, D. W. *Proc. Natl. Acad. Sci. USA* **1996**, *93*, 13770.

28. Akeson, M.; Branton, D.; Kasianowicz, J. J.; Brandin, E.; Deamer, D.W. *Biophys. J.* **1999**, *77*, 3227.

29. Li, J.; Stein, D.; McMullan, C.; Branton, D.; Aziz, M. J.; Golovchenko, J.A. *Nature* **2001**, *412*, 166.

30. Li, J.; Gershow, M.; Stein, D.; Brandin, E.; Golovchenko, J. A. *Nat. Mat.* **2003**, *2*, 611.

31. Hulteen, J. C.; Martin, C. R. *J. Mater. Chem.* **1997**, *7*, 1075.

32. Fleischer, R., L.; Price, P.; B.; Walker, R.; M. *Nuclear Tracks in Solids*; University of California Press; Berkeley, CA, 1975.

33. Hornyak, G. L.; Patrissi, C. J.; Martin, C. R. J. *Phys. Chem. B* **1997**, *101*, 1548.

34. Sun, L.; Chien, C. L.; Searson, P. C. *J. Mater. Sci.* **2000**, *35*, 1097.

35. Penner, R. M.; Martin, C. R. *Anal. Chem.* **1987**, *59*, 2625.

36. Menon, V. P; Martin, C. R. *Anal. Chem.* **1995**, *67*, 1920.

37. Cepak, V. M.; Martin, C. R. *Chem. Mater.* **1999**, *11*, 1363.

38. Cai, Z.; Martin, C. R. *J. Am. Chem. Soc.* **1989**, *111*, 4138.

39. Parthasarathy, R. V.; Martin, C. R. *Chem. Mater.* **1994**, *6*, 1627.

40. Jirage, K. B; Hulteen, L. C.; Martin, C. R. *Science* **1997**, *278*, 655.

41. Kang, M. S.; Martin, C. R. *Langmuir* **2001**, *17*, 2753.

42. Gasparac, R.; Martin, Mitchell, D. T.; C. R. *Electrochim. Acta* **2004**, *49*, 847.

43. Hulteen, J. C.; Jirage, K. B.; Martin, C. R. *J. Am. Chem. Soc.* **1998**, *120*, 6603.

44. Jirage, K. B; Hulteen, L. C.; Martin, C. R. *Anal. Chem.* **1999**, *71*, 4913.

45. Lee, S. B.; Martin, C. R. *Anal. Chem.* **2001**, *73*, 768.

46. Yu, S.; Lee, S. B.; Martin, C. R. *Anal. Chem.* **2003**, *75*, 1239.

47. Kohli, P.; Harrell, C. C.; Cao, Z.; Gasparac, R.; Tan, W.; Martin, C. R. *Science* **2004**, *305*, 984.

48. Diggle, J. W.; Dowme, T. C.; Goulding, C. W. *Chem. Rev.* **1969**, *69*, 365.

49. Jagminas, A.; Bigeliene, D.; Mikulskas, I.; Tomasiunas, *J. Crystal Growth* **2001**, *233*, 591.

50. Masuda, H.; Fukuda, K. *Science* **1995**, *268*, 1468.

51. Asoh, H.; Nishio, K.; Nakao, M.; Tamamura, T.; Masuda, H. *J. Electrochem. Soc.* **2001**, *148(4)*, B152.

52. Masuda, H.; Satoh, S. *Jpn. J. Appl. Phys. Part 2* **1996**, *35 (no. 1B)*, L126.

53. Li, A-P.; Muller, F.; Birner, A.; Nielsch, K.; Gosele, U. *Adv. Mater.* **1999**, *11(6)*, 483.

54. Masuda, H.; Asoh, H.; Watanabe, M.; Nakao, M.; Nishio, K.; Tamamura, T. *Adv. Mater.* **2001**, *13(13)*, 189.

55. Mikulskas, I.; Juodkazis, S.; Tomasiunas, R.; Dumas, J., G. *Adv. Mater.* **2001**, *13(20)*, 1573.

56. Masuda, H.; Kanezawa, K.; Nishio, K. *Chem. Lett.* **2002**, 1218.

57. Masuda, H.; Hasegawa, F.; Ono, S. *J. Electrochem. Soc.* **1997**, *144*, L277.

58. Li, A. P.; Muller, F.; Birner, A.; Nielsch, G.; Gosele, U. *J. Appl. Phys.* **1998**, *84*, 6320.

59. Thomson, G. E. *Thin Solid Films* **1997**, *297*, 192.

60. O'Sullivan, J. P.; Wood, G. C. *Proc. Roy. Soc. London A* **1970**, *317*, 511.

61. Thomson, G. E.; Furneaux, R. C.; Wood. G. C.; Richardson, J. A.; Goode, J. S. *Nature* **1978**, *272*, 433.

62. Jessensky, O.; Muller, F.; Gosele, U. *Appl. Phys. Lett.* **1998**, *72*, 1173.

63. Kaway, S.; Ueda, R. *J. Electrochem. Soc.* **1974**, *32*, 122.

64. Shiraki, M.; Wakuy, Y.; Tokushima T.; Tsuya, N. *IEEE Trans. Magn. 1985*, *MAG-21*, 1465.

65. Saito, M.; Kinikara, M.; Taniguchi, T.; Miyagi, M. *Appl. Phys. Lett.* **1989**, *55*, 607.

66. Miller, C. J.; Majda, M. *J. Am. Chem. Soc.* **1985**, *107*, 3118.

67. Tierney, M. J.; Martin, C. R. *J. Electrochem. Soc.* **1990**, *137*, 3789.

68. Yoshino, T.; Baba, N. *J. Chem. Soc. Jpn.***1983**, *1983*, 955.

69. Misuki, I.; Yamamoto, T.; Yoshino, T.; Baba, N. *J. Metal. Surf. Finish. Soc. Jpn.* **1987**, *38*, 561.

70. Masuda, H.; Mizuno, T.; Baba, N.; Ohmori, T. *J. Electroanal. Chem.* **1994**, *363*, 333.

71. Nivewarmer-Pena, S. R.; Freeman, R. G.; Reiss, B. R.; He, L.; Walton, I. D.; Cromer, R.; Keating, C. D.; Natan, M. J. *Science* **2001**, *294*, 137.

72. Hobbs, K. L.; Larson, P. R.; Lian, G. D.; Keay, J. C.; Johnson, M. B. *Nano Lett.* **2004**, *4(1)*, 167.

73. Hennesthal, C.; Steinem, C. *J. Am. Chem. Soc.* **2000**, *122*, 8085.

74. Smirnov, A. I.; Poluektov, O. G. *J. Am. Chem. Soc.* **2003**, *125*, 8434.

75. Braunstein, P.; Kormann, H-P.; Meyer-Zaika, W.; Pugin, R.; Schmidt, G. *Chem. Eur. J.* **2000**, *6(24)*, 4637.

76. Lahav, M.; Sehayek T.; Vaskevich, A.; Rubinstein, I. *Angew, Chem. Int. Ed.* **2003**, *42*, 5575.

77. Ai, S.; Lu, G.; He, Q.; Li, J. *J. Am. Chem. Soc.* **2003**, *125*, 11140.

78. Kovtyukhova, N. I.; Mallouk, T. E.; Mayer, T. S. *Adv. Mater.* **2003**, *15*, 780.

79. Lee, H.; Kepley, L. J.; Hong, H.-G.; Akhter, S.; Mallouk, T. E. *J. Phys. Chem.* **1988**, *92*, 2597.

80. Hou, S.; Harrell. C. C.; Trofin, L.; Kohli, P.; Martin, C. R. *J. Am. Chem. Soc.* **2004**, *126(18)*, 5674.

81. Mitchell, D.T.; Lee, S.B.; Trofin, L.; Li, N.; Nevanen, T.K.; Soderlund, H.; Martin, C.R. *J. Am. Chem. Soc.* **2002**, *124*, 11864.

82. Lee, S.B.; Mitchell, D.T.; Trofin, L.; Nevanen, T.K.; Soderlund, H.; Martin, C.R. *Science* **2002**, *296*, 2198.

83. Yamaguchi, A.; Uejo, F.; Yoda, T.; Uchida, T.; Tanamura, Y.; Yamashita, T.; Teramae, N. *Nature Mater.* **2004**, *3*, 337.

84. Lakshmi, B. B.; Patrissi, C. J.; Martin, C. R. *Chem. Mater.* **1997**, *9*, 2544.

85. Salem A. K.; Searson, P. C.; Leong, K. W. *Nature Mater.* **2003**, *2*, 668.

86. Mizushima. T.; Matsumoto, K.; Sugoh, J.; Ohkita, H.; Kakuta, N. *Appl. Catalysis A: General* **2004**, *265*, 53.

87. Martin, F. J.; Grove, C. *Biomed. Devices* **2001**, *3:2*, 97.

88. Yoldas, B.E. *J. Mater. Sci.* **1975**, *10*, 1856.

89. Yamane, M.; Aso, S.; Sakaino, S. *J. Mater. Sci.* **1978**, *13*, 865.

90. Livage, J.; Henry, M.; Sanchez, C. *Prog. Solid State Chem.* **1988**, *18*, 259.

91. Hench, L.L. *Sol-Gel Silica: Properties, Processing and Technology*; Noyes, Westwood, NJ, 1988.

92. Pierre, A.C. *Introduction to Sol-Gel Processing*; Kluwer, Boston, 1998.

93. Prassas, M.; Phalippou, J.; Zarzycki, J. *J. Mater. Sci.* **1984**, *19*, 1656.

94. Arkles, B. *Chemtech.* **1977**, *7*, 766.

95. Pleuddemann, F. P. *Silane Coupling Agents; Plenum Press*; New York, USA, 1982.

96. Akhond, M.; Shamsipur, M. J. Membr. Sci. 1996, 117, 221.

97. Schow, A. J.; Peterson, R. T.; Lamb, J. D. *J. Membr. Sci.* **1996**, *111*, 291.

98. Fyles, T. *US Patent 4,906,376*, 1990.

99. Cussler, E. L.; Aris, R.; Brown, A. *J. Membr. Sci.* **1998**, *43*, 149.

100. Noble, R. D. *J. Membr. Sci.* **1992**, *75*, 121.

101. Lacan, P.; Guizard, C.; Gall, P. L.; Wettling, D.; Cot, L. *J. Membr. Sci.* **1995**, *100*, 99.

102. Kang, Y. S.; Hong, J. M.; Yang, J.; Kim, U. Y. *J. Membr. Sci.* **1996**, *109*, 149.

103. Hong, J. M.; Kang, Y. S.; Yang, J.; Kim, U. Y. *J. Membr. Sci.* **1996**, *109*, 159.

104. McBride, J. D. W.; Izatt, R. M.; Lamb, J. D.; Christensen, J. J. In *Inclusion Compounds III*; Academic Press, London, 1984, pp. 571.

105. Nishide, H.; Ohyanagy, M.; Okada, O.; Tsuchida, E. *Macomolecules* **1987**, *20*, 417.

106. Nishide, H.; Ohyanagy, M.; Okada, O.; Tsuchida, E. *Macomolecules* **1988**, *21*, 2910.

107. Nishide, H.; Kawakami, H.; Kurimura, Y.; Tsuchida, E. *J. Am. Chem. Soc.* **1989**, *111*, 7175.

108. Yoshikawa, M.; Eyaki, T.; sanui, K.; Ogata, N. *Kobunshi Ronbunshu* **1986**, *43 (11)*, 729.

109. Erikse, O. I.; Aksens, E.; Dahl, I. M. *J. Membr. Sci.* **1993**, *85(1)*, 89.

110. Kim, J. H.; Park, S. M.; Won, J.; Kang, Y. S. *J. Membr. Sci.* **2004**, *236*, 209.

111. Riggs, J. A.; Smith, B. *J. Am. Chem. Soc.* **1997**, *119*, 2763.

112. Scholander, P. F. *Science* **1960**, *131*, 585.

113. Hemmingsen, E. A. *Science* **1962**, *135*, 733.

114. Schultz, J. S. In *Synthetic Membranes: Science, Engineering and Applications* 1986, Ed by Bungay, P. M., D. Reidel Publishing Company, 523.

115. Schultz, J. S.; Goddard, J. D.; Suchdeo, S. R. *AIChE J.* **1974**, *20*, 417.

116. Cooper, G. M. *The Cell – A Molecular Approach*; 2nd ed. Sunderland; MA; Sinauer Associates, Inc.;. 2000 p. 81-84, 476-491.

117. Hille, B. *Ionic Channels of Excitable Membranes*; 2nd ed. Sunderland; MA; Sinauer Associates, Inc.; 1992.

118. Kasianowicz, J. J.; Brandin, E.; Branton, D.; Deamer, W. D. *Proc. Natl. Acad. Sci. U.S.A.* **1996**, *93*, 13770.

119. Siwy, S.; Fulinski, A. *Phys. Rev. Lett.* **2002**, *89*, 158101.

120. Siwy, S.; Gu, Y.; Spohr, H. A. Baur, D.; Wolf-Reber, A.; Apel, P.; Korchev, Y. E. *Europhys. Lett.* **2002**, *60*, 349.

121. Siwy, S.; Apel, P.; Baur, D.; Dobrev, D.; Korchev, Y. E.; Neumann, R.; Spohr, R.; Trautmann, C.;Voss, K. *Surf. Sci.* **2003**, *532–535*, 1061.

122. Siwy, Z.; Dobrev, D. D.; Neumann, R.; Trautmann, C.; Voss, K.; *Appl. Phys. A: Mater. Sci. Process.* **2003**, *76*, 781.

123. Siwy, Z.; Heins, E.; Harrell, C. C.; Kohli, P.; Martin, C. R. *J. Am. Chem. Soc.* **2004**, *126*, 10850.

124. Doyle, D. A.; Cabral, J. M.; Pfuetzner, R. A.; Kuo, A.; Gulbis, J. M.; Cohen, S. L.; MacKinnon, R. *Science* **1998**, *280*, 69.

125. Jiang, Y.; Lee, A.; Chen, J.; Cadene, M.; Chait, B. T.; MacKinnon, R. *Nature* **2002**, *417*, 515.

126. Jiang, Y.; Ruta, V.; Chen, J.; Lee, A.; MacKinnon, R. *Nature* **2003**, *423*, 42.

127. Trautmann, C.; Bouffard, S.; Spohr, R. *Nucl. Instr. and Meth. B* **1996**, *116*, 429.

128. Apel, A.; Korchev, Y. E.; Siwy, Z.; Spohr, R.; Yoshida, M. *Nucl. Instr. Meth. B* **2001**, *184*, 337.

129. Siwy, Z.; Apel, A.; Dobrev, D. D.; Neumann., R.; Spohr, R.; Trautmann, C.; Voss, K. *Nucl. Instr. Meth. B* **2003**, *208*, 143.

130. Sugawara, M.; Hirano, A.; Umezawa, Y.; *Affinity Biosensors. Techniques and Protocols*; Humana Press: Totowa, 1998.

131. Mallouk, T., E.; Harrison, D., J. *Interfacial Design and Chemical Sensing, American Chemical Society*; Washinton D.C., 1994.

132. Voet, D.; Voet, J. G. *Biochemistry*; 2nd ed.; John Wiley and Sons: NY, 1995.

133. Sugawara, M.; Kojima, K.; Sakawa, H.; Umezawa, Y.; *Anal. Chem.* **1987**, *59*, 2842.

134. Buhlmann, K. P.; Umezawa, Y. *Anal. Chem.* **1999**, *71*, 1183.

135. Wu, Z.; Tang, J.; Cheng, Z.; Yang, X.; Wang, E.; *Anal. Chem.* **2000**, *72*, 6030.

136. Katayama, Y.; Ohuchi, Y.; Higashi, H.; Kudo, Y.; Maeda, M. *Anal. Chem.* **2000**, *72*, 4671.

137. Alberts, B.; Johnson, A.; Lewis, J.; Raff, M.; Roberts, K.; Walter, P. *Molecular Biology of the Cell*; 4th Ed. Garland Science, NY, 2002.

138. Steinle, E.D.; Mitchell, D.T.; Wirtz, M.; Lee, S.B.; Young, V.Y.; Martin, C.R. *Anal. Chem.* **2002**, *74*, 2416.

139. Hou, Z.; Abbott, N. L.; Stroeve, P. *Langmuir* **2000**, *16*, 2401.

140. Hillebrandt, G. W.; Tanaka, M.; Sackmann, E. *Langmuir* **1999**, *15*, 8451.

141. Ohki, K.; Tokiwa, F. *J. Chem. Soc. Jpn. Chem. Ind. Chem.* **1970**, *91*, 534.

142. Ulbricht. M. *J. Chromatogr. B* **2004**, *804*, 113.

143. Laukkanen, M-J.; Ma¨kinen-Kiljunen, S.; Isoherranen, K.; Haahtela, T.; Soderlund, H.; Takkinen, K. *J. Immun. Meth.* **2003**, *278*, 271.

144. Alenius, H.; Kalkkinen, N.; Reunala, T.; Turjanmaa, K.; Palosuo, T. *J. Immunol.* **1996**, *156*, 1618.

145. Lee, H.-I.; Broekaert, W.F.; Raikhel, N.V. *J. Biol. Chem.* **1991**, *266*, 15944.

146. Matz, M.V.; Fradkov, A.F.; Labas, Y.A.; Savitsky, A.P.; Zaraisky, A.G.; Markelov, M.L.; Lukyanov, S.A. *Nature Biotechnol.* **1999**, *17*, 969.

147. Wolpert, S. *J. Membr. Sci.* **1997**, *132*, 23.

148. Hong, J. M.; Anderson, P. E.; Quain J.; Martin, C. R. *Chem. Mater.* **1998**, *10*, 1029.

149. Arrio-Dupont, M.; Foucault, G.; Vacher, M.; Devaux, P. F.; Cribier, S. *Biophys. J.* **2000**, *78*, 901.

150. Yarbrough, D.; Wachter, R. M.; Kallio, K.; Matz, M. V.; Remington, S. J. *Proc. Natl. Acad. Sci. U.S.A.* **2001**, *98(2)*, 462.

151. Rodriguez-Romero, A.; Ravichandran, K.G.; Soriano-Garcia, M. *FEBS Lett.* **1991**, *291*, 307.

152. Lakshmi, B. B.; Martin, C. R. *Nature* **1997**, *388*, 758.

153. Yu, S.; Lee, S. B.; Kang, M.;Martin, C. R. *Nano Lett.* **2001**, *1*, 495.

154. Miller, S. A.;Young, V. Y.; Martin, C. R. *J. Am. Chem. Soc.* **2001**, *123*, 12335.

155. Templin, M. F.; Stoll, D.; Schwenk, J. M.; Potz, O.; Kramer, S.; Joos, T. O. *Proteomics* **2003**, *3*, 2155.

156. Zhu, H.; Bilgin, M.; Bangham, R.; Hall, D.; Acamayor, A.; Bertone, P.; Lang, N.; Jansen, R.; Bidlingmajer, S.; Houfek, T.; Mitchell, T.; Miller, P.; Dean, R., A.; Gerstein, M.; Snyder, M. *Science* **2001**, *293*, 2101.

157. Kawahashi, Y.; Doi, N.; Takashima, H.; Tsuda, C.; Oishi, Y.; Oyama, R.; Yonezawa, M.; Miyamoto-Sato, E.; Yanagawa, H. *Proteomics* **2003**, *3*, 1236.

158. Huang, R-P. *J. Immun. Meth.* **2001**, *255*, 1.

159. de Wildt, R. M.; Mundy, C. R.; Gorick, B. D.; Tomlinson, I., M. *Nat. Biotechnol.* **2000**, *18*, 989.

160. Joos, T. O.; Schrenk, M.; Hopfl, P,; Kroger, K.; Chowdhury, U.; Stoll, D.; Schorner, D.; Durr, M.; Herik, K.; Rupp, S.; Sohn, K.; Hammerle, H. *Electrophoresis* **2000**, *21*, 2641.

161. MacBeath, G.; Schreiber, S. L. *Science* **2000**, *289*, 1760.

162. Celis, J. E.; Gromov, P.; *Cancer Cell* **2003**, 1, 233.

163. Hunter, T. *Cell* **2000**, *1*, 113.

164. Jeong, H.; Tombor, B.; Albert, R.; Oltvai, Z., N. *Nature* **2000**, *6804*, 651;

165. Zhu, H.; Snyder, M. *Curr. Opin. Chem. Biol.* **2003**, *7*, 55.

166. Kuznezow, W.; Hoheise, J., D. *J. Mol. Recognit.* **2003**, *16*, 165.

167. Affanissiev, V.; Hanemann, V.; Wolfl, S. *Nucleic Acids Res.* **2000**, *28*, 66.

168. Walter, G.; Bussow, K.; Cahil, D.; Lueking, A.; Lehrah, H.; *Curr. Opin. Microbiol.* **2001**, *250*, 81.

169. Arenkov, P.; Kukhtin, A.; Gemmell, A.; Voloshchuck, S.; Chupeeva, V.; Mirzabekov, A. *Anal. Biochem.* **2000**, *278*, 123.

170. Lee, K-B.; Park, So-Jung; Mirkin, C.;. Smith, J. C.; Mrksich, M. *Science* **2002**, *295*, 1702.

171. Ressine, A.; Ekstrom, S.; Marko-Varga, G.; Laurell, T. *Anal. Chem.* **2003**, *75*, 6968.

172. Yan, J.; Rama Rao, G., V.; Barela, M.; Brevnov, D., A.; Jiang, Y.; Xu, H.; Lopez, G. P.; Atannasov, P. B. *Adv. Mater.* **2003**, *15*, 2015.

173. Lakshmi, B. B.; Patrissi, C. J.; Martin, C. R. *Chem. Mater.* **1997**, *9*, 244.

174. Brinker, C. J.; Scherer, G. W. *Sol-Gel Science*; Academic Press: New York, 1990.

175. Loudon, G. M. *Organic Chemistry*; 3rd ed. The Benjamin/Cummings Publishing Company, Inc. 1997.

176. Bruning, J. G. *Chem. Commun.* **1995**, *1995*, 2323.

177. Stubbings, D.; Bubb, M. O.; Conradie, J. D. *Anal. Biochem.* **1993**, *T210*, 159.

178. Henriquez, R. R.; Ito, Y.; Sun, L.; Crooks, R. M. *The Analyst* **2004**, *129*, 478.

179. Song, L.; Hobaugh, M. R.; Shustak, C.; Cheley, S.; Bayley, H.;.Gouaux, J. E. *Science* **1996**, *274*, 1859.

180. Akeson, M.; Branton, D.; Kasianowicz, J. J.; Brandin, E.; Deamer, D. W. *Biophys. J.* **1999**, *77*, 3227.

181. Meller, A.; Nivon, L.; Brandin, E.; Golovchenko, J.; Branton, D. *Proc. Natl. Acad. Sci. USA* **2000**, *97*, 1079.

182. Winters-Hilt, S.; Vercoutere, W.; DeGuzman, V. S.; Deamer, D.; Akeson,M.; Haussler, D. *Biophys. J.* **2003**, *84*, 967.

183. J. Li, D. Stein, C. McMullan, D. Branton, M.J. Aziz, J.A. Golovchenko, *Nature* **2001**, *412*, 166.

184. Li, J.; Gershow, M.; Stein, D.; Brandin, E.; Golovchenko, J. A. *Nat. Mater.* **2003**, *2*, 611.

185. Saleh, O. A.; Sohn, L. L. *Nano Lett.* **2003**, *3*, 37.

186. Storm, A. J.; van den Broek, S.; Lemay, D.; Dekker, C. *Biophys. J.* **2003**, *51*, 2002.

187. Mara, A.; Siwy, Z.; Trautmann, C.; Wan, J.; Kamme, F. *Nano Lett.* **2004**, *4*, 497.

188. Fuliński, A.; Kosińska, I.; Siwy, Z. *Physical Review E* **2004** – in press.

189. Stein, D.; Kruithof, M.; Dekker, C. *Physical Review Lett.* **2004** – in press.

190. Ulman, A. *Chem. Rev.* **1996**, *96*, 1533.

191. Gonzalez, M.; Bagatolli, L. A.; Echabe, I.; Arrondo, J. L. R.; Argarana,C. E.; Cantor, C. R.; Fidelio, G. D. *J. Biol. Chem.* **1997**, *272*, 11288.

192. Derrick, J.P.; Wigley, D.B. *J. Mol. Biol.* **1994**, *243*, 906.

193. Bjorck, L.; Kronvall, G. *J. Immunol.* **1984**, *133*, 969.

194. Akerstrom, B.; Brodin, T.; Reis, K.; Bjorck, L. *J. Immunol.* **1985**, *135*, 2589.

195. Akerstrom, B.; Bjorck, L. *J. Biol. Chem.* 1986, 261(22), 10240.

196. Spohr, R. *US Patent No. 4369370*, 1983.

197. Narhi, L. O.; Caughey, D. J.; Horan, T.; Kita, Y.; Chang, D.; Arakawa, T. *Anal. Biochem.* **1997**, *253(2)*, 236.

198. Lee, S.; Zhang, Y.; White, H.S.; Harrell, C.C.; Martin, C.R. *Anal. Chem.* **2004,** *76(20)*, 6108.

199. Poli, M.A.; Rivera, V.R.; Hewetson, J.F.; Merrill, G.A. *Toxicon* **1994**, *32*, 1371.

# BIOGRAPHICAL SKETCH

Lacramioara Trofin was born in Bucharest, Romania. She attended a very prestigious mathematics-physics high school, B.P. Hasdeu, in Buzau, Romania. Lacramioara developed an interest in chemistry since high school, when she was placed on the third place at the national Olympiads for Chemistry. She graduated with a B.S. degree in chemical engineering and a M.S. degree in organic chemistry from the Politechnica University , Bucharest, in 1993. After that she worked as a research engineer at the Research Institute for Elastomer Processing , Bucharest, Romania. In January 2000, Lacramioara entered graduate school in the Chemistry Department at the University of Florida, under the guidance of Prof. Charles R. Martin. She completed her research in December, when she received a Doctor of Philosophy degree.

I certify that I have read this study and that in my opinion it conforms to acceptable standards of scholarly presentation and is fully adequate, in scope and quality, as a dissertation for the degree of Doctor of Philosophy.

Charles R. Martin, Chairman
Professor of Chemistry

I certify that I have read this study and that in my opinion it conforms to acceptable standards of scholarly presentation and is fully adequate, in scope and quality, as a dissertation for the degree of Doctor of Philosophy.

John R. Reynolds
Professor of Chemistry

I certify that I have read this study and that in my opinion it conforms to acceptable standards of scholarly presentation and is fully adequate, in scope and quality, as a dissertation for the degree of Doctor of Philosophy.

Vaneica Young
Associate Professor of Chemistry

I certify that I have read this study and that in my opinion it conforms to acceptable standards of scholarly presentation and is fully adequate, in scope and quality, as a dissertation for the degree of Doctor of Philosophy.

Anna Brajter-Toth
Associate Professor of Chemistry

I certify that I have read this study and that in my opinion it conforms to acceptable standards of scholarly presentation and is fully adequate, in scope and quality, as a dissertation for the degree of Doctor of Philosophy.

John G. Harris
Associate Professor of Electrical and
Computer Engineering

This dissertation was submitted to the Graduate Faculty of the Department of Chemistry in the College of Liberal Arts and Sciences and to the Graduate School and was accepted as partial fulfillment of the requirements for the degree of Doctor of Philosophy.

May 2005

_____

Dean, Graduate School